University of Alberta

Analysis of the Functional Domains and Associating Proteins for the Cytochrome *c* Oxidase Assembly Factor, Cox16p

By

Jennifer Marie Ting-Yuee Zee

A thesis submitted to the Faculty of Graduate Studies and Research in partial fulfillment of the requirements for the degree of *Master of Science*

In

Medical Sciences – Medical Genetics

Edmonton, Alberta

Fall 2006

Your file Votre référence
ISBN: 978-0-494-22414-4
Our file Notre référence
ISBN: 978-0-494-22414-4

Abstract

Cox16p is a protein required for the proper assembly of cytochrome *c* oxidase (COX), the final component of the electron transport chain (ETC) located in the mitochondria. Previous studies of Cox16p determined its location in the inner mitochondrial membrane and excluded its involvement in the maturation of subunit 2, copper recruitment or heme A biosynthesis. Current studies described in this thesis characterize functional domains of Cox16p and aim to identify associating proteins within a high molecular weight complex. Analyses of various mutations have determined a functional domain within the C-terminus of the protein around amino acids 90-99. Immunoprecipitations and sucrose gradients indicate that Cox16 self-associates in a tetrameric or pentameric complex. Initial studies have also confirmed that Cox16p can be purified using a TAP epitope. The identification of a human homolog reveals the importance in determining Cox16p function as its malfunction could be an underlying cause of human COX deficiencies.

Acknowledgements

I wish to thank Dr. Rick Rachubinski for contributing the Cox16-TAP construct. I would also like to thank my committee members, Dr. Frank Nargang and Dr. Rachel Wevrick for their scientific contributions and critical reading of this thesis. I wish to thank my supervisor, Dr. Moira Glerum, for her guidance and support throughout my two years as student in her laboratory. Lastly, I would like to thank my family and my fiancé, John, for their continuing support and encouragement throughout my academic career.

Table of Contents

List of Tables

List of Figures

List of Abbreviations

ADP	Adenosine diphosphate
Amp	Ampicillin
ATP	Adenosine triphosphate
bp	Base pair
Cat	Catalase
COX	Cytochrome oxidase
EG	Ethanol/Glycerol
ETC	Electron transport chain
FAD	Flavin-adenine dinucleotide
Fe-S	Iron sulphur
FMN	Flavin mononucleotide
Gal	Galactose
Hb	Hemoglobin
IMM	Inner mitochondrial membrane
IMS	Intermembrane space
IP	Immunoprecipitation
kb	Kilobase
kDa	Kilodalton
LB	Luria Bertani
LDH	Lactate dehydrogenase
LSFC	Leigh syndrome French Canadian variant
MELAS	Mitochondrial encephalomyopathy, lactic acidosis and stroke-like episodes

mRNA	Messenger RNA
mtDNA	Mitochondrial DNA
NAD	Nicodinamide-adenine dinucleotide
nDNA	Nuclear DNA
OXPHOS	Oxidative phosphorylation
PCR	Polymerase chain reaction
P_i	Inorganic phosphate
PMS	Post mitochondrial supernatant
rpm	Rotations per minute
SDS-PAGE	Sodium dodecyl sulphate polyacrylamide gel electrophoresis
TAP	Tandem affinity purification
TCA	Trichloroacetic acid
TCA cycle	Tricarboxylic acid cycle
TIM	Translocase of the inner membrane
TOM	Translocase of the outer membrane
WO	Minimal glucose media
YPD	Yeast peptone dextrose or rich glucose medium

Chapter 1: Introduction

Mitochondria and the Respiratory Complexes

Mitochondria are organelles located in the cytoplasm of eukaryotic cells. It was hypothesized over a century ago that these double-membrane structures originated from an α-Proteobacterial ancestor (Burger et al., 2003). Since then, mitochondria have evolved, becoming an essential component in many different cellular processes, including metabolism, apoptosis and ion homeostasis, (for a more detailed list, see Figure 1-1). The most significant function of mitochondria, discovered in 1949 by Kennedy and Lehninger, is oxidative energy metabolism. This process couples electron transport with oxidative phosphorylation (OXPHOS) to generate energy for the cell in the form of adenosine triphosphate (ATP) (Figure 1-2). The transport of electrons involves four different protein complexes located in the inner mitochondrial membrane (IMM), together creating the electron transport chain (ETC). The four multimeric complexes are identified as Complex I (NADH dehydrogenase), Complex II (succinate dehydrogenase), Complex III (cytochrome bc_1) and Complex IV (cytochrome *c* oxidase). The ETC also includes two additional components, ubiquinone (also known as coenzyme Q) and cytochrome *c*. Electrons for the ETC are obtained from reduced forms of nicotinamide- and flavin-adenine dinucleotide (NADH and $FADH_2$) intermediates derived from the oxidation of carbohydrates and fatty acids (Trounce, 2000). Electrons are subsequently passed from Complex I or II to Complex III and IV, and eventually to molecular oxygen, reducing it to water. While passing electrons to the subsequent complex, Complex I, III and IV pump protons from the mitochondrial matrix into the intermembrane space (IMS), generating an electrochemical proton gradient (Pedersen, 1999; Trounce, 2000). This gradient drives the production of ATP by Complex V (ATP synthase).

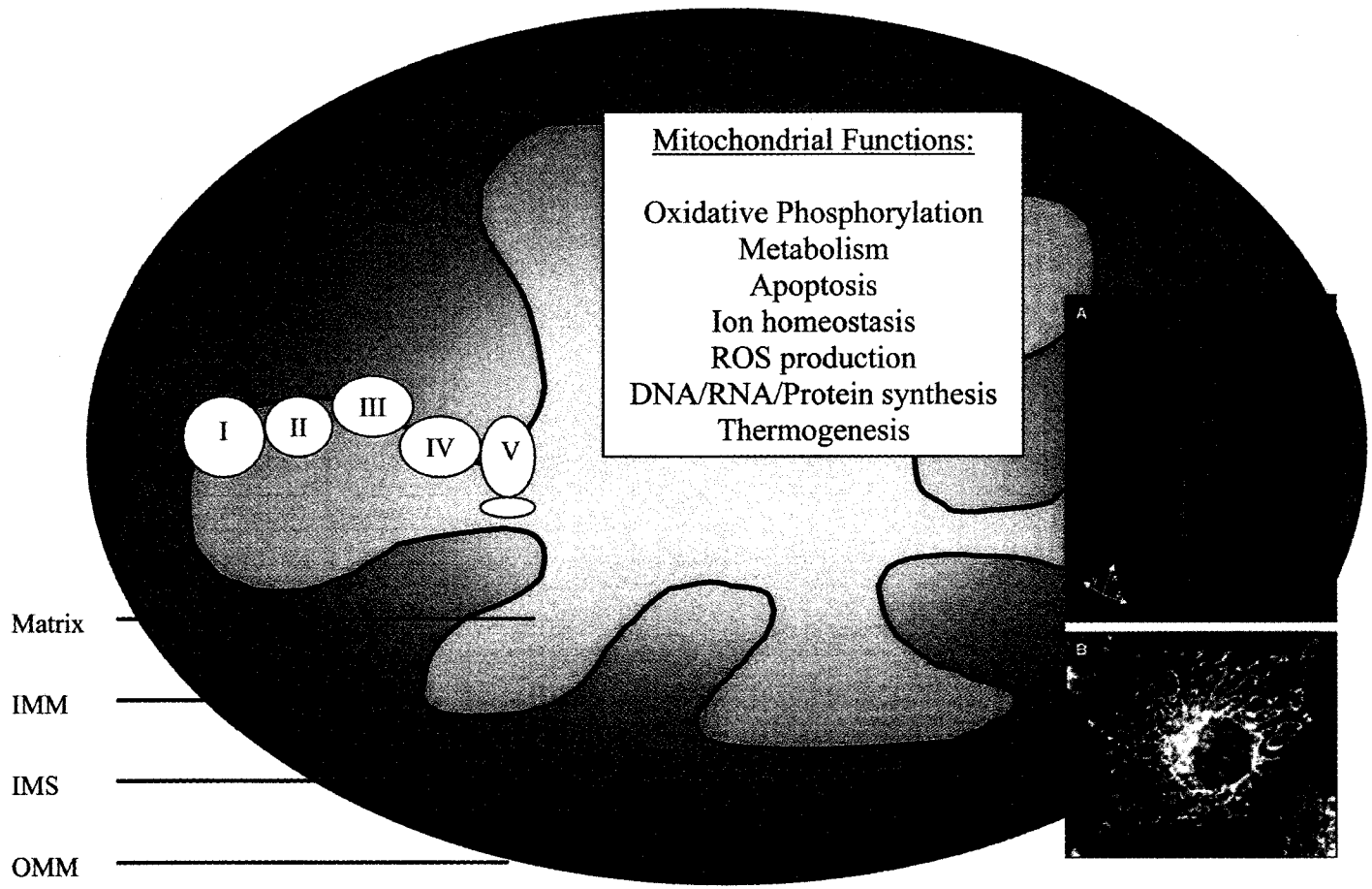

FIGURE 1-1. **Biological processes within the mitochondria and mitochondrial structure**. Components of the respiratory chain are located within the inner mitochondrial membrane and the complexes are indicated by I – V. GFP images of mitochondrial networks within *Saccharomyces cerevisiae* (top) and mammalian (bottom) cells are shown on the right (from Westermann, 2002). The regions of the mitochondria are listed as follows: OMM: outer mitochondrial membrane, IMS: intermembrane space, IMM: inner mitochondrial membrane, Matrix: mitochondrial matrix.

	Complex I	Complex II	Complex III	Complex IV	Complex V
# of subunits (Mito. encoded)	42 (7)	4 (0)	11 (1)	13 (3)	16-18 (2)
Redox centers	FMN 8-9 Fe-S	FAD 3 Fe-S heme B	Cytochrome *b* Cytochrome c_1 1 Fe-S	Heme AA_3 Cu_A Cu_B	
H^+/e^- transfer ratio	1-2	0	1	2	
	Monomer	Monomer	Dimer	Dimer	Monomer

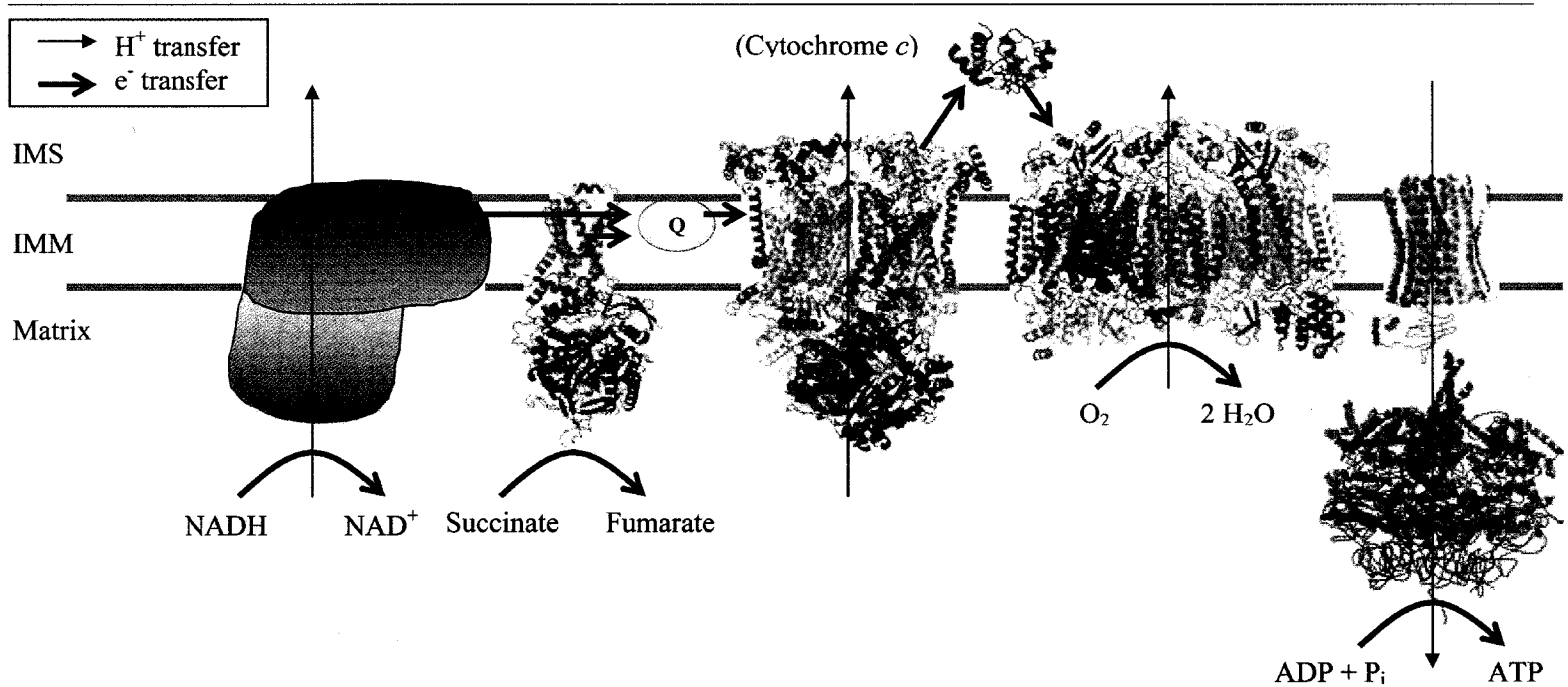

FIGURE 1-2. **Diagram of the respiratory chain in the inner mitochondrial membrane of mammalian cells.** Crystal structures were obtained from the PDB website and modified with PyMol. Accession codes: complex II = 1ZOY, complex III = 1BGY, cytochrome c = 1J3S, complex IV = 2OCC and complex V = 1QO1.

Due to their essential role in cellular growth and maintenance, the complexes involved in the ETC and ATP generation have been extensively studied. Complex I is the largest of all the complexes in the ETC, consisting of 42 subunits in humans. Seven subunits are encoded by mitochondrial DNA (mtDNA) and the remaining 35 subunits are encoded by nuclear DNA (nDNA) (Triepels et al., 2001). The "L"-shaped complex is composed of two different parts, a hydrophilic promontory (peripheral) part and a hydrophobic part. The promontory part extends into the matrix and has the ability to oxidize NADH. Electrons are transferred from NADH to FMN and eight or nine Fe-S clusters before being accepted by the lipid-soluble electron carrier, ubiquinone. Current studies have predicted that two to four protons are pumped from the matrix to the intermembrane space for every two electrons transferred. The hydrophobic part of Complex I contains all the subunits that are encoded by the mtDNA. This part of the complex is embedded in the inner mitochondrial membrane (IMM) and is hypothesized to have an involvement in ubiquinone reduction and ion transport (Yano, 2002).

Complex II is the smallest of all the complexes consisting of four subunits, all encoded by nDNA. Two subunits are hydrophilic in nature, projecting into the mitochondrial matrix (Lancaster, 2002). They contain the active sites of the complex and together form a catalytic dimer (Lemire and Oyedotun, 2002). The remaining two subunits are hydrophobic in nature and are located in the IMM (Lancaster, 2002). These subunits contain a heme B molecule and are the location of ubiquinone reduction (Lemire and Oyedotun, 2002). Although unable to pump protons into the IMS, Complex II is the only complex that is involved in both the ETC and the TCA cycle (Ackrell, 2002). Electrons are gained from the conversion of succinate to fumarate and are subsequently

passed on to FAD in the flavin subunit and the ubiquinone binding site, containing three Fe-S clusters. Electrons are then transferred to a ubiquinone pair that dissociate into the ubiquinone pool when fully reduced (Ackrell, 2002; Cecchini, 2003).

Complex III is responsible for multiple processes, including electron transfer, proton translocation and superoxide generation (Yu et al., 1999). The complex is composed of 11 subunits and exists in a dimeric form across the IMM (Cecchini, 2003; Crofts, 2004). Complex III is divided into three different regions, namely the matrix, transmembrane helix and intermembrane space. A large portion of the complex is composed of the matrix region. The transmembrane helix region consists of 13 transmembrane helices and contains the membrane-bound diheme cytochrome *b* (cytochrome b_L and b_H). The intermembrane space region contains the Rieske Fe-S protein and the functional components of cytochrome c_1 (Yu et al., 1999). Current models suggest that electrons are obtained from the ubiquinone pool and are transferred to either the Fe-S cluster or the diheme cytochrome *b*. From there, the electrons are transferred to cytochrome c_1 and eventually to cytochrome *c*. For each electron that is transferred through the complex, one proton is translocated from the matrix to the IMS (Crofts, 2004).

Complex V is a 16-18 subunit complex responsible for the production of ATP. Using the electrochemical proton gradient generated by Complex I, III and IV, the F_1F_0-type ATPase is able to catalyze the phosphorylation of ADP to generate ATP (Capaldi and Aggeler, 2002; Cecchini, 2003). Complex V is divided into two different parts. The F_0 part is composed of subunits *a, b* and *c* and transfers protons from the IMS to the mitochondrial matrix. The F_1 part is composed of α, β, γ, δ and ϵ subunits and contains

the three catalytic sites of the complex. The F_1 and F_0 parts of the complex are connected by central and peripheral stalks, with the central stock providing the rotor for the entire complex (Capaldi and Aggeler, 2002).

Cytochrome *c* Oxidase (COX)

Complex IV, also known as cytochrome *c* oxidase (COX), is the terminal electron acceptor in the ETC. It accepts electrons from cytochrome *c* and is responsible for the reduction of molecular oxygen to water.

In mammals, COX is present in a dimeric structure with each monomer consisting of 13 subunits (yeast contain 11 subunits. See Table 1-1). Three subunits are encoded by mtDNA and translated by mitochondrial ribosomes. These three subunits (CoxI, II and III) form the core of the complex. The remaining 10 subunits are encoded by nDNA and are translated by cytoplasmic ribosomes. Each nuclear-encoded subunit contains a basic mitochondrial targeting and import signal at the N-terminus of the protein (Taanman, 1997). After import through TOM and TIM complexes located in the mitochondrial outer and inner membrane respectively (Neupert, 1997; Tokatlidis and Schatz, 1999), the nuclear-encoded subunits associate with the surface of the core subunits to complete the assembly of COX.

The electron transport and catalytic properties of COX require the presence of 4 specific cofactors, Cu_A, heme A, heme A_3 and Cu_B (Figure 1-3). The functioning of COX may also be enhanced by the presence of zinc, sodium and magnesium ions and several phospholipids molecules, although the exact function of these components remains unknown (Yoshikawa, 1999). The Cu_A is the first electron acceptor and is located in the Cox2p subunit of the complex. Electrons are accepted from cytochrome *c* at a rate of

TABLE 1-1. **Comparison of Yeast and Mammal COX Subunits and Features**

Yeast	Mammals	Subunit Features
Cox1p	CoxI	Heme A, heme A_3-Cu_B
Cox2p	CoxII	Cu_A
Cox3p	CoxIII	Phospholipids
Cox4p	CoxVb	Zn^{2+}
Cox5p	CoxIVp	
Cox6p	CoxVa	
Cox6ap	CoxVIa	
Cox6bp	CoxVIb	
Cox7p	CoxVIIa	
Cox7ap	CoxVIc	
Cox8p	CoxVIIc	
-	CoxVIIb	
-	CoxVIII	

(Tsukihara et al., 1995; Yoshikawa, 1999; Khalimonchuk and Rödel, 2005)

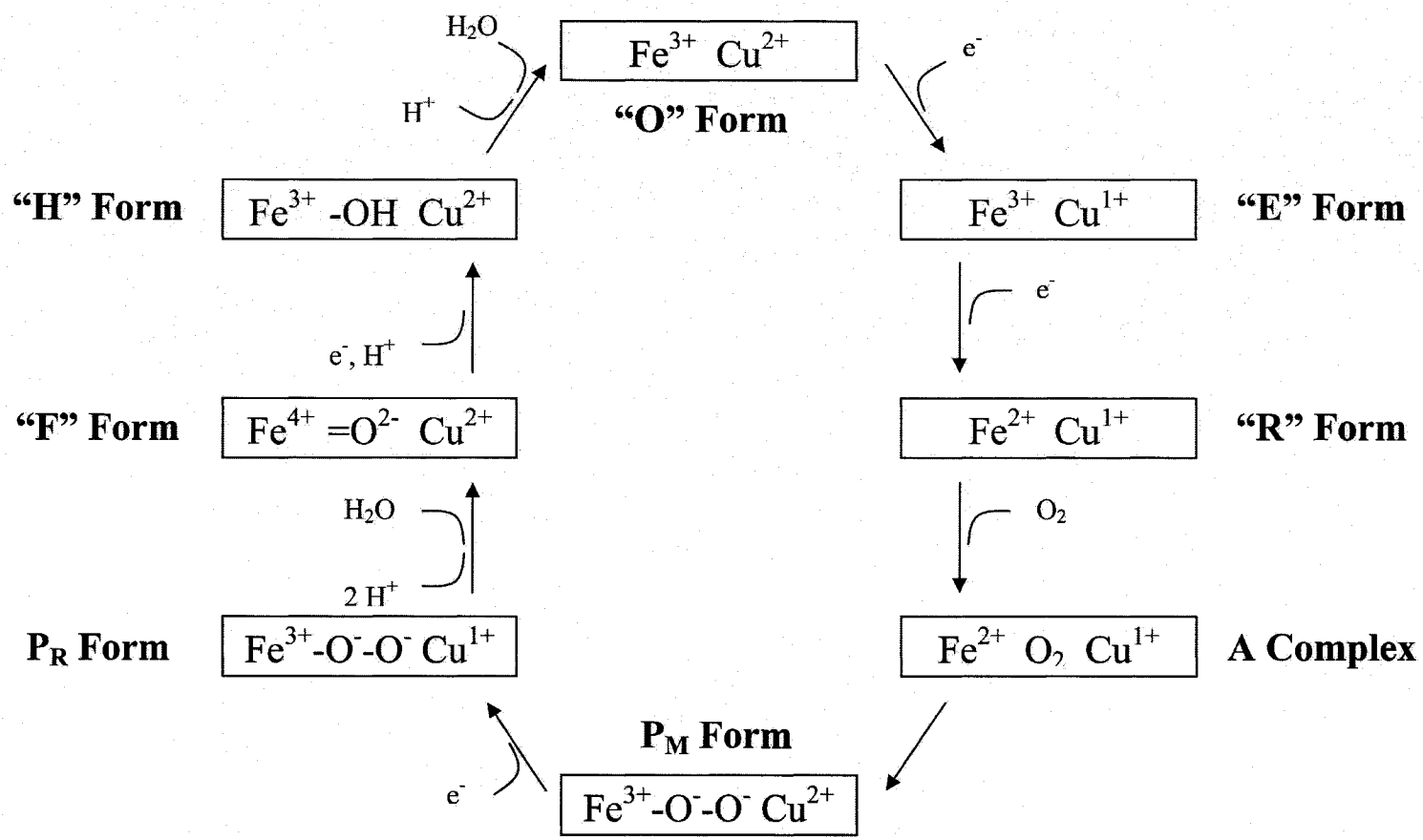

FIGURE 1-3. **The mechanism of catalysis at the heme A_3 – Cu_B site in cytochrome *c* oxidase.** Starting from the oxidized form (O), molecular oxygen is reduced to water. Cu_B and iron in the heme A_3 site undergo various oxidation and reduction steps in order to catalyze this reaction.

70,000/s. The rate of electron transfer between cytochrome *c* and the Cu_A site is limited by the rate of complex formation between cytochrome *c* and the docking site on COX (Michel et al., 1998), a crown of negatively charged residues surrounding a hydrophobic patch of 4 uncharged side chains (Brunori et al., 2005). After electron acceptance, Cu_A reduces heme A (located in the Cox1p subunit) at a rate of 20,000/s. It is speculated that this high rate of transfer is the result of a pathway consisting of 14 covalent bonds and 2 hydrogen bonds between the two sites. Electron transfer from the Cu_A site to the bimetallic heme A_3-Cu_B site is also possible although the rate of electron transfer is significantly lower (1-100/s). Instead, electrons are more frequently transferred from heme A to heme A_3-Cu_B. The electron transfer between these two sites occurs at a rate of 3000/s and is facilitated by the presence of several hydrogen bonds between the two hemes (Capaldi, 1996). The heme A_3-Cu_B is the catalytic site that reduces molecular oxygen to water (Figure 1-4). The catalytic reaction begins with both the iron of the heme A_3 and the Cu_B in an oxidized state, designated as the "O" form. The uptake of one electron by Cu_B results in the intermediate "E" form and the uptake of a second electron by iron results in a fully reduced "R" form (Brunori et al., 2005; Michel et al., 1998). Oxygen is brought to the binuclear site by one of three hypothesized hydrophobic channels. Oxygen binds to heme A_3 and electrons are subsequently transferred, resulting in an iron-bound oxygen atom. Protonation of peroxy-intermediates (P_M and P_R) at a site adjacent to heme A_3 allows the release of one water molecule from the binuclear site. A second protonation event generates an oxoferryl-state ("F" form) followed by a hydroxyl-state ("H" form) and the eventual release of a second water molecule (Michel et al., 1998).

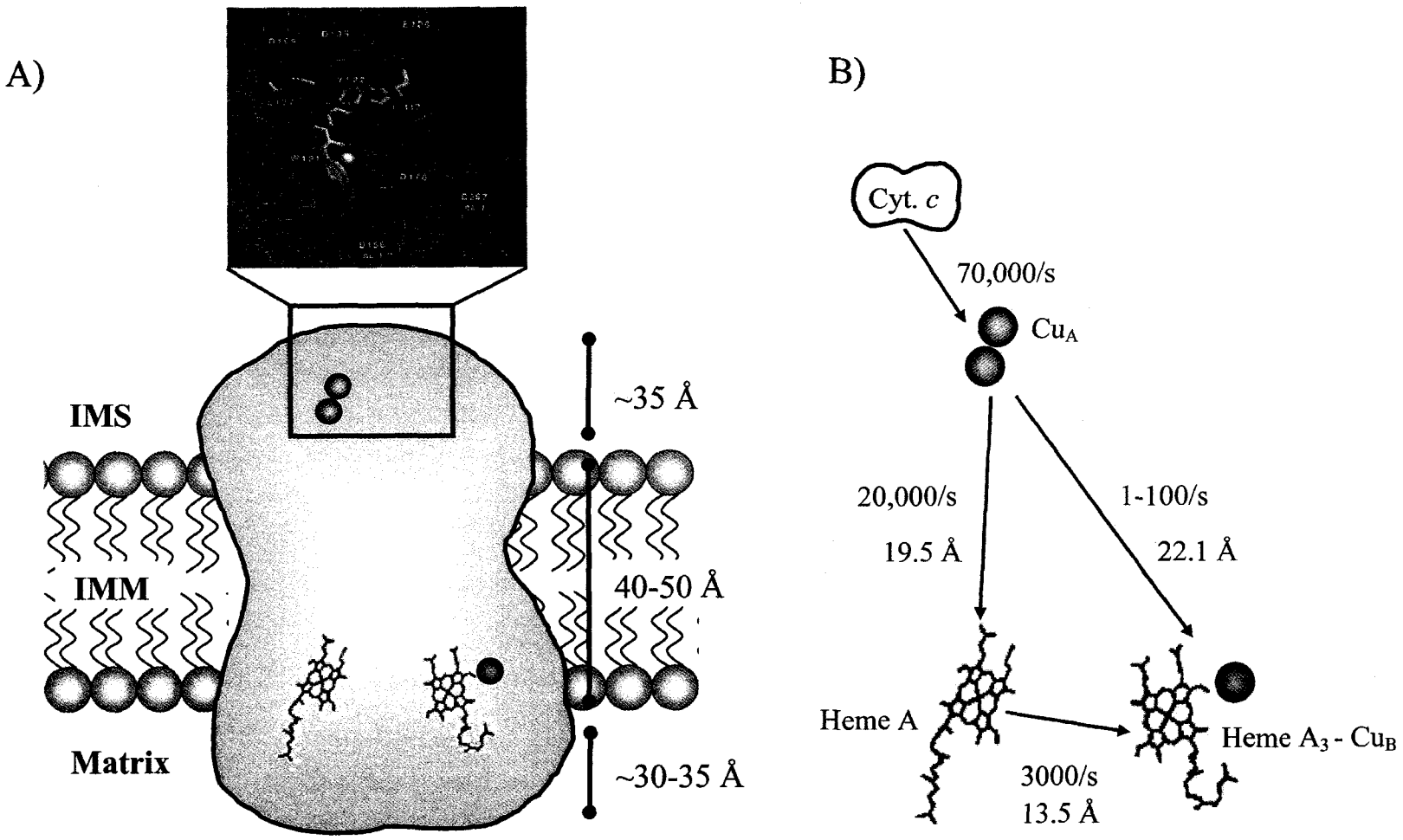

FIGURE 1-4. **COX structure and location of redox centers.** (A) An illustration of COX positioning within the IMM. The crown of negatively charged residues (red) surrounding a hydrophobic patch of uncharged side chains (green) serving as the cytochrome *c* docking site is depicted in the box above. The electron entry point is in yellow and the Cu_A site is in blue (from Brunori *et al.*, 2005). (B) A diagram depicting the speed of electron transport and distance between the redox centers of COX.

COX Assembly

The assembly of COX is a multi-step process consisting of the formation of various subcomplexes (Figure 1-5). To date, these subassembly complexes have only been identified in mammalian cells. The stepwise process begins with the presence of the mitochondrially-encoded subunit CoxI (Nijtmans et al., 1998), designated as subcomplex S1. Addition of the appropriate redox centers to S1 (heme A, heme A_3 and Cu_B) and association with the nuclear-encoded subunit, CoxIV, form the subsequent subcomplex, S2. Mitochondrially-encoded subunits CoxII and III associate with each other before association with the S2 subcomplex. The addition of nuclear-encoded subunits CoxVa, CoxVb, CoxVIb, CoxVIc, CoxVIIc and CoxVIII complete the subcomplex S3. The nuclear-encoded subunits CoxVIa, CoxVIIa and CoxVIIb are the last to be incorporated, generating the S4 subcomplex (Nijtmans et al., 1998). The assembly of COX is completed upon dimerization of the two S4 subcomplexes (Khalimonchuk and Rödel, 2005; Shoubridge, 2001; Taanman and Williams, 2001).

The formation of the subcomplexes and the functional holoenzyme require the presence of various "assembly factors". These assembly factors are not structural components of COX, yet are involved in many processes that control its assembly, such as transcription and translation of mitochondrially-encoded subunits, membrane insertion, cofactor incorporation and subunit associations. Initial investigations in *Saccharomyces cerevisiae* revealed several mutant strains that formed smaller colonies on glucose-containing media and were unable to grow on non-fermentable carbon sources, such as ethanol and glycerol. It was further discovered that the small colonies were unable to metabolize the ethanol that resulted from glucose metabolism. The accumulation of

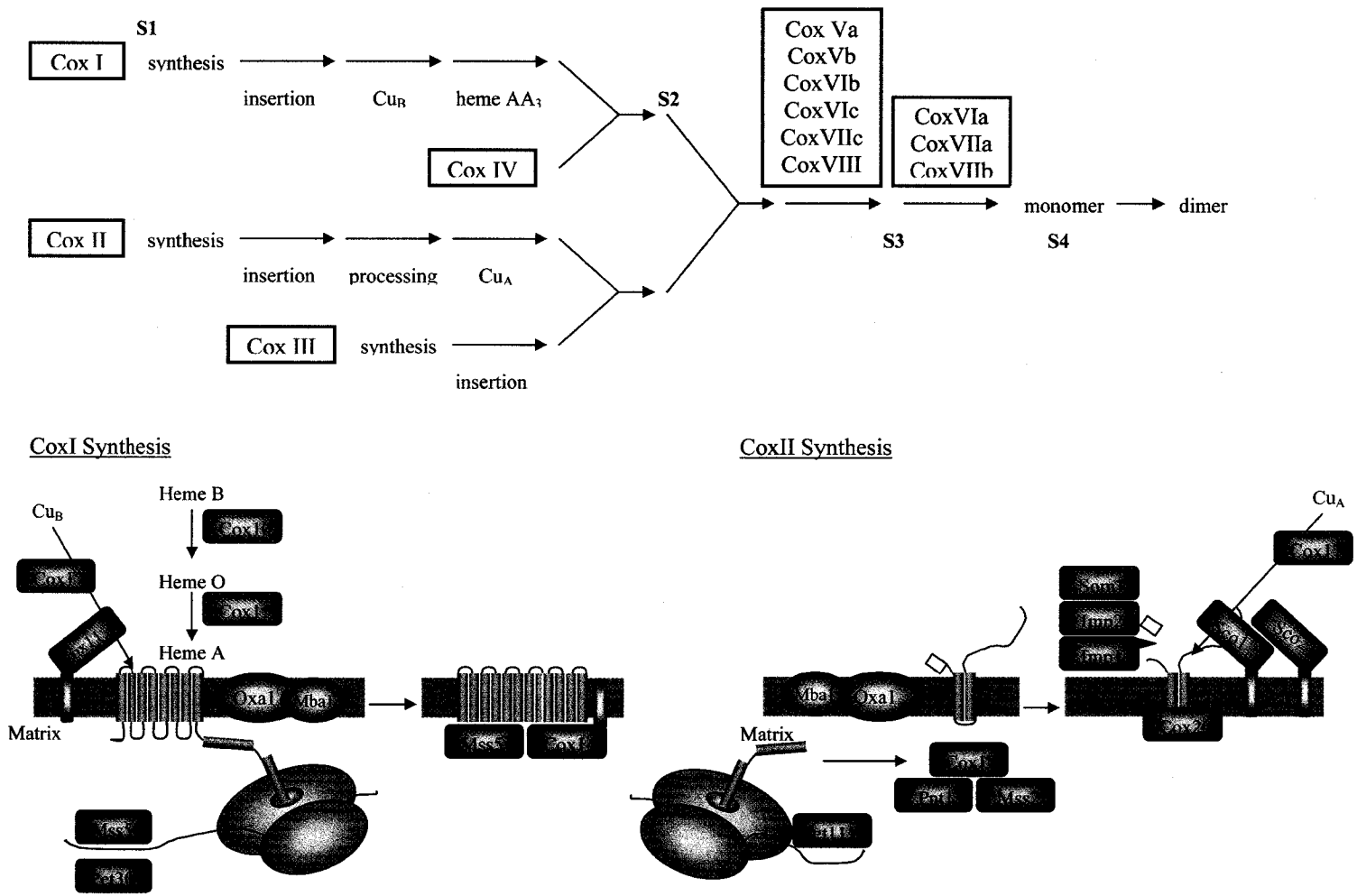

FIGURE 1-5. **COX assembly and associated assembly factors for CoxI and CoxII synthesis.** COX assembly is shown above with the various subcomplexes indicated in blue. CoxI and CoxII synthesis with the associated assembly factors is shown below. Adapted from Herrmann and Funes, 2005.

ethanol and depletion of glucose arrested the growth of these colonies, resulting in their small size. Many of these strains, referred to as nuclear *petite* or *pet* mutants, contained a mutation in the nDNA that resulted in their respiration-deficient phenotype (Tzagoloff and Dieckmann, 1990). Mutants comprising approximately 40 different genes were specifically identified to affect the assembly of a functional COX (Koerner et al., 1985). These mutants have characteristic biochemical properties including a lack of COX activity, a lack of a heme AA_3 peak at 603 nm through spectral analysis and a general decrease in Cox1p, 2p and 3p (McEwen et al., 1986; Tzagoloff and Dieckmann, 1990). Although numerous different assembly factors have been identified, the function of many is still to be determined. The assembly factors of known function in *Saccharomyces cerevisiae* will be discussed below (Figure 1-5, Table 1-2).

Translational regulation of the mitochondrial-encoded subunits is controlled by a host of different translational activators that are able to bind to the 5'-untranslated leader sequence on the mRNA transcript. These particular proteins mediate the interactions between the mRNA transcript and the mitochondrial ribosomes (Naithani et al., 2003). Cox1p synthesis is regulated by Mss51p and Pet309p, Cox2p by Pet111p and Cox3p by Pet54p, Pet122p and Pet494p (Herrmann and Funes, 2005; Khalimonchuk and Rödel, 2005). Immunoprecipitation studies have demonstrated interactions between these translational activators. The close proximity of these activators could organize the location and rate of Cox1p, 2p and 3p synthesis in the inner mitochondrial membrane, facilitating the assembly of the core complex (Naithani et al., 2003).

Before the synthesis of Cox1p, 2p and 3p is complete, the translational complex associates with Oxa1p. Oxa1p is present as a homooligomeric complex within the IMM

TABLE 1-2. **Examples of COX Assembly Factors**

Assembly Factor	Function	Localization	Human Homolog
Translational Activators			
Mss51	Cox1p translation, chaperone	Matrix	
Pet309	Cox1p translation	Matrix	LRPPRC (?)
Pet111	Cox2p translation	Matrix	
Pet54	Cox3p translation	Matrix	
Pet122	Cox3p translation	Matrix	
Pet494	Cox3p translation	Matrix	
Membrane Insertion			
Oxa1	Insertion of charged domains	IMM	OXA1
Mba1	Insertion of uncharged domains	IMM	
Cox18	Cox2p C-terminus insertion	IMM	
Mss2	Cox2p C-terminus insertion	IMM	
Pnt1	Cox2p C-terminus insertion	IMM	
Subunit Chaperones			
Cox20	Cox2p chaperone	IMM	
Cox14	Cox1p chaperone	IMM	
Copper Insertion			
Cox17	Copper chaperone	Cytosol/IMS	COX17
Cox11	Copper insertion into Cox1p	IMM	COX11
Sco1	Copper insertion into Cox2p	IMM	SCO1
Sco2	Copper insertion into Cox2p	IMM	SCO2
Heme Biosynthesis			
Cox10	Heme B to heme O conversion	IMM	COX10
Cox15	Heme O to heme A conversion	IMM	COX15
Assembly Chaperones			
Shy1	Subcomplex assembly	IMM	SURF1
Pet100	Nuclear-encoded subunit assembly	IMM	
Unknown			
Cox19	?	Cytosol/IMS	COX19
Cox23	?	Cytosol/IMS	COX23
Pet117	?	?	
Pet191	?	?	PET191
Cox16	?	IMM	COX16

and is responsible for inserting the mitochondrial-encoded subunits into the IMM. During subunit translation, the C-terminus of Oxa1p binds to the mitochondrial ribosome and inserts the subunit into the membrane cotranslationally (Herrmann and Funes, 2005; Khalimonchuk and Rödel, 2005). An additional insertion protein, Mba1p, is also responsible for proper insertion of the Cox1p, 2p and 3p subunits into the IMM. Together, these two proteins work to insert both charged and uncharged regions of the subunits into the membrane. Oxa1p is more specific to the transfer of highly charged domains whereas Mba1p is preferential to domains of few or no charge (Herrmann and Funes, 2005).

Two other proteins have also been recognized for their involvement in Cox1p insertion and assembly. Mss51p, previously mentioned for its role in Cox1p synthesis, binds to Cox1p either during or immediately after translation. Along with Cox14p, it is hypothesized that these proteins stabilize the subunit and prevent aggregation (Herrmann and Funes, 2005). Cox14p is further suggested to regulate Mss51p by binding it to Cox1p, preventing Mss51p from overexpressing Cox1p through its translational activation properties (Barrientos et al., 2004).

Cox2p insertion into the IMM is more challenging due to the small N-terminus and large hydrophilic C-terminus that are to reside in the IMS. Specific insertion factors, Cox18, Mss2p and Pnt1p, interact on the matrix side of the IMM and are required to translocate the large C-terminus (Saracco and Fox, 2002; Souza et al., 2000). After translocation, a presequence of 15 amino acids is cleaved off the N-terminus by Imp1/Imp2 and Som1 proteases in the IMS (Carr and Winge, 2003). Cleavage by these proteases is facilitated by the binding of Cox20p, a chaperone protein for newly synthesized Cox2p subunits. The association with Cox20p is maintained after proteolytic

cleavage and suggests a possible role for this chaperone in further Cox2p assembly (Hell et al., 2000).

Copper insertion into COX is a multi-step process that requires the presence of several different proteins. Known assembly factors associated with copper transport include Cox17p, Cox11p, Sco1p and Sco2p. The exact mechanism of copper import into the IMS remains unknown. Initially, the role of copper transport into the mitochondrion was thought to depend on Cox17p, a soluble protein found in both the cytoplasm and the IMS (Punter and Glerum, 2003). Cox17p is able to bind copper ions through a $C^{23}CXC^{26}$ motif (Cobine et al., 2006). Upon further investigation, it was found that COX function was not altered when Cox17p was tethered to the IMM, suggesting it was unlikely that Cox17p was able to chaperone copper into the mitochondria (Cobine et al., 2006; Horng et al., 2004). Instead, Cox17p is a specific copper donor for several proteins responsible for copper insertion into COX.

Sco1p and Sco2p are integral IMM proteins with a single transmembrane domain of ~17 amino acids (Lode et al., 2002). *In vitro* studies with purified proteins demonstrated that Sco1p was directly obtaining copper from Cox17p (Horng et al., 2004). Further investigations through immunoprecipitation (IP) revealed interactions between Sco1p, Sco2p and Cox2p, suggesting that the copper obtained from Cox17p was being incorporated into the bimetallic Cu_A site (Dickinson et al., 2000; Lode et al., 2000; Lode et al., 2002). Sco1p and Sco2p are able to bind copper with high affinity (Beers et al., 2002) through a CXXXC motif and a conserved histidine residue located at the C-terminus of the protein (Lode et al., 2002; Nittis et al., 2001; Rentzsch et al., 1999). Homomeric and heteromeric complexes of Sco1p and Sco2p interact with the C-terminal

region of Cox2p through electrostatic interactions to incorporate copper into Cox2p after translocation of the C-terminus (Cobine et al., 2006; Lode et al., 2002; Winge, 2003).

Copper insertion into the Cu_B site of Cox1p is likely mediated by Cox11p, an dimeric integral IMM protein (Banting and Glerum, 2006; Carr et al., 2002; Khalimonchuk et al., 2005). *In vitro* studies with purified proteins demonstrated that Cox11p was also obtaining copper from Cox17p (Horng et al., 2004). In contrast to the Sco proteins, copper obtained from Cox17p is incorporated into the Cu_B site of Cox1p. Three conserved cysteine residues, two located in a highly conserved CXC motif, provide a copper binding site for Cox11p (Carr et al., 2002). The incorporation of copper into the Cu_B site is postulated to occur during the synthesis of Cox1p. Sucrose gradient fractionations and IPs have suggested that Cox11p associates with mitochondrial ribosomes, specifically MrpL36p, a component of the large mitoribosome subunit. From this result, it is suggested that copper insertion by Cox11p occurs during Cox1p synthesis and Oxa1p-mediated translocation across the IMM (Khalimonchuk and Rödel, 2005).

Two other proteins, Cox19p and Cox23p, are located in both the cytosol and the IMS and have been implicated in copper homeostasis for COX. A CX_9C motif present in Cox17p is conserved in both these protein, suggesting a role similar to Cox17p (Barros et al., 2004; Cobine et al., 2006). Other research has suggested that these proteins are simply members of a protein family that require this particular motif for import into the IMS (Mesecke et al., 2005). Further investigations are required to determine the role of these proteins in COX assembly.

Heme A found in COX is originally derived from a more abundant heme B. The conversion of heme B to heme A involves an intermediate, heme O, as well as specific

heme assembly factors. Cox10p is a membrane-bound farneysltransferase responsible for the conversion of heme B to heme O. The conversion is the result of a stereospecific nucleophilic addition generating a hydroxyethyfarnesyl group (Carr and Winge, 2003). Further conversion to heme A is mediated by Cox15p, the ferredoxin Yah1p and the ferredoxin reductase Arh1p (Barros et al., 2001). These proteins work together to oxidize the C8 pyrrole methyl moiety into an aldehyde, generating heme A (Khalimonchuk and Rödel, 2005). Currently, the mechanism for heme A incorporation into COX remains unknown. It is hypothesized that the insertion of the heme moieties occurs during Cox1p translation and insertion into the IMM (Carr and Winge, 2003), although this remains to be proven.

Additional proteins involved in COX assembly have been identified, but to date, have not been well characterized. Shy1p (Surf Homolog of Yeast) is localized to the IMM and has been implicated in COX assembly although the exact role of this protein remains unclear (Mashkevich et al., 1997). 2D-PAGE analyses have identified an interaction between Shy1p and Cox2p (Nijtmans et al., 2001), whereas a pulse-chase labeling experiment suggested the requirement of Shy1p for Cox1p assembly with no visible effect on Cox2p (Barrientos et al., 2002b). This protein is of great significance as mutations in the human homolog (SURF1) have been associated with mitochondrial diseases such as Leigh Syndrome.

Pet100p is another protein for which a function has not been confirmed. Experiments have suggested that this protein acts as a molecular chaperone, ensuring the proper assembly of several nuclear-encoded subunits (VII, VIIa and VIII) into COX (Church et al., 2005). Further investigations are required to confirm this result.

Proteins of undetermined function also exist. Null mutants of these particular assembly factors indicate that these proteins are involved with the assembly of COX, yet their exact role within the assembly pathway remains unknown. These proteins include Pet117p, Pet191p and Cox16p. Previous studies of Cox16p revealed that it is a small protein located in the IMM with a C-terminus residing in the IMS. The N-terminus contains a putative mitochondrial targeting sequence followed by a single transmembrane domain. This particular protein does not appear to be involved in the maturation of Cox2p, heavy metal recruitment or heme A synthesis (Carlson et al., 2003). Further investigation is required to determine the role of Cox16p and other unidentified assembly factors in the assembly of COX.

Human COX Deficiencies

As described above, many additional proteins other than the structural components are necessary for the proper assembly and functioning of COX. Due to the importance of the COX within the respiratory chain, mutations in the subunits or assembly factors affecting their function can result in detrimental effects. In 1988, the first pathogenic mutation in mtDNA was reported by Holt *et al.* Since then, numerous other mutations resulting in respiratory complex defects have been identified in both mtDNA and nDNA. Generally, the term "mitochondrial disease" is used to encompass all pathogenic mutations in the respiratory complexes. As the requirement for oxidative metabolism varies between different organs and tissues, the clinical phenotypes vary as well, although encephalomyopathies are often observed due to the high energy demands of the brain and muscles (Hirano, 2001). Mutations in respiratory complexes can give rise to clinical features at any age and in any organ or tissue. At a cellular level, respiratory

complex defects cause an increase in reducing equivalents, a decrease in mitochondrial ATP formation, an increase in monovalent reduction of O_2 (superoxides) and an impairment of numerous metabolic pathways that depend on the respiratory chain (Munnich and Rustin, 2001). The clinical phenotypes of mitochondrial disease are not consistent between patients as a result of the complexity of mitochondrial segregation and varying energy requirements for each cell type (Barrientos et al., 2002a). Several clinical presentations are suggestive of mitochondrial disease, including combinations of neuromuscular and non-neuromuscular symptoms, the involvement of seemingly unrelated organs and/or tissues and an overall progressive worsening (Munnich and Rustin, 2001).

Mitochondrial disease resulting from defects in COX can be divided into three subtypes (Shoubridge, 2001). Primary COX deficiency resulting from mtDNA mutations include pathogenic mutations within *COXI, II* and *III*. Primary COX deficiency resulting from nDNA mutations include pathogenic mutations within the nuclear-encoded subunits. Secondary COX deficiency resulting from nDNA mutations encompass pathogenic mutations in any assembly factor that causes the misassembly or misfunctioning of COX itself. These three subtypes of COX mitochondrial disease will be discussed in further detail below (Table 1-3).

Primary COX deficiency resulting from mtDNA mutations are maternally inherited. To date, pathogenic mutations have been found in *COXI, COXII* and *COXIII*. Mutation types identified in these genes include nonsense, missense, deletion and frameshift. An example of a nonsense mutation was found in a patient with a multisystem mitochondrial disorder. A G→A transition at nucleotide position 6930 was detected,

TABLE 1-3. **Examples of mutations observed in mtDNA and nDNA in patients with mitochondrial disease due to COX deficiency**

Gene	Mutation	Type	Clinical Manifestations	Reference
mtDNA				
COX1	Δ6019-6023	Del, FS	Spastic tetraparesis, dysphagia and dysarthria with active pharyngeal reflex	Comi *et al.*, 1998
	G6930A	Nonsense	Progressive sensorineural hearing loss, myoclonic epilepsy, cerebellar ataxia, muscle atrophy, visual defect, cerebellar atrophy	Bruno *et al.*, 1999
	G5920A	Nonsense	Exercise intolerance, myoglobinuria	Karadimas *et al.*, 2000
COX2	T7671A	Missense	Muscle weakness, fatigue	Rahman *et al.*, 1999
	T7587C	FS	Progressive gait ataxia, severe congnitive impairment, bilateral optic atrophy, pigmentary retinopathy, mild muscle wasting	Clark *et al.*, 1999
COX3	T9957C	Missense	Hemiparesis, facial motor seizures, blindness, ptosis, hearing loss, limb weakness	Manfredi *et al.*, 1995
	Δ (15bp)	Del, FS	Myoglobinuria, muscle cramps	Keightley *et al.*, 1996
	G9952A	Nonsense	Exercise fatigue, hyperflexia, muscle weakness, myalgia	Hanna *et al.*, 1998
	$9537C_{ins}$	Ins, FS	Progressive spastic paraparesis, opthalmoparesis, moderate metal retardation, lactic acidosis, Leigh-like lesions of putamina	Tiranti *et al.*, 2000
nDNA				
SURF-1	C765T	Nonsense	Leigh Syndrome	Zhu *et al.*, 1998
	337+2T→C	Splice site	Leigh Syndrome	Zhu *et al.*, 1998
	$868T_{ins}$	Ins, FS	Leigh Syndrome	Tiranti *et al.*, 1998
SCO1	Δ363-364	Del, FS	Neonatal-onset hepatic failure and encephalopathy	Valnot *et al.*, 2000
	C520T	Missense		
SCO2	G1541A	Missense	Rapidly progressive hypertrophic cardiomyopathy in the neonatal period, respiratory distress, metabolic acidosis, hypotonia	Tay *et al.*, 2004
	C1280T	Nonsense		
COX10	C612A	Missense	Muscle weakness, hypotonia, ataxia, proximal tubulopathy, neurological deterioration	Valnot *et al.*, 2000
COX15	C700T	Missense	Early-onset fatal hypertrophic cardiomyopathy	Antonicka *et al.*, 2003
	C4473G	Splice site		
LRPPRC	C1119T	Missense	Leigh Syndrome French Canadian	Xu *et al.*, 2004

Note: Del = deletion, Ins = insertion, FS = frameshift

resulting in a premature stop codon and the translational loss of ~170 amino acids. The mutant CoxI was only two-thirds the length of the normal CoxI and does not encode the α-helices IX-XII (Bruno et al., 1999). Consequently, the mutant CoxI is likely unable to promote the proper assembly of COX. An example of a deletion in the *COXI* gene was found in a patient diagnosed with a motor neuron disease. This individual contained a 5 bp deletion that caused a frameshift and premature stop codon. The deletion abolished one of two CGAGC sequences and suggests the occurrence of slippage and mispairing during mtDNA replication. The mutant CoxI contains only a short amino terminus (Comi et al., 1998) and again suggests the inability for proper COX assembly, resulting in the observed clinical manifestations. A similar deletion is observed in the *COXIII* gene of a patient with recurrent myoglobinuria. The 15 bp deletion eliminates one of two AAAAAGA sequences, suggesting another incidence of slippage and improper pairing during mtDNA replication (Keightley et al., 1996). Missense mutations have been identified in the *COXII* and *COXIII* genes. A T→C transition has been detected in a patient previously diagnosed with mitochondrial encephalomyopathy, lactic acidosis and stroke-like episodes (MELAS). This transition results in the change of a highly conserved phenylalanine to leucine. It was suggested that this mutation may affect proton pumping (Manfredi et al., 1995), although this cannot be confirmed until the actual function of CoxIII has been confirmed. A T→C transition observed in *COXII* alters the initiating methionine to threonine. As a result, transcription of the protein either occurs at the next available methionine or does not occur at all. The next available methionine is located in a different reading frame and transcription that begins at this initiation site results in an

out-of-frame protein consisting of 5 amino acids (Clark et al., 1999). A mutation as such would cause the complete absence of CoxII and the inability of a functional COX to form.

The second type of primary COX deficiency results from nDNA mutations. To date, no pathological mutations have been identified in nDNA encoding for COX subunits (Borisov, 2002).

Secondary COX deficiency resulting from nDNA mutations presents with a wide array of clinical manifestations. To date, mutations have been identified in a variety of different assembly factors, including *SURF-1*, *SCO1, SCO2, COX10* and *COX15*. An additional mutation in the *LRPPRC* gene has been associated with COX misassembly to which the yeast *PET309* gene is suggested to be a distant homolog.

Human *SURF1* is located on chromosome 9q34 and consists of nine exons spread over ~4.7 kb (Péquignot et al., 2001). SURF1 contains two transmembrane domains and is localized to the inner mitochondrial membrane (Yao and Shoubridge, 1999). Studies in the yeast homolog, Shy1p, suggest that SURF1 has a role in COX assembly. Many different mutations in *SURF1* have been identified and associated with the mitochondrial disease, Leigh syndrome. Leigh syndrome associated with COX deficiency presents as a subacute necrotizing encephalomyelopathy occurring in infancy, inherited in an autosomal recessive fashion (Péquignot et al., 2001). To date, a wide range of pathogenic mutations have been identified in the *SURF1* gene, including nonsense and missense mutations, insertions and deletions causing frameshift mutations and alterations in splice sites (Tiranti et al., 1998; Zhu et al., 1998). A series of deletion constructs were transduced into patient cells and examined for their ability to rescue COX function. By generating this series of deletion mutants, the regions necessary for protein function could

be assessed. Results of the study demonstrated that both the transmembrane domains and the central loop are required for proper protein insertion into the IMM, whereas the terminal six amino acids are not essential for SURF1 function (Yao and Shoubridge, 1999). Upon analysis of the mutations detected in patient samples, it was observed that many of the mutations resulted in the truncation of the C-terminus of the protein due to the presence of a premature stop codon. Additionally, splice site mutations resulted in a deletion within a transmembrane domain or central loop. Thus, it is likely that the COX deficiency observed in many of these patients is caused by the inability of the SURF1 to properly insert and function within the IMM.

Human homologs for the yeast Sco proteins have been identified and localized to chromosome 17p13.1 and 22q13.33. The function of human SCO1 and SCO2 is dependant on copper binding through a three coordinate site containing two cysteine residues and one histidine residue. Together, these residues exist in a planar trigonal geometry (Horng et al., 2005). Similar to the yeast homologs, the Sco proteins are required for the correct insertion of copper into COX. Mutations in COX deficient patients have been identified in both *SCO1* and *SCO2*. Although their functions are similar, mutations in each protein result in noticeably different clinical phenotypes. Identified pathogenic *SCO1* mutations include a 2 nucleotide deletion resulting in a frameshift mutation and premature stop codon and C520T missense mutation that alters a highly conserved proline to a leucine. These mutations, presenting as hepatic failure and encephalopathy during the neonatal period, typically result in death by a ketoacidotic coma. It is postulated that the deletion produces a non-functional truncated protein, whereas the missense mutation changes the structure of the adjacent CXXXC copper-

binding motif (Valnot et al., 2000a). *SCO2* mutations have also been identified in patients afflicted with these clinical manifestations. A G1541A transition causes a missense mutation (Glu → Lys) at amino acid 140 of the 266 amino acid protein and a C1280T transition causes a nonsense mutation at amino acid 53. These mutations present with a fatal infantile encephalocardiomyopathy (Papadopoulou et al., 1999; Tay et al., 2004). Additional studies revealed that the E140 mutation occurs in close proximity to the CXXXC copper binding domain and the missense mutation to a lysine disturbs the copper binding site of SCO2 (Foltopoulou et al., 2004). For both *SCO1* and *SCO2* mutations, the protein would not be functional, causing a lack of copper insertion into CoxII at the Cu_A site. In turn, the lack of the Cu_A site would damage the electron transfer mechanism in COX resulting in the observed COX deficiency.

The human homolog for Cox10p is a protein located in the IMM. This protein contains seven to nine transmembrane domains with a II/III loop essential for the catalytic conversion of heme B to heme O. A C612A transition resulting in a missense mutation (N204K) has been identified and associated with COX deficiency presenting with tubulopathy and leukodystrophy. It is predicted that the alteration of the conserved uncharged asparagine residue to a basic lysine residue affects the catalytic activity of COX10, as the mutation is located in the second transmembrane segment of the II/III loop junction (Valnot et al., 2000b). The observed COX deficiency and associated clinical manifestations result from the lack of heme AA_3 incorporation into CoxI and damage of the electron transfer mechanism in COX.

Studies on human *COX15* have identified two different mutations associated with COX deficiency. These pathogenic mutations clinically present as an early-onset fatal

hypertrophic cardiomyopathy. A C700T transition causes a R217W missense mutation within a string of highly conserved residues. This mutation is located in the 21-amino acid loop between the third and fourth transmembrane domains. A second mutation (C447-3G) alters the splice site in intron 3 causing a complete deletion of exon 4. Mitochondria from these patients containing either of these mutations have demonstrated decreased levels of heme A by reverse phase HPLC (Antonicka et al., 2003), suggesting that both of these mutations are able to cause COX deficiency.

An additional mutation in *LRPPRC* (leucine-rich pentatricopeptide repeat cassette) has been implicated in COX deficiency, although a yeast homolog has not been confirmed. It is suggested that this protein is a distant homolog of Pet309p, a translational activator for *Cox1* (Xu et al., 2004). The LRPPRC protein is predicted to contain a cleavable leader sequence and localize to the mitochondria, in addition to being an mRNA-binding protein. A mutation in *LRPPRC* was first identified in association with the Leigh syndrome French Canadian variant (LSFC). A C1119T transition causes a missense mutation (A354V), resulting in significantly lower levels of LRPPRC expression in mitochondria. These low levels of LRPPRC are associated with reduced levels of COX mRNA transcripts within the mitochondria (Xu et al., 2004).

Concluding Remarks

COX is the final complex in the ETC and functions as the terminal electron acceptor, reducing molecular oxygen to water. The assembly of COX is a complex process involving the coordination between DNA from the mitochondria and the nucleus. The assembly process is assisted by a variety of nuclear-encoded assembly factors that are involved in transcription and translation of mitochondrially-encoded subunits,

membrane insertion, cofactor incorporation and subunit association(s). Investigations in the model system, *Saccharomyces cerevisiae*, have identified many of these assembly factors and determined their role in the assembly of COX. Presently, researchers have a general understanding of COX assembly although the exact details of processes such as cofactor insertion and subcomplex assembly remain unknown. Mutations have been identified in the human homologs of several assembly factors, including *SURF1, SCO1, SCO2, COX10, COX15* and possibly *PET309*. Patients with mutations in these particular assembly factors present with mitochondrial disease due to COX deficiency, although the specific clinical manifestations are dependent on the affected assembly factor. These initial studies have identified key mutations in these specific assembly factors, yet the underlying cause of disease in a large number of COX deficient patients is still to be determined. Through continued studies of particular assembly factors in *Saccharomyces cerevisiae*, further understanding of their molecular function in COX assembly will provide additional insight into the pathogenic mechanisms in the human homologs by which mitochondrial disease arises. Investigations presented in this thesis aim to characterize the assembly factor, Cox16p, and determine its role in the assembly of COX. The identification of a human homolog has made this protein a good candidate for further characterization due to its possible implication in human mitochondrial disease associated with COX deficiency.

Chapter 2: Materials and Methods

Strains and Media: Bacterial and Yeast

E. coli were grown either in Luria Bertani (LB) liquid media (0.5% yeast extract; 1% tryptone; 0.5% NaCl; 0.1% glucose) or on plates of LB solid media (0.5% yeast extract; 1% tryptone; 0.5% NaCl; 0.1% glucose; 2% agar), containing ampicillin (Amp) at a concentration of 50 μg/ml (Sigma).

The yeast strains utilized in the experimental procedures include the wild-type yeast strain, aW303 (*a ade2-1 his3-11,15 leu2-3,112 trp1-1 ura3-1*) and the *cox16* null mutant strain, aW303Δcox16 (*a ade2-1 his3-11,15 leu2-3,112 trp1-1 ura3-1 cox16::URA3*). Disruption of the *COX16* gene was the result of a 1.1 kb insertion of a *URA3* fragment at the internal *Hind*III site in *COX16* (Carlson *et al.*, 2003).

Dependent on the experimental procedure, yeast were grown in different media. A solid YPD medium (1% yeast extract; 2% peptone; 2% glucose; 2% agar) is rich in glucose and was used as growth media for yeast. A liquid YPD medium (1% yeast extract; 2% peptone; 2% glucose) was used for yeast transformations and yeast cultures prior to growth curves. Plates with minimal media (WO – 0.067% nitrogen base without amino acids; 2% glucose; 2% agar) supplemented with specific amino acids for prototrophic selection were used after yeast transformations. To determine respiratory competence, various yeast strains were grown on solid ethanol/glycerol (EG) media (1% yeast extract; 1% peptone; 2% ethanol; 2% glycerol; 2% agar), a non-fermentable carbon source. For mitochondrial isolations, yeast were grown in liquid galactose (GAL) media (1% yeast extract; 1% peptone; 2% galactose) to promote mitochondrial proliferation. All media generated were autoclaved prior to use.

DNA Clones and Constructs:

Construction of a C-terminal Cox16p-V5 Fusion

The V5 epitope tag is 14 amino acids (GKPIPNPLLGLDST) derived from the paramyxovirus of simian virus 5 (SV5). A reverse primer encoding the V5 sequence, followed by a *BamH*I restriction enzyme site (Cox16-V5 in Table 2-1A), was used to generate a V5 epitope tag on the C-terminus of Cox16p. The forward primer (Cox16-*Pst*I in Table 2-1A) incorporated a *Pst*I site 113 nucleotides upstream of the *COX16* start codon. A 548-bp polymerase chain reaction (PCR) product was digested with the appropriate restriction enzymes and ligated into the low copy (CEN) vector, YCplac111, containing a *LEU2* marker. The *COX16-V5* fusion construct was also ligated into the CEN vector, YCplac22, which contains a *TRP1* marker.

Construction of N-terminal V5-Cox16p Fusions

Cox16 primers, as well as V5 epitope-specific primers, were designed to incorporate the V5 epitope tag into the Cox16 sequence either before or after the putative transmembrane domain through a 2-step PCR (Figure 2-1). In the first step, the 5'- and 3'-ends of the construct are generated separately such that there are two different PCR products from two different reactions: the 5'-end of the *COX16* gene containing the V5 epitope at the 3'-end of the construct and a 3'-end of the *COX16* gene containing the V5 epitope at the 5'-end of the construct. The 5'-end was generated with the Cox16-*Pst*I in Table 2-1A) that incorporated a *Pst*I site 113 nucleotides upstream of the *COX16* start codon and a reverse primer that encoded the V5 epitope (N-term V5 reverse or V5-Cox16

reverse in Table 2-1A). The 3'-end was generated with a reverse primer (Cox16-*EcoR*I in Table 2-1A) that incorporated a *BamH*I site 23 nucleotides downstream of the *COX16* termination codon and a forward primer that encoded the V5 epitope (N-term Cox16 forward or V5-Cox16 forward in Table 2-1A). 1-10 ng of DNA from *COX16* in YCplacIII was used as a template. 5 pmol of each forward and reverse primer were used in a single reaction. In addition, 20 pmol of dNTP, 75 pmol $MgCl_2$, 1x PCR buffer (10x stock from Invitrogen) and 2.5 U of Taq polymerase were added to the reaction. The PCR was held at 95°C for 2 minutes before 35 cycles of 95°C for 45 seconds, 60°C for 45 seconds and 72°C for 1 minute. The reaction was finished with 3 minutes at 72°C before cooling to 4°C. The PCR efficiency was determined by visualizing the PCR products on an agarose gel. The band of interest was isolated from the agarose gel using the Gel Extraction Kit (Qiagen) according to the manufacturer's protocol, eluting the DNA with 30 μl of sterile water. The second PCR joined the 5'- and 3'-fragments and amplified the final product through Cox16-specific primers (Cox16-*Pst*I and Cox16-*EcoR*I in Table 2-1A). 5 μl of the isolated DNA from the 5'- and 3'-end was used in the second PCR. In addition, 5 pmol of Cox16-*Pst*I and Cox16-*EcoR*I primers were added to the reaction to amplify the final product. Again, 20 pmol of dNTP, 75 pmol $MgCl_2$, 1x PCR buffer (10x stock from Invitrogen) and 2.5 U of Taq polymerase were added to the reaction. The PCR was held at 95°C for 2 minutes before 35 cycles of 95°C for 45 seconds, 60°C for 45 seconds and 72°C for 1 minute. The reaction was finished with 3 minutes at 72°C before cooling to 4°C. The PCR efficiency was determined by visualizing the PCR product on an agarose gel. Two different PCR products of 653-bp were further used in a PCR with the forward primer (Cox16-*Pst*I) and reverse primer (Cox16-*BamH*I) to insert an

alternative restriction site after *COX16*. This PCR product was digested with the restriction enzymes, *Pst*I and *BamH*I, and ligated into the CEN vector, YCplac111, containing a *LEU2* marker. The constructs were verified by automated sequencing (ABI PRISM® 3100-*Avante* Genetic Analyzer, Applied Biosystems Inc.)

Construction of a C-terminal Cox16p-FLAG Fusion

The FLAG epitope is 11 amino acids (DYKDDDDK) derived from gene-10 of the bacteriophage T7. A reverse primer encoding the FLAG sequence followed by a *BamH*I restriction enzyme site (Cox16-FLAG in Table 2-1A) was used to generate a FLAG epitope tag on the C-terminus of Cox16p. The Cox16-*PstI* primer, as described above, was used as the forward primer. A 529-bp PCR product was digested with the appropriate restriction enzymes and ligated into the CEN vector, YCplac111, containing a *LEU2* marker. The *COX16-FLAG* fusion construct was also ligated into the CEN vector, YCplac22, which contains a *TRP1* marker.

Construction of a C-terminal Cox16p-Tandem Affinity Protein (TAP) Fusion in a CEN Vector

A Cox16p-TAP construct available from Open Biosystems was kindly given to us by Dr. Rick Rachubinski. The TAP epitope tag is 186 amino acids and was originally constructed by Dr. B. Séraphin (Rigaut *et al.*, 1999). After ensuring the presence of *COX16* through PCR, the *COX16-TAP* construct was PCR amplified with a *TAP*-specific reverse primer containing a *Kpn*I restriction enzyme site (TAP-*Kpn*I in Table 2-1A). The Cox16-*PstI* primer, as described above, was used as the forward primer. A 1054-bp PCR

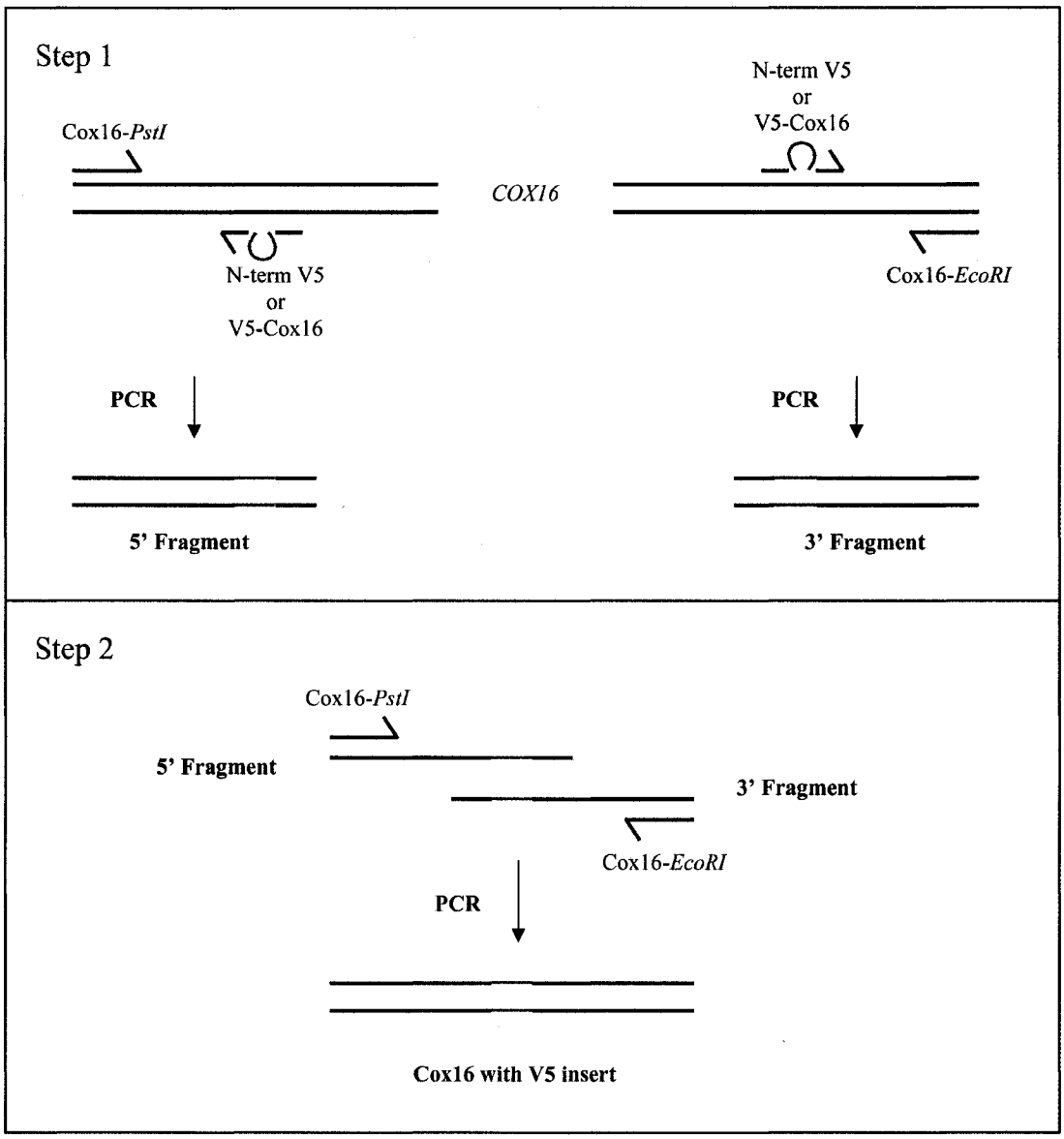

FIGURE 2-1. **Two-step PCR for the construction of N-terminal V5-Cox16p Fusions.** Addition of the V5 epitope to Cox16p either before or after the putative transmembrane domain involved two sequential PCR reactions, in which the product from the first reaction was used as a template in the second reaction. The first step involves the generation of separate 5'- and 3'-fragments. The second step joins the two products from the first step and amplifies the final construct with additional primers. The *COX16* gene is represented in black and the V5 epitope is represented in light blue. Forward primers used in the PCR reactions are indicated above the template whereas reverse primers are indicated below.

product was digested with the appropriate restriction enzymes and ligated into the CEN vector, YCplac111, containing a *LEU2* marker. The construct was verified by automated sequencing (ABI PRISM® 3100-*Avante* Genetic Analyzer, Applied Biosystems Inc.)

Construction of a Factor X_a Protease Site in Cox16p-TAP

A site for the protease, Factor X_a, was generated in the previously described construct, Cox16p-TAP. Through specific primers (Factor X_a forward and reverse in Table 2-1A), the protease site was inserted through site-directed mutagenesis and verified by automated sequencing (ABI PRISM® 3100-*Avante* Genetic Analyzer, Applied Biosystems Inc.)

TABLE 2-1A: PRIMERS GENERATED FOR VARIOUS COX16P CONSTRUCTS.

General Cox16 Primers		
Primer Name:	**Type:**	**Primer Sequence (5' to 3'):**
Cox16-*Pst*I	Forward	GTT ATT AGA CTG CAG ATA CAC TTC C
Cox16-*Sma*I	Reverse	CGT TTT GAA TGT TCC CGG GCA TTC
Cox16-*Eco*RI	Reverse	CAA TCA TTT CCT AGG AAT TCT CGT GGT C
Cox16-*BamH*I	Reverse	GCG GAC GGA TCC CAA AGA TGT TCA CG
Primers for Epitope Tags and Cleavage Sites:		
Primer Name:	**Type:**	**Primer Sequence (5' to 3'):**
Cox16-V5	Reverse	GCG GAC GGA TCC TTA CGT AGA ATC GAG ACC GAG GAG AGG GTT AGG GAT AGG CTT ACC CCA GAC ATT CTC AGA TTC ATC C
Cox16-FLAG	Reverse	GCG GAC GGA TCC TTA CTT ATC GTC GTC ATC CTT GTA ATC CCA GAC ATT C
TAP-*BamH*I	Reverse	GCG GAC GGA TCC TCA CTG ATG ATT CGC G
TAP-*Kpn*I	Reverse	GCG GAC GGT ACC TCA CTG ATG ATT CGC G
Factor Xa	Forward SDM	GAA TGT GGA TCG AAG GTC GAC GG
Factor Xa	Reverse SDM	CCG TCG ACC TTC GAT CCA GAC ATT C
N-term V5	Forward SDM	GCA TTG AGT AAG CAC GTT AAG CCT ATC CCT AAC CCT CTC CTC GGT CTC GAT TCT ACG CCC TTT CTT TTT TTT GG
N-term V5	Reverse SDM	CAA AAA AAA GAA AGG GCG TAG AAT CGA GAC CGA GGA GAG GGT TAG GGA TAG GCT TAA CGT GCT TAC TCA ATG C
V5-Cox16	Forward SDM	CGA TCA AGT ACG AGG GTA AGC CTA TCC CTA ACC CTC TCC TCG GTC TCG ATT CTA CGC AAG GCG ATC G
V5-Cox16	Reverse SDM	CGA TCG CCT TGC GTA GAA TCG AGA CCG AGG AGA GGG TTA GGG ATA GGC TTA CCC TCG TAC TTG ATC G

TABLE 2-1B: PRIMERS GENERATED FOR VARIOUS MUTAGENIC COX16P CONSTRUCTS.

Primers for Single Amino Acid Mutagenesis:		
Primer Name:	**Type:**	**Primer Sequence (5' to 3'):**
Cox16 R83E	Forward SDM	GGA AGA ATC AAG AGG AAT TTG ATA TTA AAG
Cox16 R83E	Reverse SDM	CTT TAA TAT CAA ATT CCT CTT GAT TCT T
Cox16 E90K	Forward SDM	GAT ATT AAA GAA AAA TAT TAT CGT TTA CAA GG
Cox16 E90K	Reverse SDM	CCT TGT AAA CGA TAA TAT TTT TCT TTA ATA TC
Cox16 Y91D	Forward SDM	GAT ATT AAA GAA GAA GAT TAT CGT TTA CAA CG
Cox16 Y91D	Reverse SDM	CCT TGT AAA CGA TAA TCT TCT TCT TTA ATA TC
Primers for a C-Terminus Truncation:		
Primer Name:	**Type:**	**Primer Sequence (5' to 3'):**
Δ115-118	Reverse	GCG GAC GGA TCC TTA AGA TTC ATC CTT TAA CCT AGC G
Δ110-118	Reverse	GCG GAC GGA TCC TTA CCT AGC GAC GCG CAC AGG CTC CC
Δ105-118	Reverse	GCG GAC GGA TCC TTA AGG CTC CCA ATC CTC TTC AGA AAG ACC
Δ100-118	Reverse	GCG GAC GGA TCC TTA TTC AGA AAG ACC TTG TAA ACG
Δ95-118	Reverse	GCG GAC GGA TCC TTA TAA ACG ATA ATA TTC TTC TTT AAT ATC AAA TTC C
Δ90-118	Reverse	GCG GAC GGA TCC TTA TTC TTT AAT ATC AAA TTC CC
Primers for Cox16 Deletions:		
Primer Name:	**Type:**	**Primer Sequence (5' to 3'):**
Δ28-32 deletion	Forward SDM	CGA TAC AAA AAA CCC TTT CTT TTT TTT GG
Δ28-32 deletion	Reverse SDM	CCA AAA AAA AGA AAG GGT TTT TTG TAT CG
Δ33-37 deletion	Forward SDM	GCA TTG AGT AAG CAC GGT TTA CCA TTT TGT GC
Δ33-37 deletion	Reverse SDM	GCA CAA AAT GGT AAA CCG TGC TTA CTC AAT GC

Δ90-94 deletion	Forward SDM	GGA ATT TGA TAT TAA AGA ACA AGG TCT TTC TGA AGA GG
Δ90-94 deletion	Reverse SDM	CCT CTT CAG AAA GAC CTT GTT CTT TAA TAT CAA ATT CC
Δ95-99 deletion	Forward SDM	GAA TAT TAT CGT TTA GAG GAT TGG GAG CC
Δ95-99 deletion	Reverse SDM	GGC TCC CAA TCC TCT AAA CGA TAA TAT TC
Δ80-89 deletion	Forward SDM	GGA TAT CTT GAA AAT AAG GGA ATA TTA TCG
Δ80-89 deletion	Reverse SDM	CGA TAA TAT TCC CTT ATT TTC AAG ATA TCC
Δ90-99 deletion	Forward SDM	GAA ATT TGA TAT TAA AGA AGA GGA TTG GGA GCC
Δ90-99 deletion	Reverse SDM	GGC TCC CAA TCC TCT TCT TTA ATA TCA AAT TCC

Molecular Biology Techniques:

Transformation of Competent *E. coli* Cells

200 μl of DH5α *E. coli* were thawed and incubated with 10 μl of plasmid on ice for 30 minutes. DH5α were heat shocked at 42°C for 30 seconds before the addition of 800 μl liquid LB and incubation at 37°C for 60 minutes. 100 μl of the sample was plated onto an AMP^R selective LB plate and grown at 37°C overnight.

Modified *E. coli* Plasmid Miniprep

Lysis buffer was made by combining 1ml of Miniprep buffer (50 mM glucose; 25 mM Tris-Cl, pH 8.0; 10 mM EDTA), 5 mg of lysozyme (Sigma) and 20 μg of ribonuclease A. The lysis buffer was divided into Eppendorf tubes in 100 μl aliquots and placed on ice. *E. coli* patches on an AMP selective LB plate were scraped off with an autoclaved toothpick and mixed into the lysis buffer. The cells were incubated on ice for 1 minute before the addition of 200 μl of 0.2 M NaOH, 1% SDS. The solutions were mixed by inversion. 150 μl of 7.5 M ammonium acetate was added and the solutions were centrifuged at 14,000 rpm for 8 minutes (Eppendorf Centrifuge 5417C). After centrifugation, the supernatant was collected and combined with 300 μl of isopropanol containing 0.2% TritonX-100. The solutions were centrifuged again at 14,000 rpm for 8 minutes. The supernatant was removed and the pellet was washed with 80% ethanol containing 0.2 mM EDTA followed by 80% ethanol. After the supernatants were removed, the pellets were dried in the Savant Speed Vac Plus SC110A for 10 minutes. The dried pellet was dissolved in 30 μl of sterile water.

DNA Extraction from Agarose

The band of interest was excised from the agarose gel and melted in 3 volumes of NaI (100 g NaI dissolved in 110 ml ddH_2O, to which 1.67 g Na_2SO_3 was added) at 55-65°C in a 1.5 ml Eppendorf tube. 10 μl of glassmilk (Sigma) was added to the sample and incubated at room temperature for 10 minutes with agitation at 2 minute intervals. The sample was centrifuged at 14,000 rpm for 30 seconds before washing the pellet 3 times with a NEET solution (100 mM NaCl; 1 mM EDTA; 50% ethanol; 10 mM Tris, pH 7.5). After the third wash, the supernatant was removed and the pellet was resuspended in 10 μl of sterile water and incubated at 55-65°C for 5 minutes. The glassmilk was pelleted by centrifugation at 14,000 rpm for 30 seconds and the supernatant was collected in a separate tube. The pellet was resuspended in another 10 μl of sterile water and incubated again before centrifugation at 14,000 rpm for 30 seconds. After pooling the supernatants, they were centrifuged at 14,000 rpm for 1 minute. The supernatant was collected and the DNA content was visualized on an agarose gel.

Triton Plasmid DNA Preparation

Solution was made by combining 1 ml of Sucrose buffer (5% sucrose; 50 mM Tris, pH 8.0), 1ml Tris buffer (25 mM Tris, pH 8.0; 125 mM EDTA), 5 mg of lysozyme and 1 mg of ribonuclease A in a 15 ml conical tube (Falcon). Using a sterile spatula, a lawn of *E. coli* cells grown on an AMP selective LB plate was scraped and mixed into the buffer. The cells were incubated on ice for 30 minutes. 1 ml of TritonX-100 lysis buffer (0.3% TritonX-100; 185 mM EDTA, pH 8.0; 150 mM Tris, pH 8.0) was added to the cells and mixed by inversion before transferring the solution to a polyallomer thick wall

centrifuge tube (Beckman). The solution was centrifuged at 40,000 rpm for 15 minutes at 4°C in a TLA-110 rotor (Beckman Optima™ TLX Ultracentrifuge) and the supernatant was transferred to another 15 ml conical tube. An equal volume of water-saturated phenol (Sigma) was added and the solution was mixed by inversion before centrifugation at 4000 rpm for 5 minutes at 4°C (Beckman J6-MI Centrifuge). After centrifugation, the upper aqueous phase was carefully collected and transferred into another 15 ml conical tube. The solution was washed 3 times with equal volumes of ether, mixing the solutions by vigorous shaking and removing the top layer for each wash. 0.05 volumes of 5 M NaCl was added and mixed before 3 volumes of 100% ethanol was added. The solutions were mixed by inversion, and then centrifuged at 4000 rpm for 10 minutes at 4°C. The supernatant was removed and the oily pellet was dissolved in 2 ml of 2M ammonium acetate. 3 volumes of 100% ethanol was added and the samples were centrifuged at 4000 rpm for 10 minutes at 4°C. The supernatant was carefully removed before the pellet was dissolved in 300 μl of 2 M ammonium acetate and transferred to a 1.5 ml Eppendorf tube. 2.5 volumes of 100% ethanol was added before centrifugation at 14,000 rpm for 5 minutes. The supernatant was removed and the pellet was washed with 80% ethanol containing 0.2 mM EDTA followed by a wash with 80% ethanol. After the supernatant was removed, the pellet was dried in the speedvac for 10-15 minutes. The dried pellet was dissolved in 100 μl of sterile water and the DNA content was quantified by an OD ratio of 260:280.

Lithium Acetate Yeast Transformation

10 ml of liquid YPD was inoculated with the desired yeast strain in a 50 ml conical tube (VWR). The inoculate was grown overnight at 30°C in a shaker at 225 rpm

(New Brunswick Scientific C24 Incubator Shaker). 2 ml of the overnight culture was used to inoculate 100 ml of liquid YPD in a sterile 250 ml flask. The cells were grown for 3-4 hours at 30°C in a shaker at 225 rpm. Two 50 ml conical tubes were filled with 50 ml of the inoculate and centrifuged at 4000 rpm for 5 minutes at 4°C (Sorvall RC 5B Plus). The supernatant was removed and the pellet was resuspended in 10 ml of TEL (10 mM Tris-Cl, pH 7.5; 1 mM EDTA; 0.1 M LiAc). The cells were centrifuged again at 4000 rpm for 5 minutes at 4°C. The supernatant was removed and the cells were resuspended in 450 μl of TEL. 100 μl of the cell suspension was aliquoted into 1.5 ml Eppendorf tubes. 2 μl of the transforming DNA and 50 μg of carrier salmon sperm DNA (previously heated for 10 minutes at 95°C) were added to the cell suspension before incubation at room temperature for 30 minutes. 700 μl of PEG/TEL (40% PEG; 10 mM Tris-Cl, pH 7.5; 1 mM EDTA; 0.1 M LiAc) was mixed into the suspension and the cells were incubated at room temperature for an additional 45 minutes. The cells were heat shocked at 42°C for 13 minutes before centrifugation at maximum speed for 10 seconds (Eppendorf Centrifuge 5417C). The supernatant was removed and the cells were resuspended in 200 μl of TE (10 mM Tris-Cl, pH 7.5; 1 mM EDTA). The cells were centrifuged at maximum speed for 10 seconds and the supernatant was removed. The cells were resuspended in 100 μl of TE and were plated on WO plates with appropriate nutrients. The plates were incubated for 3 nights at 30°C.

Polymerase Chain Reaction (PCR)

Epitope tags and C-terminal truncations were generated in *COX16* through PCR. 1-10 ng of DNA from *COX16* in YCplacIII was used as a template. Primers used for the

addition of an epitope tag are listed in Table 2-1A and primers used to generate C-terminal truncation mutants are listed in Table 2-1B. 2.5 pmol of each forward and reverse primer were used in a single reaction. In addition, 10 pmol of dNTP, 37.5 pmol $MgCl_2$, 1x PCR buffer (10x stock from Invitrogen) and 2.5 U of Taq polymerase were added to the reaction. The PCR was held at 95°C for 2 minutes before 35 cycles of 95°C for 45 seconds, 55°C for 1 minute and 72°C for 1 minute. The reaction was finished with 3 minutes at 72°C before cooling to 4°C (MJ Research Peltier Thermal Cycler PTC-200). The PCR efficiency was determined by visualizing the PCR product on an agarose gel.

Site-Directed Mutagenesis Polymerase Chain Reaction (SDM-PCR)

Single and double point mutations as well as deletion mutations were generated in *COX16* through SDM-PCR. The Factor X_a site was also inserted into *COX16-TAP* through SDM-PCR. The mutations and insertions through SDM-PCR were performed with the Quikchange Site-Directed Mutagenesis Kit (Stratagene) as per the manufacturer's protocol. Briefly, 1-10 ng of DNA from *COX16* or *COX16-TAP* in YCplac111 was used as a template. Primers used for single and double amino acid mutagenesis as well as deletion mutations are listed in Table 2-1B whereas primers used for generating the Factor X_a site are listed in Table 2-1A. 10 pmol of each forward and reverse primer were used in a single reaction. In addition, dNTP, 10x reaction buffer and PFU Turbo DNA Polymerase were also added to the reaction. The PCR was held at 95°C for 30 seconds before 16 cycles of 95°C for 30 seconds, 55°C for 1 minute and 68°C for 7 minutes. The reaction was then cooled to 4°C. *Dpn*I was added to the reaction and

incubated at 37°C for 60 minutes before cooling to 4°C. The PCR efficiency was determined by visualizing the PCR product on an agarose gel.

Biochemical Techniques:

Growth Curves in Liquid EG

10 ml of liquid YPD was inoculated with the desired yeast strain in a 50 ml conical tube and incubated overnight at 30°C, shaking at 225 rpm. After setting the absorbance to 600 nm, the spectrophotometer (Shimadzu UV-1601PC) was blanked with liquid EG. The YPD inoculate was added to 10 ml of liquid EG in a conical tube such that the absorbance read ~0.1000. The absorbance was recorded and the liquid EG inoculate was returned to 30°C, shaking at 225 rpm. The inoculates were read at intervals of 2-3 hours for a total of 9-10 hours, then read again at 24 hours. The results were plotted on Excel to obtain the relative rate of growth.

Preparation of Intact Yeast Mitochondria by Zymolase

10 ml of liquid GAL was inoculated with the desired yeast strain in a 50 ml conical tube and incubated overnight at 30°C, shaking at 225 rpm. 2 ml of the overnight culture was used to inoculate 100 ml of liquid GAL in a sterile 250 ml flask. This inoculate was incubated overnight at 30°C, shaking at 225 rpm. 33 ml of the overnight culture was used to inoculate 800 ml of liquid GAL in a sterile 2 L flask. This inoculate was incubated overnight at 30°C, shaking at 225 rpm (New Brunswick Scientific C25KC Incubator Shaker). The overnight culture was transferred to a plastic Beckman centrifuge

bottle and centrifuged at 2000 rpm for 7 minutes at 4°C (Beckman J6-MI Centrifuge). The supernatant was removed and the cells were resuspended in 150 ml of 1.2 M sorbitol, transferring the suspension to a plastic 250 ml Nalgene bottle. The cells were centrifuged at 6000 rpm for 10 minutes at 4°C in a SLA-1500 rotor (Sorvall RC 5B Plus). The supernatant was removed and the weight of the cells was determined. The cells were resuspended in 3 ml of digestion buffer per 1 g of cells (1.2 M sorbitol; 75 mM NaPi, pH 7.5; 1 mM EDTA; 1% β-mecaptoethanol; 0.45 mg/ml zymolase 20,000 – Seikagaku Corporation) and digested at 37°C until the cells were converted into spheroplasts. Digestion times were approximately 1.5-2.5 hours for respiration deficient strains and 2-3 hours for respiratory competent strains. After digestion, 1.2 M sorbitol was added to a total volume of 200 ml. The cells were centrifuged at 6000 rpm for 10 minutes at 4°C. Two additional washes with 1.2 M sorbitol were performed before resuspending the cells in STE buffer (0.5 M sorbitol; 20 mM Tris, pH 7.5; 0.5 mM EDTA) at the same volume as the digestion buffer. The spheroplasts were homogenized in a pre-cooled Waring blender for 20 seconds and 0.4 mg of PMSF was added. Cells were centrifuged at 2500 rpm for 10 minutes at 4°C. The supernatant was collected and centrifuged again at 2500 rpm for 10 minutes at 4°C. The supernatant was transferred to 40 ml Nalgene tubes and centrifuged at 14,000 rpm for 15 minutes at 4°C in a SA-600 rotor. A sample of the supernatant was collected for immunoblot analysis (post-mitochondrial supernatant fraction). The pellet was washed 3 additional times with STE buffer, centrifuging at 12,000 rpm for 15 minutes at 4°C. After removing the supernatant, the pellet was resuspended in 20 mM Tris, pH 7.5 with 0.6 mg of PMSF.

Folin Procedure for Protein Determination

In separate 1.5 x 15 cm test tubes, 5 μl of the mitochondrial fraction and 10 μl of the post-mitochondrial supernatant fraction was diluted in ddH_2O to a total volume of 600 μl. The fractions were tested in duplicate. 3 ml of copper reagent (0.01% $CuSO_4$; 0.02% NaK tartrate; 1.96% Na_2CO_3 in 0.1 M NaOH) was added to each dilution and mixed by vortexing. The samples were incubated at room temperature for 10 minutes. 0.3 ml of Folin reagent (1:1 dilution of stock - Sigma) was added and the solutions were mixed by vortexing before incubating at 95°C for 2 minutes. The solutions were then cooled on ice and re-equilibrated to room temperature before reading the absorbance on the spectrophotometer (Shimadzu UV-1601PC) at 750 nm.

Immunoblot Analysis of Protein Samples

Protein samples were prepared at desired concentrations in a loading buffer (4x stock: 0.19 M Tris-Cl, pH 6.8; 3.85% SDS; 38.5% glycerol; 3.85% β-mercaptoethanol; 0.02-0.05% bromophenol blue w/v). Proteins were separated on a 12% SDS-PAGE (sodium dodecyl sulphate polyacrylamide gel electrophoresis), running the gel at 150 V for 75 minutes in running buffer (25 mM Tris; 190 mM glycine; 0.8 mM SDS). The proteins were transferred to a nitrocellulose membrane using the Mini-Protean II system (Bio-Rad) in cold transfer buffer (200 mM glycine; 25 mM Tris-Cl; 20% methanol) at 100 V for 30 minutes. After the transfer, the nitrocellulose membrane was stained with Ponceau S (2% Ponceau S; 30% trichloroacetic acid; 30% sulfosalicylic acid) for 10 seconds and rinsed with water until the protein bands were clearly visible. The protein standards were marked before the remaining Ponceau S stain was rinsed off with water.

The membranes were incubated in a blocking solution (3% skim milk powder w/v in rinse buffer: 10 mM Tris-Cl, pH 8.0; 1 mM EDTA; 150 mM NaCl; 0.1% TritonX-100) for 60 minutes on a rocking platform at room temperature. The blot was then incubated in fresh blocking buffer containing a specific dilution of primary antibody (Table 2-2) and left on a rocking platform at 4°C overnight. The primary antibody was removed and the blot was rinsed for two intervals of 10 minutes with rinse buffer before the addition of a specific dilution of secondary antibody conjugated to horseradish peroxidase. The blot was incubated with the secondary antibody for 60 minutes on a rocking platform at room temperature. The blot was rinsed for three intervals of 10 minutes, followed by exposure for 1 minute to 1:1 volumes of enhanced chemiluminescence (ECL) detection reagents (Solution 1: 0.4 mM coumaric acid; 10 mM luminol; 100 mM Tris, pH 8.0, Solution 2: 0.02% H_2O_2; 100 mM Tris, pH 8.0) or exposed for 5 minutes to 1:1 volumes of Immobilon Western Chemiluminescent HRP Substrate (Millipore). The blot was wrapped in Saran wrap, immediately exposed to film (Super RX – Fujifilm) and developed with the M35A X-OMAT processor (Kodak). Densitometry was performed by scanning the developed film and analyzing the protein bands with the Quantity One® software (Bio-Rad).

TABLE 2-2: ANTIBODY CONCENTRATIONS FOR WESTERN BLOT ANALYSIS OF PROTEINS.

Antibody Concentrations for ECL Detection Reagents				
Primary Antibody	**Primary Dilution**	**Company**	**Secondary Antibody**	**Secondary Dilution**
Yeast CoxI	1:2000	Molecular Probes	Anti-mouse	1:5000
Yeast CoxII	1:2000	Molecular Probes	Anti-mouse	1:5000
Yeast CoxIII	1:2000	Molecular Probes	Anti-mouse	1:5000
Yeast CoxV	1:2000	Molecular Probes	Anti-rabbit	1:5000
FLAG (A)*	1:2000	Sigma	Anti-mouse	1:5000
FLAG (B)*	1:5000	Sigma	Anti-rabbit	1:1000
Myc	1:2500	Molecular Probes	Anti-mouse	1:4000
V5	1:2500	Invitrogen Life Technologies	Anti-mouse	1:4000
TAP	1:2000	Open Biosystems	Anti-rabbit	1:2000
CBP	1:2000	Upstate Cell Signaling	Anti-rabbit	1:2000
Porin	1:10,000	Molecular Probes	Anti-mouse	1:7500
Antibody Concentrations for Immobilon Western Chemiluminescent HRP Substrate (Millipore)				
Primary Antibody	**Primary Dilution**	**Company**	**Secondary Antibody**	**Secondary Dilution**
Yeast CoxI	1:5000	Molecular Probes	Anti-mouse	1:7500
Yeast CoxII	1:5000	Molecular Probes	Anti-mouse	1:7500
Yeast CoxIII	1:5000	Molecular Probes	Anti-mouse	1:7500

Anti-mouse secondary antibodies were purchased from BD Pharmingen.

Anti-rabbit secondary antibodies were purchased from either Transduction Laboratories or Cell Signaling Technology.

* FLAG (A) is a monoclonal antibody generated in mouse. FLAG (B) is a polyclonal antibody generated in rabbit.

Coomassie Staining for proteins separated by SDS-PAGE

After the dye front in the SDS-PAGE reached the bottom of the gel, the gel was incubated in Coomassie stain (0.25% Coomassie Brilliant Blue R250; 45% methanol; 10% glacial acetic acid) for 1-3 hours on a rocking platform at room temperature. The stain was then removed and the gel was incubated in destain (45% methanol; 10% glacial acetic acid) on a rocking platform at room temperature until the protein bands were clearly visible.

Silver Nitrate Staining for proteins separated by SDS-PAGE

After the dye front in the SDS-PAGE reached the bottom of the gel, the gel was incubated in 50% methanol/10% glacial acetic acid for two intervals of 15 minutes followed by incubation in 10% methanol/10% glacial acetic acid for two intervals of 15 minutes on a rocking platform. The gel was then incubated in 0.01% $KMnO_4$ (w/v) for 7 minutes. The gel was rinsed three times in filtered water for 5 minutes each before incubation in 0.2% $AgNO_3$ (w/v) for 15 minutes. The gel was briefly rinsed with filtered water, then exposed to a developer solution (2% Na_2CO_3; 1 μl/ml formaldehyde) until the protein bands were clearly visible. When the gel was sufficiently developed, the reaction was stopped by immersing the gel in 5% glacial acetic acid.

Molecular Weight Determination by Sucrose Gradients

2 ml of a 7-20% or 7-40% sucrose gradient (7, 20 or 40% sucrose w/v; 0.1% TritonX-100; 10 mM Tris, pH 7.5; 0.5 M NaCl) was made in a 11 x 34 mm polyallomer centrifuge tube (Beckman) and chilled to 4°C in the cold room for 60 minutes. A

deoxycholate protein extraction was performed (0.1% deoxycholate; 0.5 M NaCl) on 3 mg of isolated yeast mitochondria by centrifugation at 40,000 rpm for 20 minutes in a TLA-110 rotor. The supernatant was applied to the sucrose gradient. Internal protein standards of hemoglobin (Sigma), lactate dehydrogenase (Boehringer Mannheim) and, for the 7-40% sucrose gradient, catalase (Sigma) were also prepared. 50 μl of lactate dehydrogenase was centrifuged at 10,000 rpm for 10 minutes. The supernatant was removed and the pellet was dissolved in 50 μl of 30 mM NaPi, pH 7.5 and applied to the gradient. 2.5 mg of hemoglobin and 0.25 mg of catalase dissolved in water were also applied to the gradient. Using the TLS 55 rotor (Beckman), the gradient was centrifuged at 55,000 rpm for 14-15 hours at 4°C. The rotor was left to decelerate without braking before the sample was removed from the centrifuge. The gradient was divided into 11-12 fractions of 200 μl. Each fraction was carefully removed from the top of the gradient using a pipette. Hemoglobin levels were determined by diluting 50 μl of the sample in 950 μl of sterile water and reading the absorbance at 410 nm in the spectrophotometer. Lactate dehydrogenase levels were determined by an activity assay, diluting 10 μl of the sample in 50 μl of sterile water, then using 10 μl of the dilution to combine with 860 μl of 30mM NaPi, pH 7.5, 30 μl of 10 mM pyruvate and 100 μl of 2 mM NADH. In comparison to a control (860 μl of 30 mM NaPi, pH 7.5, 30 μl of 10 mM pyruvate), the activity was read at 340 nm for 10 seconds by a spectrophotometer. To determine catalase levels, 10 μl of the dilution used in the lactate dehydrogenase assay was combined with 1 ml of 0.06% H_2O_2 solution. Setting the wavelength at 240 nm, the time required for a 0.05 nm the decrease in absorbance was recorded. The level of the protein of interest in

each fraction was determined by immunoblot. The estimated weight of the protein complex was calculated by the following equation (Martin and Ames, 1961):

$$\frac{D_x}{D_s} = \left(\frac{mw_x}{mw_s}\right)^{2/3}$$

Where: D = distance to the meniscus

mw = molecular weight

x = unknown protein complex

s = protein standard

Spectral Analysis of Mitochondrial Cytochromes

13 mg of isolated yeast mitochondria were prepared in a thick wall polyallomer ultracentrifuge tube (Beckman) with 1% deoxycholate, 50 mM Tris pH 8.0 and 80 mg KCl in a total volume of 2 ml. To extract the cytochromes, the sample was centrifuged at 40,000 rpm for 20 minutes at 4°C in a TLA-110 rotor. The supernatant was transferred to 1.5 x 15 cm test tubes, cholate was added to a final concentration of 1% and the solutions were mixed by inversion. The solution was split into two cuvettes for the rear and front holders of the spectrophotometer (Shimadzu UV-1601 PC). Solution in the rear cuvette was oxidized with KFeCN whereas the solution in the front cuvette was reduced with $Na_2S_2O_4$. The oxidized minus reduced spectra of the extracted cytochromes was measured at intervals of 0.2 nm from 650 to 450 nm with the "Spectrum" function of UV Probe.

Activity Assay for Cytochrome Oxidase

10 μl of isolated yeast mitochondrial (with a concentration >10 mg/ml) were diluted with 10 μl of 20 mM Tris, pH 7.5. 10 μl of the diluted mitochondria were then extracted with 10 μl of 0.5% deoxycholate for 40 seconds at room temperature before the addition to a cuvette containing 920 μl of 10 mM KPi, pH 7.0 and 80 μl of 1% oxidized cytochrome c. The activity was compared to the background activity of 920 μl of 10 mM KPi, pH 7.0 and 80 μl of 1% reduced cytochrome c. Cytochrome oxidase activity was measured for 10 seconds at a wavelength of 550 nm with the "Kinetics" function of UV Probe.

Yeast Whole Cell Lysate

10 ml of liquid YPD was inoculated with the desired yeast strain in a 50 ml conical tube and grown overnight at 30°C, shaking at 225 rpm. The cells were centrifuged at 2500 rpm for 7 minutes at 4°C. The supernatant was removed and the cells were washed in 1.2 M sorbitol, centrifuging at 2500 rpm for 7 minutes at 4°C. The supernatant was removed and the cells were resuspended in 600 μl of digestion buffer (0.3 M sorbitol; 75 mM NaPi, pH 7.0; 1 mM EDTA; 1% β-mercaptoethanol; 0.045% zymolase w/v) before a 90 minute incubation at 37°C. After digestion, 600 μl of 1.2 M sorbitol was added before centrifugation at 6000 rpm for 10 minutes at 4°C. The supernatant was removed and the pellet was washed twice more with 1.2 M sorbitol. After the last wash, the pellet was resuspended in 1 ml of 20 mM Tris, pH 7.5 and

sonicated for 20 seconds with the output control set at 4 (Branson Sonifier 450). PMSF was added to a final concentration of 0.4 mg/ml.

Immunoprecipitation with Mitochondrial Proteins

Immunoprecipitation (IP) was performed with 200 μg of isolated yeast mitochondria diluted in 20 mM Tris, pH 7.5 to a final volume of 300 μl. 3 μl of primary antibody was added to the sample before rotating overnight at 4°C (Fisher Scientific Hematology/Chemistry Mixer 346). After rotation, 15 μl of a Protein G Plus/Protein A Agarose Suspension (Calbiochem) was added to the sample. The samples were rotated for 60 minutes at 4°C. The samples were centrifuged at 10,000 rpm for 1 minute to pellet the bead complexes and the supernatant was removed. The pellet was washed twice with 20 mM Tris, pH 7.5, centrifuging and removing the supernatant between washes. After the final wash, the supernatant was removed and the pellet was resuspended in a loading buffer (4x stock: 0.19 M Tris-Cl, pH 6.8; 3.85% SDS; 38.5% glycerol; 3.85% β-mercaptoethanol; 0.02-0.05% bromophenol blue w/v) to a final volume of 40 μl. The sample was heated at 95°C for 5 minutes, then kept on ice before loading onto a SDS-PAGE.

Tandem Affinity Protein (TAP) Column Purification

Two small Econo-Columns (Bio-Rad) were each loaded with 500 μl of IgG Sepharose beads (Amersham Biosciences). The beads were washed with 5 ml of TST (50 mM Tris, pH 7.6; 150 mM NaCl; 0.05% Tween 20), dislodging beads with the wash. The beads were washed twice with 2-3 ml of 0.5 M acetic acid, then TST to remove any

contaminants from the beads. The beads were then normalized with TST until the pH >7.0. The beads were then washed with 1 ml of IPP150 buffer (10 mM Tris, pH 8.0; 150 mM NaCl; 0.1% Igepal) before sealing the bottom of the columns. 40 mg of isolated mitochondria were prepared (150 mM NaCl; 0.1% Igepal) in a total volume of 4 ml and then sonicated for 2 x 6 seconds with the output control set at 4. Half of the sonicated sample was loaded onto each column and the columns were rotated overnight at 4°C. After rotation, the columns were drained by gravity flow. The beads were washed with 10 ml of IPP150 buffer followed by 3 ml of TEV cleavage buffer (10 mM Tris-Cl, pH 8.0; 150 mM NaCl; 0.1% Igepal; 0.5 mM EDTA; 1 mM fresh DTT), dislodging the beads to wash. The bottoms of the columns were sealed before the addition of 1 ml TEV cleavage buffer and 75 U of TEV protease (Invitrogen) to each column. The columns were rotated overnight at 4°C. After rotation, both columns were drained into a separate column containing 700 μl of Calmodulin beads (Stratagene) that were previously washed with 3 volumes of IPP 150 calmodulin binding buffer (10 mM Tris-Cl, pH 8.0; 150 mM NaCl; 1 mM magnesium acetate; 1 mM Imidazole; 2 mM calcium chloride; 10 mM β-mercaptoethanol; 0.1% Igepal). The dead volume from the IgG Sepharose columns was drained by gravity flow by the addition of 500 μl of TEV cleavage buffer. After the addition of 4 ml IPP 150 calmodulin binding buffer, calcium chloride was added to a final concentration of 3 mM. The beads were rotated for 2 hours at 4°C. By gravity flow, the flowthrough was drained and the beads were washed with 5 ml of IPP150 calmodulin binding buffer, dislodging the beads to wash. The bottom of the column was sealed before adding 1 ml of IPP 150 calmodulin elution buffer (10 mM Tris-Cl, pH 8.0; 150 mM NaCl; 1 mM magnesium acetate; 1 mM Imidazole; 20 mM EGTA; 10 mM β-

mercaptoethanol; 0.1% Igepal). The column was incubated on ice for 10 minutes, after which the elution was collected by gravity flow. The final elution step was repeated twice more for a total of 3 elution fractions.

Trichloroacetic acid (TCA) Precipitation of Protein

Samples were adjusted to 25% TCA from a 100% stock (w/v). The samples were placed on ice for 30 minutes, mixing the solutions at 10 minute intervals. The samples were centrifuged at 14,000rpm for 30 minutes at 4°C (Eppendorf Centrifuge 5417 C) and the supernatant was removed. The pellets were washed once with cold acetone (-20°C) with 0.05 M HCl, followed by centrifugation at 14,000 rpm for 5 minutes at 4°C. After the supernatants were removed, the pellets were then washed once with cold acetone (-20°C), followed by centrifugation at 14,000 rpm for 5 minutes at 4°C. The supernatants were carefully removed before drying the pellets in the speedvac for 10 minutes. The dried pellets were resuspended in a loading buffer (4x stock: 0.19 M Tris-Cl, pH 6.8; 3.85% SDS; 38.5% glycerol; 3.85% β-mercaptoethanol; 0.02-0.05% bromophenol blue w/v) to a final volume of 30 μl.

Metal Supplementation of EG Plates

10% (w/v) stock solutions were made for a various metals of interest, including copper ($CuSO_4 \cdot 5H_2O$), iron ($Fe(NH_4)SO_4$), manganese ($MnSO_4 \cdot H_2O$), zinc ($ZnSO_4 \cdot 7H_2O$), magnesium ($MgSO_4$), calcium ($CaCl_2$), potassium (KCl) and sodium (NaCl). The stock solutions were filter sterilized before further use. EG media was made in 2 L flasks and autoclaved. A working concentration of 10 ml was made for each metal of interest

such that when added to 50 ml of molten EG (for a total volume of 60 ml), the following concentrations were generated: 0.01, 0.02, 0.05, 0.1, 0.2, 0.4 and 0.8%. The molten EG and working concentrations of metal solutions were mixed in a sterile 250 ml flask before pouring 25-30 ml into 100 x 15 mm plates (Fisher). The plates were left to dry for two nights at room temperature.

Chapter 3: Results

Single Mutants Identify an Important Domain in Cox16p

Previous investigations of Cox16p had determined that its presence is required for cytochrome oxidase (COX) assembly. The function of Cox16p in the assembly of the COX complex remains unknown. To elucidate the function of Cox16p, the protein was examined to determine important protein domains and motifs required for proper functioning and interactions. Through SDM-PCR, a series of 18 different *cox16* point mutants had previously been generated and confirmed by sequencing by a former M.Sc. student, Chris Carlson. These mutants contained amino acid substitutions for several conserved residues within the putative transmembrane domain and C-terminus of the protein (Figure 3-1). Investigations for this thesis began with the characterization of these point mutants. The point mutants were transformed into a yeast *cox16* null strain (aW303Δcox16) and tested for growth on the non-fermentable carbon sources, ethanol/glycerol (EG). Of the 18 different point mutations generated, two strains demonstrated a slow-growing phenotype on solid EG media: R83E and Y91D. A 24-hour growth curve in liquid EG identified an additional slow-growing strain (E90K) that was not detectable by growth on solid EG media. The growth rates of the yeast strains were determined at OD600 with an absorbance of 0.1 representing 1×10^6 cells. In comparison to the wild-type growth rate of 6.49×10^5 cells/hr, the R83E, E90K and Y91D mutants had reduced growth rates of 5.52, 6.17 and 3.59×10^5 cells/hr respectively (Table 3-2). These strains were not completely respiratory deficient as their growth rates were notably higher than the growth rate of the Δcox16 strain (0.18×10^5 cells/hr). The remainder of the point mutants grew at rates similar to the wild-type yeast, Cox16st5, a Δcox16 strain transformed with a wild-type COX16 construct. None of the point mutations rendered the

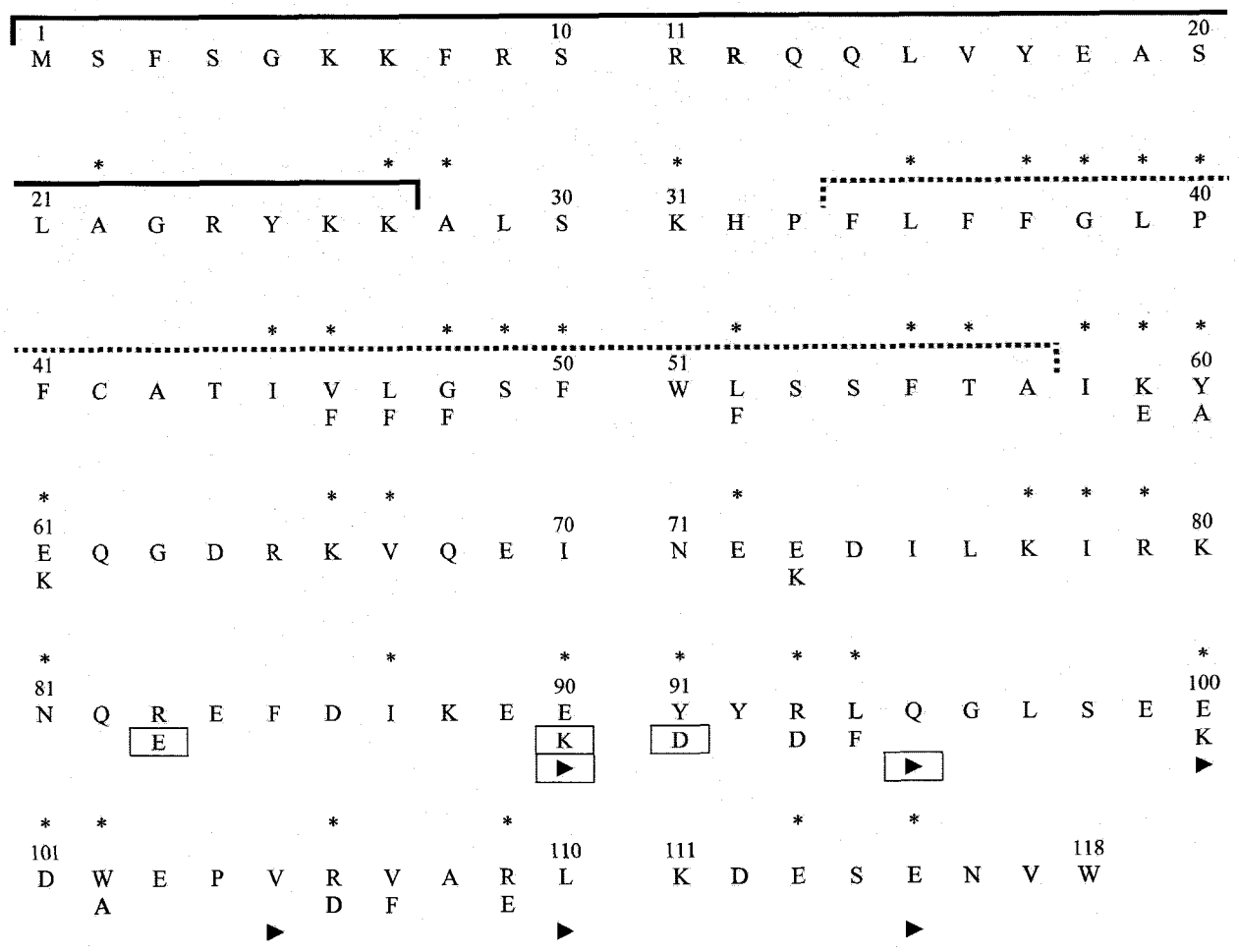

FIGURE 3-1. **Schematic of *cox16* mutants generated.** The sequence of Cox16p is given in the single-letter code. The amino acid substitutions that were studied are provided below the sequence. Substitutions that resulted in a respiration-deficient phenotype are indicated by *boxed amino acids*. The regions of truncation that were studied are indicated below the sequence by *black arrows* (▶). Truncations that resulted in a respiration-deficient phenotype are indicated by *boxed black arrows*. Identical and conserved residues between yeast and human Cox16 are designated with an *asterisk* above the sequence. The putative mitochondrial targeting sequence is labeled with the *solid bracket* and the putative transmembrane domain is labeled with the *dotted bracket* above the sequence.

	Cox16st5	aW303Δcox16	R83E	E90K	Y91D
Growth Rate (x 10^5 cells/hr)	6.49	0.18	5.52	6.17	3.59
COX Activity (μmol/min/mg)	3.16	1.44	2.58	3.07	2.52
CoxI (38kDa)	100	0	64	130	57
CoxII (33kDa)	100	0	110	126	103
CoxIII (27kDa)	100	0	81	97	82
Porin (30kDa)					

FIGURE 3-2. **Cox16p single point mutants identified as respiratory-deficient**. The growth rates of the single mutant strains were determined from an average of five growth curves in which respiration-deficient yeast were grown in liquid ethanol/glycerol and the cell density was measured at 600 nm. Cytochrome oxidase (COX) activity measurements are an average of three separate assays. 13 μg of isolated mitochondrial protein were used for Western blot analysis of cytochrome oxidase subunits I, II and III. Protein levels were densitometrically quantified by a Quantity-One® software, normalized to the porin control and measured as a % of wild-type.

yeast completely respiratory deficient. In addition, none of the point mutants demonstrated a temperature-sensitive respiration growth defect at 15°C, room temperature or 37°C.

Most COX-deficient strains have a detectable decrease in protein levels of the Cox subunits, some subunits with lower levels than others depending on the effect of the mutation. The severity of the mutation is often correlated with a more dramatic decrease in protein levels of the subunits. Analysis of the mitochondrially-encoded subunits, CoxI, II and III, in the respiration-deficient strains demonstrated a decrease in protein levels that paralleled the decrease in growth rate (Figure 3-2). CoxI levels of R83E and Y91D mutant strains were decreased in comparison to wild-type levels (64 and 57% respectively). Although slightly altered from wild-type, there was no noticeable change in protein levels of CoxII and III in the mutant strains examined. The E90K mutant strain did not demonstrate a decrease in protein levels for CoxI, II or III. Furthermore, analysis of nuclear-encoded CoxV did not reveal any difference in protein level among the different point mutants.

A decrease in cytochrome oxidase (COX) activity that paralleled the decrease in growth rate was also observed in the three point mutant strains (Figure 3-2). Again, R83E and Y91D were severely affected, with activity levels at 2.58 and 2.52 μmol/min/mg respectively. Activity levels of E90K (3.07 μmol/min/mg) resembled wild-type levels. COX-deficient strains have also demonstrated a lack of spectrally detectable cytochromes *a* and a_3. Again, the severity of the mutation is mirrored in the spectral signal, either by a shifted peak, a decrease in amplitude, or both. Spectral analysis of mitochondrial cytochromes was performed for the respiration-deficient strains to determine the presence

or absence of the heme aa_3 cytochromes. In comparison to the wild-type strain, the aa_3 cytochrome peak for both the R83E and E90K single mutant strains was shifted 1nm towards the blue. The Y91D single mutant strain was more affected, with the aa_3 peak shifting 3nm toward the blue (Figure 3-3).

These results suggest the importance of the region of amino acids 83-91 in Cox16p. Mutations in this region are altering the structure or function of the protein, and as a result, are affecting the assembly of cytochrome oxidase.

A Cox16p Double Point Mutation Results in Severe Respiratory Deficiency

To further analyze the region containing the single point mutations, two combinations of double point mutations were generated: R83E/E90K and R83E/Y91D. To determine if there was an additive effect, the double point mutations were transformed into a yeast *cox16* null strain (aW303Δcox16) and tested for growth on EG. Both strains demonstrated a respiratory-deficient phenotype. The growth rates of these mutant strains were confirmed by a 24-hour growth curve in liquid EG and compared to wild-type and Δcox16 growth rates, 7.60 and 0.12 x 10^5 cells/hr respectively. The growth rate for the R83E/E90K mutation was reduced to approximately 65% of the wild-type level whereas the R83E/Y91D had a growth rate that was minimally greater than the Δcox16 strain (Table 3-4).

Analysis of the mitochondrial subunits, CoxI, II and III, in the double mutant strains was performed by immunoblot (Figure 3-4). The R83E/E90K mutant did not have any observable reduction in the protein levels for CoxI, II and III in comparison to wild-type levels. In contrast, the R83E/Y91D double mutant strain had reduced levels of both

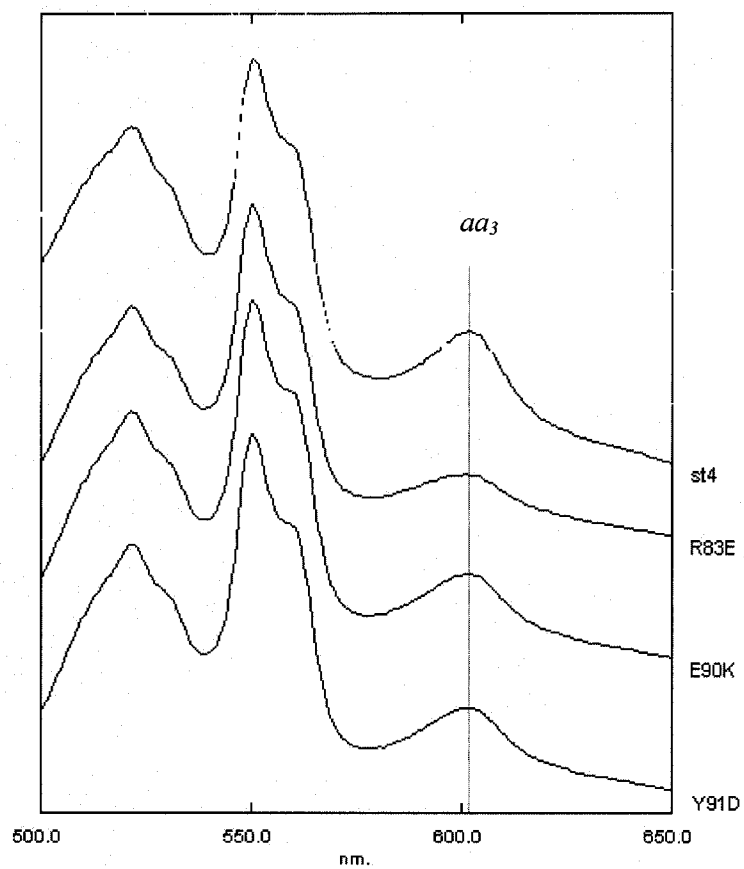

FIGURE 3-3. **Spectral analysis of mitochondrial cytochromes in respiratory-deficient Cox16p single point mutants**. Cytochromes were extracted from 13 mg of mitochondria from the wild-type and single point mutants. The position of cytochrome aa_3 is marked.

	Cox16st5	aW303Δcox16	R83E/E90K	R83E/Y91D
Growth Rate (x 10^5 cells/hr)	7.60	0.12	4.87	0.16
COX Activity (μmol/min/mg)	3.16	1.44	2.37	1.54
CoxI (38kDa)	100	0	107	65
CoxII (33kDa)	100	0	99	42
CoxIII (27kDa)	100	0	110	97
Porin (30kDa)				

FIGURE 3-4. **Cox16p double point mutants are respiratory-deficient.** The growth rate is an average of two separate growth curves performed in liquid EG. The growth rate, COX activity and protein levels for CoxI, II and III of the double mutant strains were determined as described in the legend of Figure 3-2.

CoxI and II (65 and 42% respectively) while CoxIII levels remained similar to wild-type levels.

COX activity for the double mutant strains demonstrated a reduction in activity proportional to the growth rate on EG (Figure 3-4). The COX activity for the R83E/E90K double mutant strain was 2.37 μmol/min/mg whereas the COX activity for the R83E/Y91D double mutant strain was 1.54 μmol/min/mg.

Spectral analysis of mitochondrial cytochromes was performed for the strains containing the double point mutations (Figure 3-5). In comparison to the wild-type strain, the aa_3 cytochrome peak for the R83E/E90K double mutant strain was shifted 0.8nm towards the blue. The R83E/Y91D double mutant strain was more affected, shifting 1.4nm toward the blue.

The additive effect of the mutations observed by these analyses further support the importance of this region in Cox16p.

Cox16p Truncation Mutants Identify an Important Region in the C-terminus

Further characterization of the Cox16 single and double mutants was to be performed through the addition of an epitope tag, such as FLAG or V5, to the C-terminus of Cox16p. The addition of an epitope tag to the C-terminus did not alter the growth rate of wild-type or single mutant strains on EG. In contrast, the addition of an epitope tag to the double mutant strains dramatically altered the growth rate on EG, giving previously severely respiration-deficient strains the ability to grow at wild-type levels in the presence of the tag. This effect was observed with both the FLAG and V5 epitope tags. As a result, further characterization of mutant strains with C-terminal epitope tags was

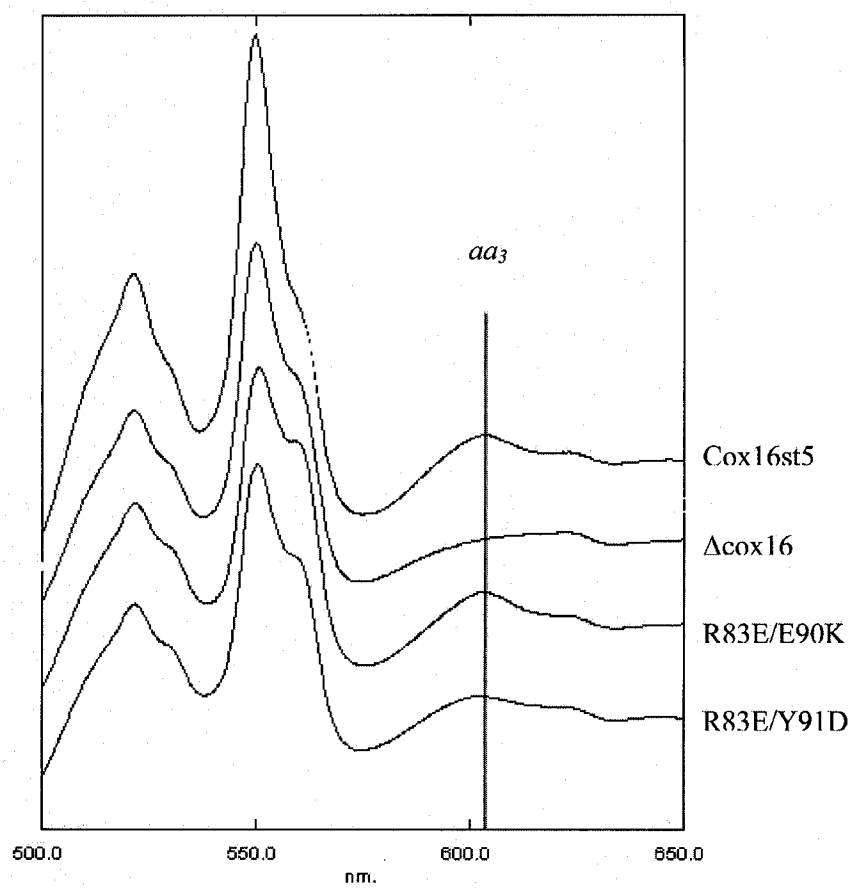

FIGURE 3-5. **Spectral analysis of mitochondrial cytochromes in respiratory-deficient Cox16p double point mutants**. Cytochromes were extracted from 13 mg of mitochondria from the wild-type and double point mutants. The position of cytochrome aa_3 is marked.

considered unreliable and thus not performed.

The altered growth rate of the double point mutants upon the addition of a C-terminal epitope tag suggested the importance of the C-terminus to the functioning of Cox16p. To further investigate this effect, successive 5-amino acid truncations were made at the C-terminus of Cox16p. Six different truncation mutants were generated (Figure 3-1). The truncation mutations were transformed into aW303Δcox16 and tested for growth on EG.

The growth rates were confirmed with a 24-hour growth curve in liquid EG (Table 3-1). Truncations up to (and including) 19 amino acids (Δ100-118) grew at rates comparable to wild-type in liquid EG. Truncations expanding to 24 and 29 amino acids (Δ95-118 and Δ90-118 respectively) resulted in a growth rate similar to the Δcox16 strain indicating a respiratory-deficient phenotype. Due to the apparent ability of these truncations to either grow or not grow in EG media, this region was further investigated by deletion mutants. No further characterization of the truncation mutants was performed. The growth rate of these truncation mutants not only confirms the importance of this particular region, it also demonstrates that a large portion of the Cox16p C-terminus is not required for proper functioning of this protein.

TABLE 3-1. **Growth rates of Cox16p truncation mutants in liquid EG.** The growth rate of the mutant strains was determined from a 24-hour growth curve in which Cox16p truncation mutants were grown in liquid ethanol/glycerol and the cell density was measured at 600 nm. The growth of the mutant strains is presented as a percent of the wild-type strain growth rate.

	Growth Rate ($x\ 10^5$ cells/hr)
Cox16st5	6.47
Δcox16	0.20
Δ90-118	0.18
Δ95-118	0.18
Δ100-118	6.44
Δ105-118	6.49
Δ110-118	6.49
Δ115-118	6.52

Deletion Mutations Further Characterize Important Regions of Cox16p

The necessity of specific regions of Cox16p was investigated through the creation of 5 and 10 amino acid deletion mutants. Specific primers were used to generate two 5 amino acid deletions (Δ90-94 and Δ95-99) and two 10 amino acid deletion (Δ80-89 and Δ90-99) at the C-terminus of the protein. The deletion mutants were transformed into aW303Δcox16 and tested for growth on EG. The 5 amino acid deletion strains were partially respiratory deficient whereas both of the 10 amino acid deletion strains were completely respiratory deficient on EG. The growth rates of the 5 amino acid deletion strains were confirmed with a 24-hour growth curve in liquid EG (Figure 3-6). Further characterization of the deletion strains focused on the 5 amino acid deletions, as it was apparent that 10 amino acid deletions rendered the protein completely non-functional. Analysis of the mitochondrial subunits, CoxI, II and III, in the 5 amino acid deletion strains was performed by immunoblot (Figure 3-6). The Δ90-94 deletion strain had noticeably reduced levels of CoxI (60% of wild-type) while CoxII and III levels remained similar to wild-type levels. The levels of the CoxI, II and III subunits in the Δ95-99 deletion strain were similar to the wild-type levels.

The deletion strains demonstrated a reduction in COX activity in comparison to wild-type activity (3.16 μmol/min/mg). Unlike the single and double mutant strains, the reduction in COX activity was not proportional to the growth rate of the strain on EG. The Δ90-94 deletion strain had a higher COX activity than the Δ95-99 deletion strain (2.48 vs. 2.14 μmol/min/mg).

	Cox16st5	aW303Δcox16	Δ28-32	Δ33-37	Δ90-94	Δ95-99
Growth Rate (x 10^5 cells/hr)	5.77	0.20	6.26	0.22	1.53	4.70
COX Activity (μmol/min/mg)	3.16	1.44	3.76	1.85	2.48	2.14
CoxI (38kDa)	100	0	1361	-14	60	117
CoxII (33kDa)	100	0	118	26	102	93
CoxIII (27kDa)	100	0	132	3	103	111
Porin (30kDa)						

FIGURE 3-6. **Cox16p deletion mutant strains demonstrate a range of respiratory competence.** The growth rate is determined from two separate growth curves performed in liquid EG. The growth rate, COX activity and protein levels for CoxI, II and III of the deletion mutant strains was determined as described in the legend of Figure 3-2.

Note: The immunoblot for CoxI protein levels is not what is expected as protein levels for wild-type should be a strong band similar to what is observed in CoxII and CoxIII immunoblots.

The spectral analysis of mitochondrial cytochromes showed a similar trend (Figure 3-7). The Δ90-94 deletion strain had an aa_3 peak similar to the wild-type (0.2nm shift towards the red) whereas the Δ95-99 deletion strain had an aa_3 peak shifted 1.6nm towards the blue.

Further characterization by deletion analysis of Cox16p was performed at the N-terminus of the protein out of interest of an alternative site for an epitope tag that would not interfere with the growth rate of the mutants. Two different 5 amino acid deletions were generated. The first deletion (Δ28-32) was located immediately before the putative transmembrane domain whereas the second deletion (Δ33-37) included the first 4 amino acids of the putative transmembrane domain. The N-terminal truncation mutants were transformed into aW303Δcox16 and tested for growth on EG, later confirming their growth rate by a 24-hour growth curve in liquid EG. The Δ28-32 deletion strain grew at rates similar to wild-type on EG whereas the Δ33-37 deletion strain was completely respiratory deficient.

Analysis of the mitochondrial subunits, CoxI, II and III, in the N-terminal deletion strains was performed by immunoblot (Figure 3-6). Surprisingly, the Δ28-32 deletion strain had drastically higher levels of CoxI (1361%), whereas CoxII and III levels resembled wild-type levels. The Δ33-37 deletion strain had dramatically lower levels of all three subunits in comparison to wild-type levels, (-14% CoxI, 26% CoxII and 3% CoxIII).

COX activity in the Δ28-32 deletion strain was slightly elevated in comparison to the wild-type (3.76 vs. 3.16 μmol/min/mg) whereas the COX activity in the Δ33-37 deletion strain was considerably reduced (1.85 μmol/min/mg).

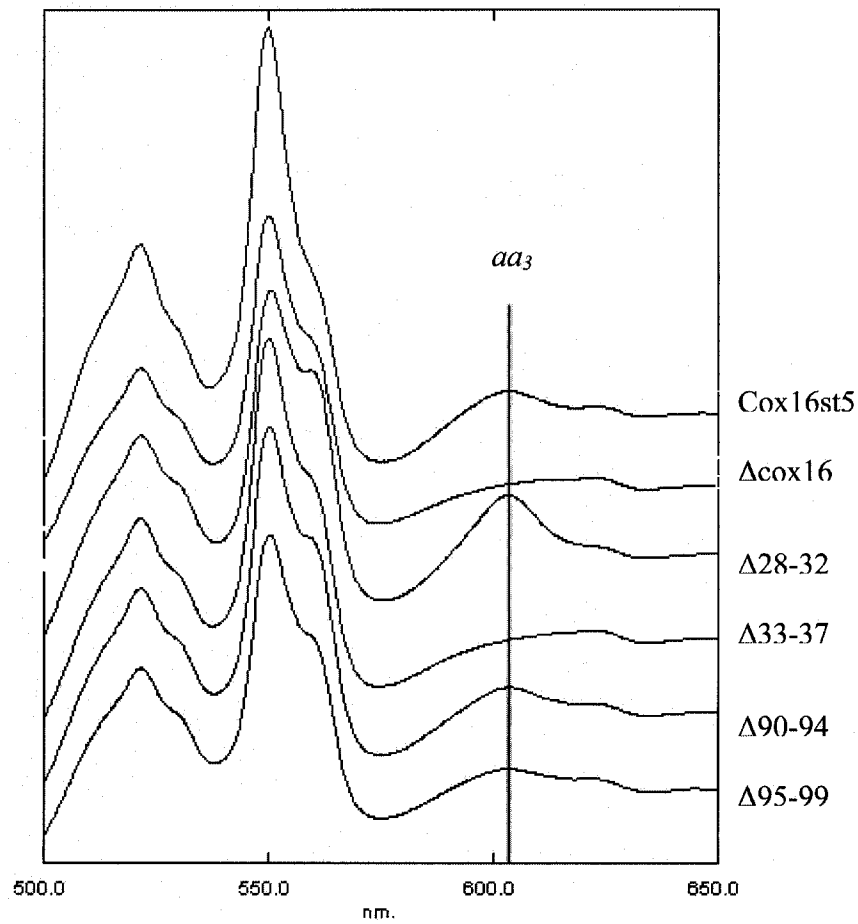

FIGURE 3-7. **Spectral analysis of mitochondrial cytochromes in Cox16p deletion mutant strains**. Cytochromes were extracted from 13 mg of mitochondria from the wild-type and deletion mutant strains. The position of cytochrome aa_3 is marked.

Spectral analysis of the mitochondrial cytochromes in the Δ28-32 deletion strain revealed an increased aa_3 peak, approximately 2.3 times larger than wild-type levels. The Δ33-37 deletion strain demonstrated a complete loss of the aa_3 peak, resulting in a spectrum similar to the aW303Δcox16 strain.

N-terminal Epitope Tags in Cox16p Result in a Respiration-Deficient Phenotype

Creation of an epitope-tagged Cox16p that does not interfere with the growth rate would allow many of the previously generated mutations to be further analyzed. Mitochondrial localization of various mutants could be examined through immunoblot and changes in protein associations could be assessed through immunoprecipitations. Previously, FLAG and V5 epitope tags were generated at the C-terminus of Cox16p. Although the tags did not alter the growth rate of wild-type and single point mutants, the tags dramatically altered the growth rate of double mutants, restoring respiratory competence in respiratory-deficient mutants. As a result, epitope tagging at the C-terminus would be unreliable for other mutant constructs, such as truncations and deletions.

Given that the Δ28-32 deletion mutant did not result in an altered growth rate, it appeared that the addition of an epitope tag within this region would not affect the localization or function of the protein. V5 epitope tags were constructed at two alternative locations in hopes that the tag would not interfere with the growth rate of wild-type or mutant strains. The first location was immediately before the putative transmembrane domain, in between the amino acids H32 and P33. This construct was designated N-terminal V5-Cox16. The second location was after 4 highly conserved residues (IKYE)

that immediately followed the putative transmembrane domain. This second construct was designated Middle V5-Cox16.

The constructs were generated by a two-step PCR and transformed into aW303Δcox16. Their growth was tested on EG and subsequently confirmed by a 24-hour growth curve in liquid EG (Figure 3-8). The V5 epitope resulted in severe respiratory deficiency in both the N-terminal and Middle V5-Cox16p strains. The N-terminal V5-Cox16p strain grew at about a fifth of the wild-type rate and the middle V5-Cox16p strain was completely respiratory deficient, growing at a rate identical to aW303Δcox16. As the location of either tag alters the growth rate of the strain, these constructs also could not be used for further analyses. Alternative methods of protein detection, such as the generation of a Cox16-specific antibody, will have to be explored.

Cox16p Self-Associates in a High Molecular Weight Complex

Cox16p has previously been tagged with a myc epitope and been detected by immunoblot. Sucrose gradients have demonstrated that Cox16p associates with additional proteins, forming a high molecular weight complex of ~84kDa, (Carlson *et al.*, 2003). Current experiments focus on the composition of this high molecular weight complex. Initial experiments were aimed at identifying if Cox16p was able to associate with itself within the complex. Self-association of Cox16p was determined by generating two different constructs of Cox16p with a C-terminal epitope tag, *COX16-myc* and *COX16-FLAG*. Each tagged construct was transformed into aW303Δcox16 and tested for growth on EG. Both strains grew at similar rates as the wild-type, indicating that the epitope tag did not appear to interfere with the protein function. The *COX16-FLAG* construct was

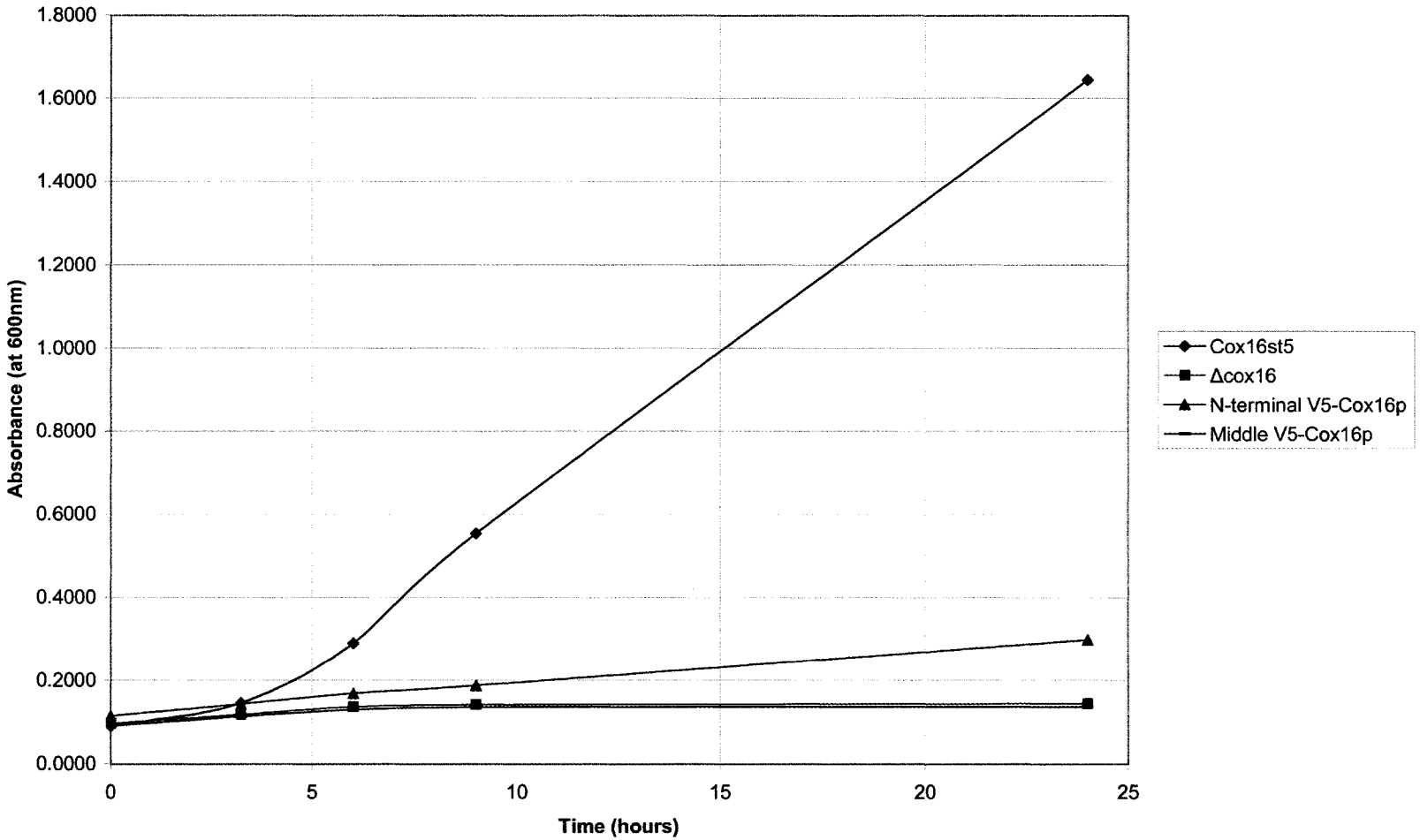

FIGURE 3-8. **N-terminal and Middle V5-Cox16p strains are respiratory deficient in liquid EG**. The growth rate of the V5-tagged Cox16p strains was determined from a 24-hour growth curve in liquid ethanol/glycerol, measuring the cell density at 600 nm.

transformed into the Cox16-myc strain to generate a strain that expressed Cox16p with two different epitope tags. Isolated mitochondria from this strain were used for immunoprecipitation (IP), performing the IP against one epitope tag and subsequent immunoblotting against the other. Reciprocal IPs were also performed. IP studies with the myc- and FLAG-tagged Cox16 strain suggested self-association of Cox16p, but the light chain of the antibody remaining from the IP interfered with the interpretation of the immunoblot. This problem was caused by the antibodies used in the IP, as both were derived from mouse. Antibodies in the IP samples resulted in interfering bands in the immunoblot when probed with the secondary anti-mouse antibody. Detection of the FLAG epitope with an antibody derived in rabbit was unsuccessful due to the low specificity of the antibody. To eliminate this problem, the *COX16-FLAG* construct was replaced with a *COX16-V5* construct. The antibody against the V5 epitope is derived from rabbit and as a result, would not interfere with the secondary antibody in the immunoblot analysis. In addition, the antibody has been previously used and determined to have a high specificity for the V5 epitope. The Cox16-V5 strain was determined to grow at wild-type levels on EG, indicating that the epitope tag was not interfering with the protein function. The *COX16-V5* construct was transformed into the Cox16-myc strain and the IP experiment was repeated. IP and reciprocal IP studies with the myc- and V5-tagged Cox16 strain demonstrated self-association of Cox16p (Figure 3-9). A band of 21kDa was detected in the IP and reciprocal IP sample through immunoblot, corresponding to a band of the same size in the lysed mitochondria control lanes.

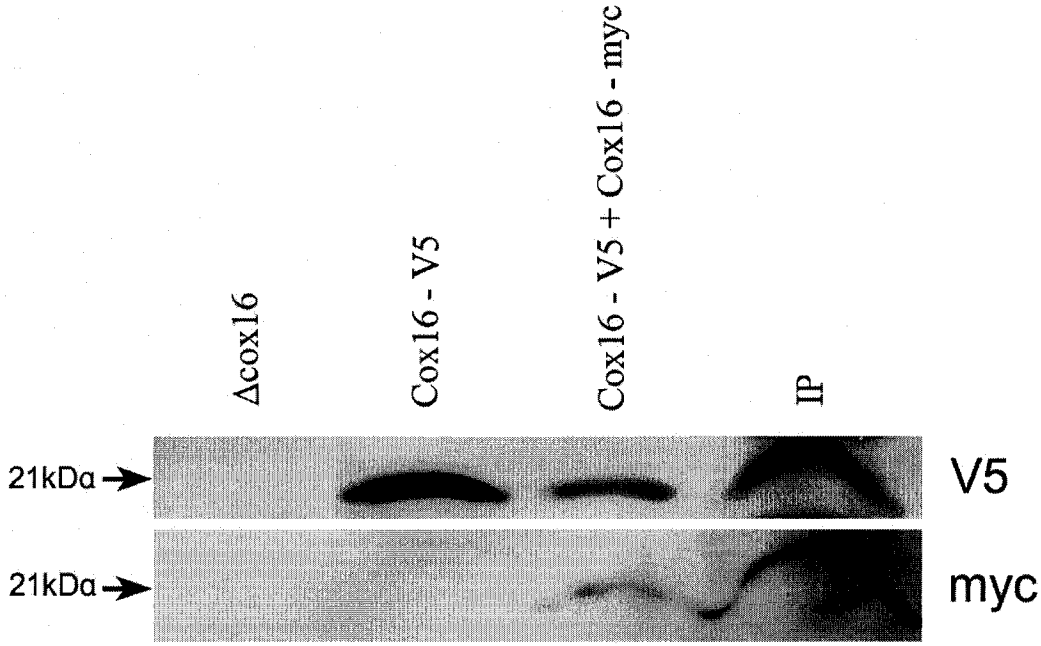

FIGURE 3-9. **Immunoprecipitation of tagged Cox16 demonstrates Cox16 self-association.** A Δcox16 yeast strain was transformed with both Cox16-V5 and Cox16-myc. The mitochondria from the transformant (Cox16-V5 + Cox16-myc) were isolated, lysed and immediately used for immunoprecipitation (IP). IP was performed with an α- myc antibody in the top blot and an α-V5 antibody in the bottom blot. The IP was then analyzed through Western Blot and compared to control mitochondria samples (first 3 lanes). The antibodies used in Western Blotting are indicated to the right of the blot. The band present in both the IP lanes suggests self-association of Cox16.

Cox16-TAP can be Isolated by Column Purification

Previous attempts to identify proteins that are associating with Cox16p in the high molecular weight complex through sucrose gradients and subsequent IPs were unsuccessful. The amount of protein in the sucrose gradient sample was not high enough to perform IP. An alternative method to investigate protein associations involves a TAP epitope tag. This particular tag has previously been used for protein purification through two different columns under conditions that minimize the disruption between protein-protein associations.

A yeast strain containing a TAP epitope tag on the C-terminus of Cox16 was kindly provided by Dr. Rick Rachubinski. This strain was originally purchased from Open Biosystems. Upon receiving the strain, a PCR was performed to ensure the presence of *COX16*, using primers specific to the 5'- and 3'-sequence of *COX16* (Figure 3-10a). After confirming the presence of *COX16*, an additional PCR was performed to ensure the presence of a *COX16-TAP* fusion, using primers specific to the 5'-end of *COX16* and the 3'-end of the *TAP* sequence (Figure 3-10b).

The *COX16-TAP* construct was transformed into aW303Δcox16 and tested for growth on EG. When compared to wild-type strains, the Cox16-TAP strain grew at similar rates. An immunoblot of whole-cell lysates from the Cox16-TAP strain confirmed that the fusion protein was present in the yeast strain and could be detected, resulting in a band of ~40kDa (Figure 3-11a). Previous investigations have demonstrated that Cox16 is located in the inner mitochondrial membrane. To determine that the Cox16-TAP protein was properly localizing within the mitochondria, two different fractions from a mitochondrial isolation were analyzed by immunoblot (Figure 3-11b). The post-

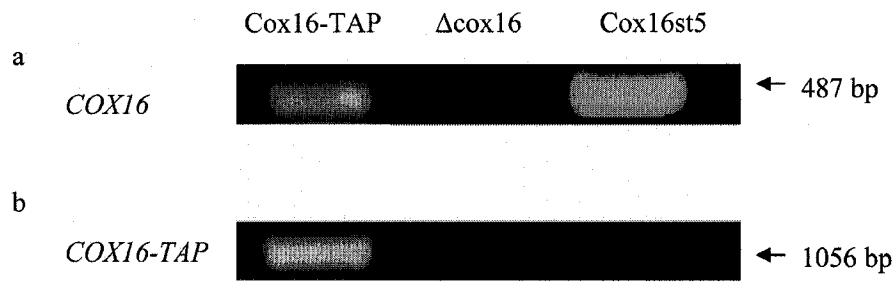

FIGURE 3-10. **Yeast colony PCR confirmed the presence of *COX16-TAP* in the yeast strain.** Yeast colony PCR was performed on the Cox16-TAP strain and compared to the *cox16* null mutant (Δcox16) and wild-type (Cox16st5). PCR was used to confirm (a) the presence of the *COX16* sequence and (b) the presence of the *COX16-TAP* fusion sequence.

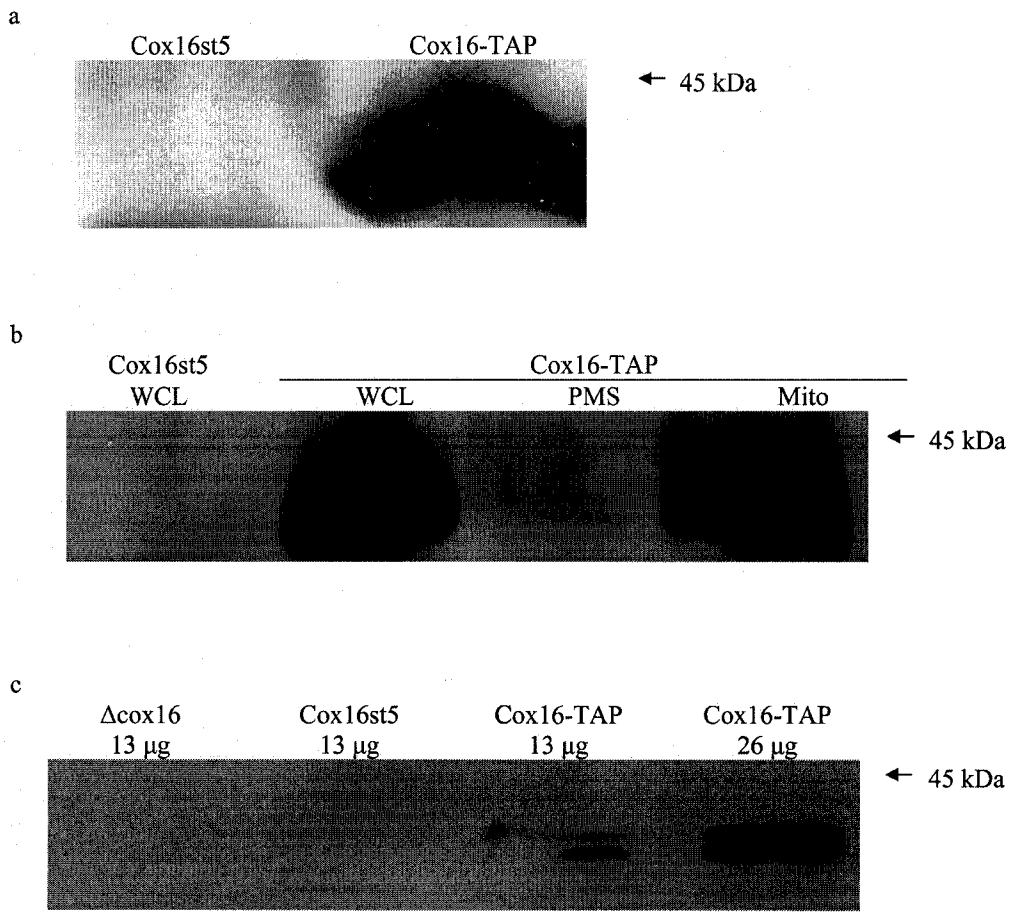

FIGURE 3-11. **The Cox16-TAP fusion product localizes to the mitochondria and is detected through Western blot**. (a) 13 μg of the Cox16-TAP fusion protein from a yeast whole cell lysate is detected by Western blot using an antibody against the TAP epitope. The fusion protein is detected at ~40 kDa. (b) The Cox16-TAP protein (13 μg) is localized to the mitochondria, indicated by a ~40 kDa band on a Western blot. (WCL = whole cell lysate, PMS = post mitochondrial supernatant, Mito = mitochondrial fraction). The membrane was probed with an antibody against the TAP epitope. (c) The Cox16-TAP protein from mitochondrial samples is clearly detected as a ~40 kDa band by Western blot when probed with an antibody against the TAP epitope. Mitochondrial samples from the *cox16* null mutant (Δcox16) and the wild-type (Cox16st5) serve as controls.

mitochondrial supernatant (PMS) fraction did not contain a signal for Cox16-TAP whereas the mitochondrial sample had a strong signal. This result indicated that the protein was properly localizing to the mitochondria. An additional immunoblot from isolated mitochondria demonstrates that the TAP antibody is clearly able to recognize the Cox16-TAP protein, identified by a band at ~40kDa (Figure 3-11c).

A method for preparing mitochondrial samples for TAP column purification requires mitochondrial disruption by sonication. It was important to confirm that the Cox16 complex would not be disrupted if the sample was sonicated. Two mitochondrial samples were prepared and one sample was subjected to sonication while the other was left as a control. The samples were run on separate 7-40% sucrose gradients and analyzed by immunoblot (Figure 3-12). Cox16-TAP signals of ~40kDa were detected in the same fraction of both sucrose gradients, indicating that the high molecular weight complex was not disrupted by sonication.

Mitochondrial samples from the Cox16-TAP expressing strain were prepared by sonication and subjected to TAP column purification. Conditions to purify Cox16-TAP were optimized for each column before the isolation of Cox16-TAP. Initial purifications have demonstrated that the protein of interest can be purified from this method as demonstrated by immunoblot of the column elution (Figure 3-13). When compared to uncleaved and cleaved Cox16-TAP controls, a single band corresponding to the cleaved Cox16-TAP protein (~25kDa) is present in the column elution. None of the uncleaved protein (~40kDa) remains in the fraction eluted from the column.

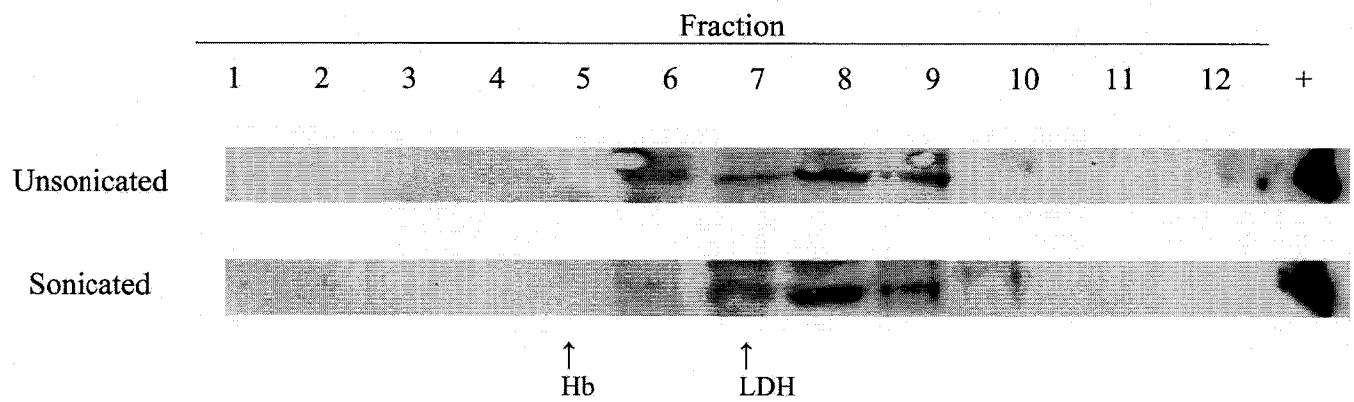

FIGURE 3-12. **Sonication does not affect the structure of the high molecular weight Cox16p complex**. Two samples of mitochondrial lysate from Cox16p-TAP were prepared and one was treated with 2 x 6 seconds of sonication. The samples were subjected to a 7-40% sucrose gradient and separated into 12 fractions, with 1 as the top fraction and 12 as the bottom. The samples were analyzed on a 12% SDS-PAGE and probed against the TAP epitope. A 40 kDa protein was detected in the fractions that corresponded to the Cox16-TAP control (right lane). Fractions that contained the internal protein standards for the sucrose gradient are indicated below the blots, (Hb = hemoglobin, 67 kDa, LDH = lactate dehydrogenase, 130 kDa).

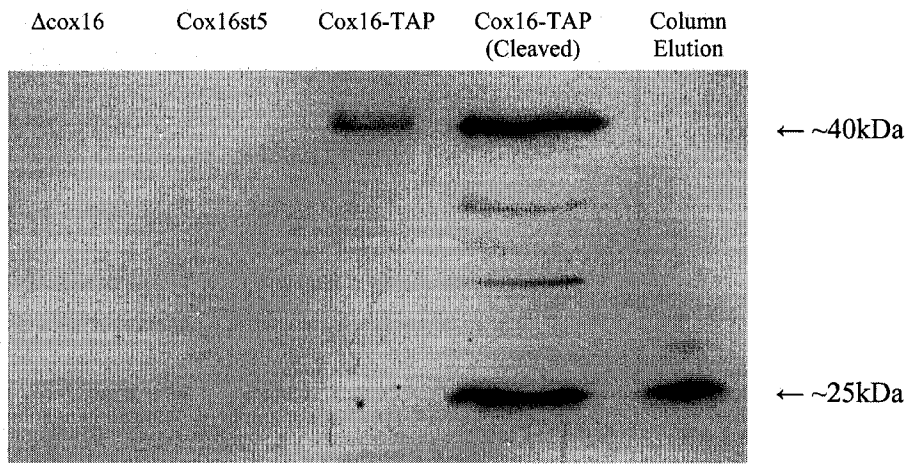

FIGURE 3-13. **Cleaved Cox16-TAP in the TAP column purification elution is detectable by Western Blot**. Isolated mitochondria from a Cox16-TAP strain were purified by TAP column purification. The elution was separated on a 12% SDS-PAGE and probed against the TAP epitope. The fraction from the column elution was compared to Cox16-TAP controls that were uncleaved or cleaved with TEV protease.

To identify proteins that associate with Cox16-TAP, the column elutions were resolved on a 12% SDS-PAGE gel and stained with either Coomassie or Silver Nitrate (Figure 3-14). A possible band for the isolated cleaved Cox16-TAP was detected at ~25kDa. In addition, many high molecular weight proteins were detected that did not correspond with the complex of interest, as the sum of the size of the proteins greatly exceeded the size of the Cox16-TAP complex identified from the sucrose gradients. Additional optimization experiments must be performed to minimize proteins that are non-specifically binding to the complex without disrupting the complex itself.

Cox16p is Present in a Tetrameric or Pentameric Complex

Two different Cox16 fusion proteins had been generated that were dramatically different in size. The first, Cox16-V5, is detected as a ~21kDa band through immunoblot whereas the second, Cox16-TAP, is detected at ~40kDa. The notable difference in size, ~19kDa, allowed the complex to be analyzed through comparative 7-40% sucrose gradients. The size of each complex could be calculated and the difference in size would be divided by the size difference of the individual fusion proteins to determine the multiples of Cox16 in the complex.

This experiment was performed twice. On average, the Cox16-TAP complex sedimented at a position corresponding to 177.01kDa and the Cox16-V5 complex was 92.79kDa (Figure 3-15). When the difference of the complex size (84.22kDa) was divided by the difference of the fusion protein size (19kDa), the multiple of Cox16 within the complex was calculated as 4.4. Due to the inaccuracy of this particular technique, this result could mean that Cox16 is present in either a tetrameric or pentameric structure.

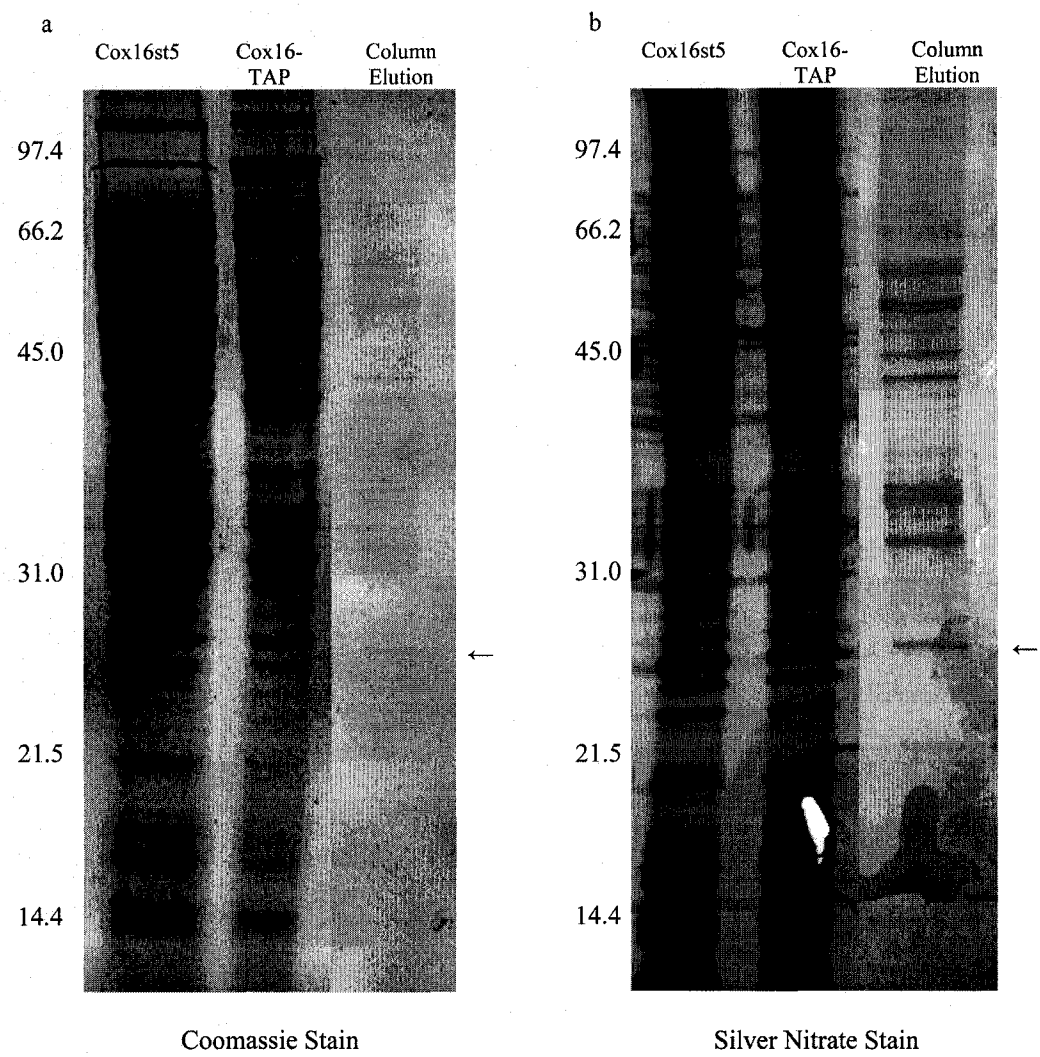

FIGURE 3-14. **Coomassie and Silver Nitrate Stains reveal non-specific proteins in the column elution.** Column elutions were resolved on a 12% SDS-PAGE and stained with either Coomassie or Silver Nitrate to compare proteins in the elution to control samples. Arrows (←) indicate a band that possibly represents the isolated cleaved Cox16-TAP protein that corresponds to the detected band after immunoblotting with the TAP antibody. The molecular weight ladder is listed on the left of the blot in kDa. Many additional bands are observed in the column elutions, particularly those of higher molecular weight.

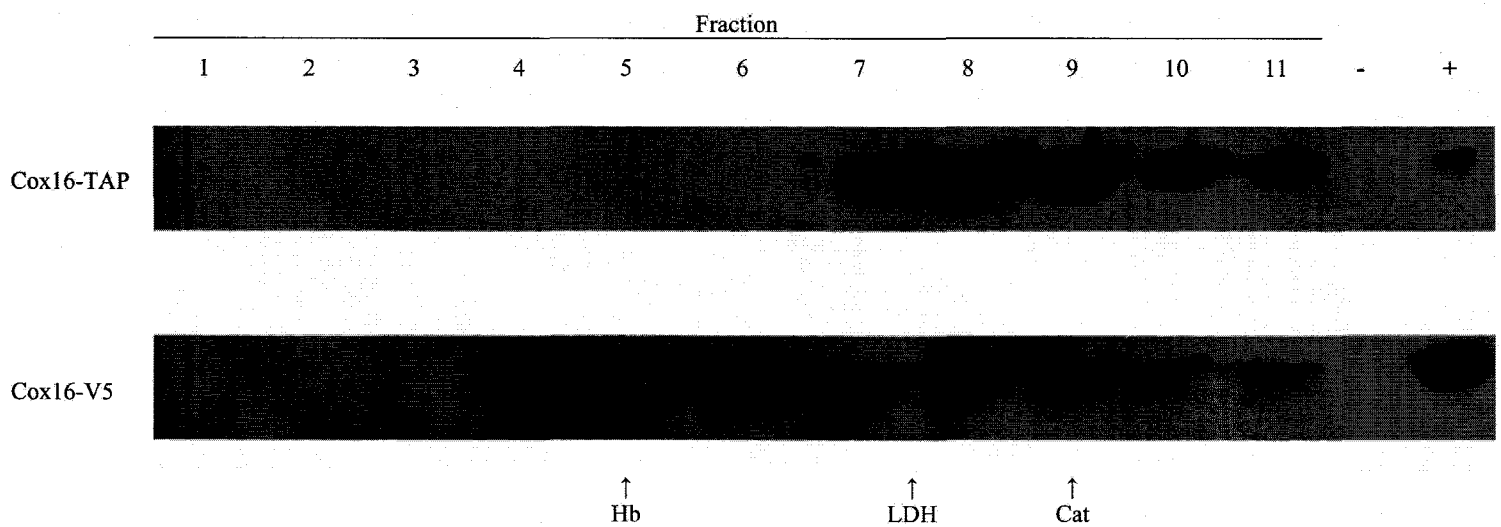

FIGURE 3-15. **Comparative sucrose gradients suggest a tetrameric or pentameric structure for Cox16p**. Isolated mitochondria from Cox16-TAP and Cox16-V5 fusion strains were each separated on a 7-40% sucrose gradient and divided into 11 fractions, with 1 as the top fraction and 11 as the bottom. The fractions were resolved on a 12% SDS-PAGE and probed with antibodies against the respective epitope tags. Δcox16 negative controls (-) and Cox16-TAP or Cox16-V5 positive controls (+) are indicated in the right lanes. The complex size was calculated and the difference in complex size was divided by the difference in individual fusion protein size to determine the multiple of Cox16 in the complex. Fractions that contained the internal protein standards for the sucrose gradient are indicated below, (Hb = hemoglobin at 67 kDa, LDH = lactate dehydrogenase at 130 kDa, Cat = catalase at 232 kDa).

Although this technique does provide a rough estimate of the Cox16 multiple, other more sensitive techniques must be applied to provide a more definite answer.

Native Gels are Unable to Confirm the Tetrameric or Pentameric Complex

An alternative method for analyzing the size of a complex is a native gel, a PAGE lacking SDS. Multiple different preparations of mitochondrial samples were loaded onto a 12% native gel and subsequently stained with Coomassie to determine if the proteins were properly resolved (Figure 3-16a). Upon staining, it was clear that the mitochondrial proteins were not running properly through the gel, as most of the proteins for the control and test samples remained at the top of the gel. For proper migration of the proteins through the gel, a minimal amount of SDS was added to the running buffer at two different concentrations (0.01 and 0.1%). The samples and the gel remained without SDS. The addition of a minimal amount of SDS is predicted to be enough to allow proper migration of the complex without disrupting the protein-protein associations within the complex. The gels were transferred to nitrocellulose and probed with an antibody against the TAP epitope (Figure 3-16b). The addition of 0.01% SDS in the running buffer did not appear to be a high enough concentration. The proteins were able to migrate through the gel although the migration was not even. In addition, the lack of SDS caused the molecular marker to resolve differently when compared to a normal SDS-PAGE. By increasing the concentration to 0.1% SDS, the proteins ran evenly throughout the gel, yet a strong band corresponding to the size of the Cox16 monomer was present. This indicated that the concentration of SDS was too high and as a result, had disrupted the majority of the protein-protein interactions in the complex. In both blots, a band was

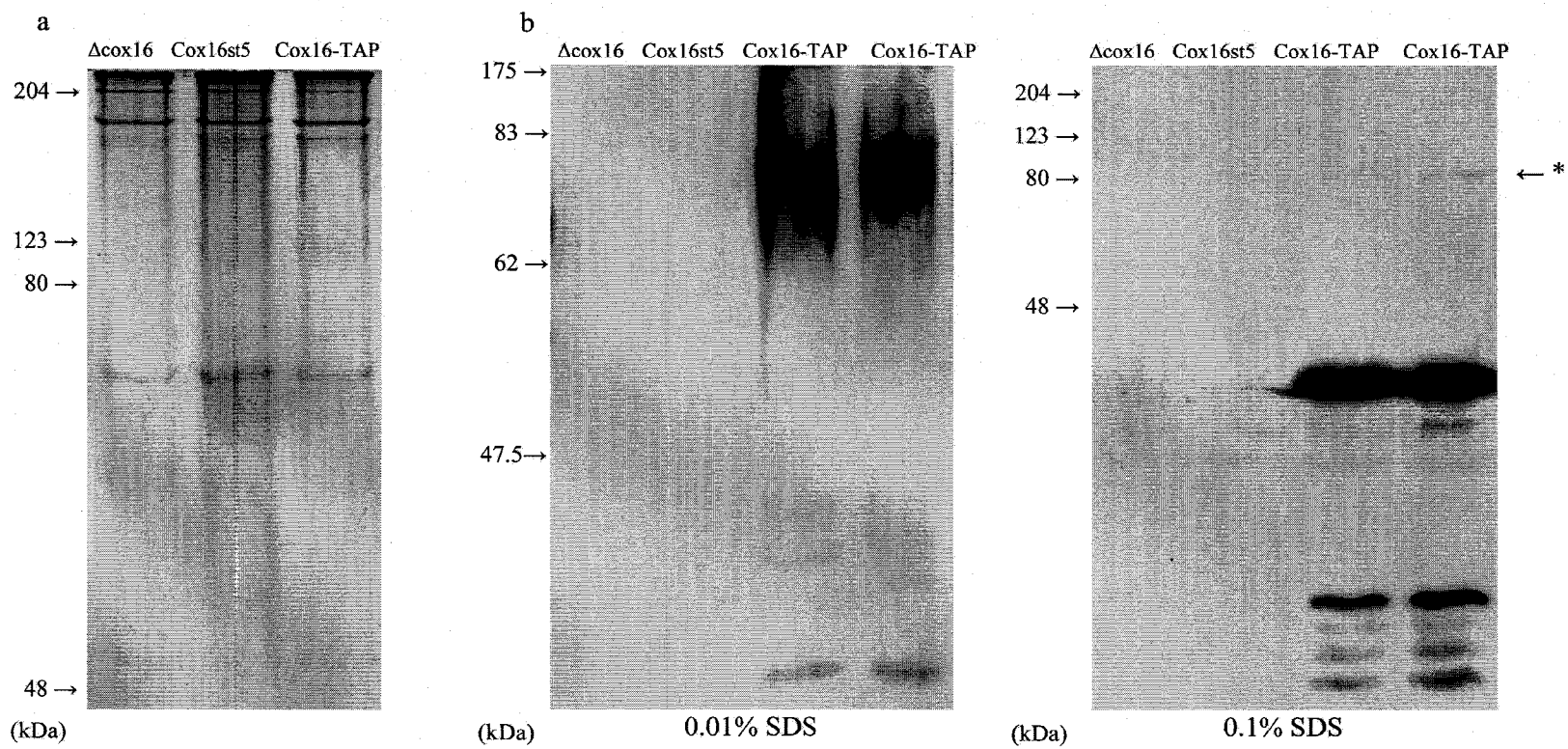

FIGURE 3-16. **Native gels are unable to confirm the tetrameric or pentameric complex of Cox16p**. (a) Mitochondrial samples run on a 12% Native Gel were not properly resolved as determined by Coomassie staining. (b and c) Mitochondrial samples run on a 12% Native Gel with various concentrations of SDS in the running buffer (stated below blot) were transferred to nitrocellulose and probed with an antibody against the TAP epitope. Although the blots were unable to detect any signal large enough to represent a complex, a dimer complex was detected at ~80 kDa and is indicated by an asterisk (*). Molecular markers are listed on the left of the blots in kDa.

present at ~80kDa, likely representing a dimeric form of Cox16p.

Cox16p is Unlikely to be Involved in the Transport of Metals

Previous work had determined that the *cox16* null strain could not be rescued by metal supplementation (Carlson et al., 2003). Various different metals were tested, including calcium, copper, iron, magnesium, manganese and zinc. The recent discovery that Cox16p may be involved in a tetrameric or pentameric complex prompted further investigations into the role of other tetrameric or pentameric complexes. Other proteins able to form pentameric complexes were found to act as pores within a membrane, transporting small molecules such as calcium and glutamate. This suggested that the Cox16p complex might create a pore in the mitochondrial inner membrane. To determine if the hypothesized pore was associated with any particular metal or ion, we tested the growth of the *cox16* null mutant, along with an array of different mutations, truncations and deletions that had previously shown a detectable respiration-deficient phenotype on EG plates. The growth of these mutant strains was tested in EG plates with the supplementation of calcium, copper, iron, magnesium, manganese, potassium, sodium and zinc. The metals were tested at different concentrations (0.01, 0.02, 0.05, 0.1, 0.2, 0.4 and 0.8% w/v). Although previous studies had shown the inability of the *cox16* null to be rescued by metal supplementation, alterations in the Cox16p structure that reduce the protein function may be rescued by metal supplementation as the protein itself is still present.

Growth of the various strains was compared to the growth on EG plates that were not supplemented with any metal or ion. None of the strains demonstrated an increased

growth rate in comparison to the EG control, suggesting that the complex is not involved in the transport of the metals tested, nor does the complex require these metals for proper functioning (data not shown).

Chapter 4: Discussion

Analysis of Cox16p Functional Domains and Associating Proteins

COX is the final electron acceptor in the ETC and is involved in the process of ATP generation within the mitochondria. Proper COX assembly and function is essential for the survival of many living organisms, including humans. Thirteen subunits, three mitochondrially-encoded and 10 nuclear encoded, form the COX structure. The assembly of this multimeric complex requires the interaction of many nuclear-encoded components that are not a part of the COX structure itself. These proteins, termed assembly factors, are involved in many different aspects of COX assembly including translational activation, cofactor biogenesis and insertion, subunit stabilization and complex assembly. The absence of a single assembly factor is able to cause detrimental effects on this sequential assembly process, resulting in a misassembled or non-functional COX. Several examples have been observed in human patients suffering from mitochondrial disease associated with specific COX deficiency. To date, mutations altering protein function have been identified in six different COX assembly factors: *SURF1, SCO1, SCO2, COX10, COX15* and *LRPPRC*. Unfortunately, the underlying cause of COX deficiency in a large majority of patients remains unknown.

Homologs for these particular assembly factors, in addition to multiple others, were initially identified by functional complementation in the yeast, *Saccharomyces cerevisiae*. This particular model system has allowed for extensive genetic and biochemical characterization of COX assembly factors. This thesis focuses on the characterization of one particular assembly factor, Cox16p, in the *Saccharomyces cerevisiae* model system.

COX16 is a nuclear gene that was first identified in *Saccharomyces cerevisiae* by its ability to restore respiratory competence to a group of *pet* mutants in the complementation group G22. Further investigation revealed that these mutants were COX deficient, characterized by the lack of a spectrally detectable peak for cytochrome aa_3 (Tzagoloff and Dieckmann, 1990). Previous studies by Carlson *et al.* confirmed that Cox16p, encoded by the yeast ORF YJL003W, was a COX assembly factor. Δcox16 mutants demonstrated a partial to complete loss of the cytochrome aa_3 peak, in addition to visibly reduced levels for mitochondrially-encoded subunits. Cox16p was excluded in the involvement of inserting Cox2p into the IMM, the synthesis of heme O or heme A and the transport of heavy metals to COX. Preliminary characterization identified Cox16p as a 118 amino acid protein with a predicted mass of 14.1 kDa, containing a putative mitochondrial targeting sequence and transmembrane domain, both located at the N-terminus. Studies with a C-terminally myc-tagged Cox16p revealed that Cox16p was located in the IMM with the C-terminus located in the IMS. The fusion protein was able to restore growth to the *cox16* null mutant with no detectable decreases in the mitochondrially-encoded COX subunits. A linear sucrose gradient found Cox16p associating in a high molecular weight complex of approximately 84 kDa (Carlson *et al.*, 2003).

Research for this thesis initially began by identifying specific domains of Cox16p necessary for protein function, generating single point mutations through site-directed mutagenesis. Eighteen different point mutations at several conserved residues were generated and tested for growth on non-fermentable carbon sources (EG). Of these 18 mutations, three (R83E, E90K and Y91D) demonstrated a detectable phenotype, growing

at slower rates than the wild-type strain. Alterations in COX activity with respect to wild-type activities suggest that these mutations are altering the function of the Cox16p, yet not to the extent that the protein is rendered completely non-functional. Spectral analyses of cytochrome aa_3 indicate a shifted peak in the single point mutants, suggesting that the heme molecules may be misplaced within subunit 1 of COX. Protein levels for Cox1p were also decreased, particularly in the single point mutants R83E and Y91D. Cox2p levels were also decreased although to a lesser extent. Studies from the single point mutations suggest that the region of amino acids 83 to 91 is required for some aspect of Cox16p function, perhaps involving subunit 1 of COX.

R83E/E90K and R83E/Y91D double point mutant strains were generated and tested for growth on EG. Both double point mutants demonstrated a slower growth rate in comparison to their single point mutant counterparts, indicating that a combination of the single point mutants alters the function of Cox16p to a greater degree. The effect of the mutations was also observed in the COX activity, as these strains again demonstrated a reduced growth rate in comparison to the single point mutations alone. The R83E/Y91D mutation had a greater effect on the growth rate and COX activity, emphasizing the importance of these two particular residues in Cox16p function. The severity of the R83E/Y91D mutation was further demonstrated by a marked decrease in the levels of Cox1p and Cox2p and a decrease in amplitude and blue shift of the cytochrome aa_3 peak. The decrease in amplitude in the spectral analysis suggests reduced levels of cytochrome aa_3, which correlate with the decreased levels of Cox1p, as the heme molecules are located within this particular subunit. The decreased levels of Cox1p may be causing destabilization of Cox2p during complex formation, resulting in proteolytic degradation.

This, unfortunately, does not provide an explanation for levels of Cox3p that are similar to wild type levels. Decreases in mitochondrially-encoded subunit levels and cytochrome aa_3 peaks were not observed in the R83E/E90K mutant. It is likely that the E90K mutation is not an amino acid directly involved in Cox16p function, but instead the amino acid alteration affects an adjacent site that is involved in Cox16p function, particularly Y91D. This may explain why no dramatic effect on the assays performed in the E90K single point mutant and in the double point mutation containing the E90K mutation.

C-terminal truncations of Cox16p revealed that the terminal 18 amino acids are not required for the proper functioning of this protein. Truncations of 23 amino acids or greater altered the function of the protein, as observed by its complete respiration-deficient phenotype. Truncations to this degree could eliminate a functional domain within the protein or simply eliminate a region too large for the protein to function properly. To determine which scenario was more likely, 5 and 10 amino acid deletions were generated that spanned the region of the respiration-deficient truncations.

The 10 amino acid deletions (Δ80-89 and Δ90-99) resulted in a completely respiration-deficient phenotype and could not distinguish if the deletion was too large to allow for proper Cox16p functioning or if the deletion had actually eliminated a functional domain of the protein.

The 5 amino acid deletion (Δ90-94 and Δ95-99) strains were partially respiratory competent, with the Δ95-99 strain having a greater ability to grow on EG than the Δ90-94 strain. Unlike the single and double point mutants, the amount of COX activity and decrease in amplitude in the cytochrome aa_3 spectra did not directly correlate to the

growth rate on EG for these two deletion mutants. The Δ95-99 deletion strain had a much faster growth rate on EG but a lower COX activity and reduced spectral peak than the Δ90-94 deletion strain. It may be possible that Cox16p is involved in the generation of a mature subunit, perhaps Cox1p. The Δ95-99 deletion may allow Cox16p to still associate with Cox1p but lack the region required for some form of subunit processing and as a result, generate a Cox1p that is present but lacking function. In contrast, the Δ90-94 deletion may be within the region of Cox16p that associates with Cox1p. A deletion in this region would reduce the amount of Cox16p able to associate with Cox1p, leading to proteolytic degradation of this particular subunit. The Cox1p subunits that are still able to associate with Cox16p would undergo proper processing, resulting in a functional subunit. The lower levels of Cox1p observed in the Δ90-94 deletion in comparison to the Δ95-99 deletion would correlate with this proposed model. As the isolated mitochondria used for these biochemical analyses originated from a single purification isolation, an alternative explanation may be that the integrity of the mitochondria from one of the deletion strains was destroyed, resulting in the conflicting results. Duplication of these results using freshly isolated mitochondria would eliminate the second explanation as the cause of the discrepancy. Additional experiments would then be required to determine the validity of the first explanation.

Two additional 5 amino acid deletions were generated at the N-terminus of Cox16p. The first deletion was located immediately before the putative transmembrane domain (Δ28-32) whereas the second deletion contained 4 amino acids of the putative transmembrane domain (Δ33-37). Preliminary examination of the Δ28-32 deletion suggested that it had no effect on Cox16p, as the growth rate of the deletion strain was

almost identical to the wild-type rate. Further investigations revealed that, although the growth rate was similar, the COX activity, amplitude of the cytochrome spectral signal and Cox1p levels were all elevated. In contrast, the Δ33-37 mutant, with the exception of a low amount of COX activity, had biochemical characteristics similar to that of the *cox16* null strain.

Previous investigations have shown no detectable role for Cox16 in the insertion of heme or copper into Cox1p. Experiments using *in vivo* labeling further indicated that the three mitochondrially encoded subunits of COX are correctly expressed (Carlson et al., 2003). Other processes involved in Cox1p generation include the stabilization of Cox1p prior to the association with the Cox4p subunit. Proteins involved in Cox1p stabilization include Cox14p, an IMM protein with a single putative transmembrane domain, and Mss51p, a mitochondrial matrix protein. These two proteins work together to stabilize and also control the rate of production for Cox1p. In high abundance of Cox1p, Cox14p is able to bind and together with Mss51p, stabilizes the Cox1p subunit for further processing. When the levels of Cox1p decrease, Cox14p no longer has the Cox1p subunit to bind to and as a result, releases Mss51p (Barrientos et al., 2004). The unbound Mss51p serves as a transcriptional activator on the 5'-untranslated leader sequence of the *COX1* mRNA to increase the rate of Cox1p production.

Barrientos and coworkers have identified the presence of Cox14p and Mss51p in a high molecular weight complex through sucrose gradient sedimentation experiments. After subtracting the molecular weight of the GST tag fused to their Cox14p, the molecular weight of the complex containing Cox14p and Mss51p is strikingly similar to

the molecular weight of the Cox16p complex, both being approximately 90kDa. This suggests the possible association between Cox16p, Cox14p and Mss51p.

It is possible that the Δ28-32 deletion removed the domain of Cox16p required for association with Mss51, as the region of this deletion is located on the matrix side and Mss51p is a matrix protein. If this were the case, it is likely that the overproduction of Cox1p is a result of the unregulated transcriptional activation properties of Mss51p on the *COX1* mRNA. As Cox1p itself is the first subcomplex (S1) of COX assembly, overproduction of this particular subunit could lead to increased production of COX, due to higher amounts of the initial component. The regulation of COX assembly in this case would depend instead on the availability of the other subunits, such as Cox2p, Cox3p and the nuclearly-encoded subunits.

The lack of growth on EG of the Δ33-37 mutant may be the result of the inability of Cox16p to associate with other proteins in the complex, namely itself and Cox14p, through the transmembrane domain. Numerous proteins containing a single transmembrane domain have been found to associate with each other or other proteins through residues in the transmembrane region. With the inability to associate with other proteins in the complex, Cox16p along with other associating proteins would not be able to stabilize Cox1p. As a result, Cox1p would be degraded and unavailable for COX production, correlating to the respiratory-deficient phenotype observed in this strain.

Epitope tags within the N- and C-terminal regions of Cox16p have been generated. The epitope tags generated at the N-terminus altered the growth rate of the wild type Cox16p when grown on EG. An epitope tag at the C-terminus did not affect the growth of the wild type Cox16p, but was able to alter the growth rate of multiple different mutant

strains such that the growth rate on EG of the tagged and untagged strains did not correlate with each other. As epitope tags for Cox16p containing mutations are not feasible due to alterations in growth rates, antibodies specific to this protein would help to decipher the effect of the Δ33-37 deletion. Localization studies, generating isolated fractions of mitochondria and mitoplasts from a Cox16p strain containing the Δ33-37 deletion, could identify if the protein is properly localizing to the IMM. Further immunoprecipitation studies with a strain containing an epitope tagged wild-type Cox16 and Cox16p containing the Δ33-37 deletion could investigate the role of the transmembrane domain in Cox16p association, as these studies have shown that Cox16p can self-associate (discussed below).

Cox16p was discovered to self-associate through immunoprecipitation (IP) studies using a strain containing two different constructs of epitope-tagged Cox16p. Mitochondrial lysate containing Cox16-V5 and Cox16-myc were subject to IP with V5 and myc specific antibodies and their association was detected on immunoblot, as a band was present in both the IP and reciprocal IP lanes. The bands present were of similar size to the bands in the control lanes of mitochondrial samples. This indicated that the previously identified high molecular weight complex contained a minimum of two molecules of Cox16p.

Further studies of comparative sucrose gradients utilized the difference in size between two different epitope-tagged Cox16 constructs to determine the number of molecules within this particular high molecular weight complex. The initial identification of a high molecular weight complex was through the use of a linear sucrose gradient and a Cox16-myc strain. To determine the number of molecules of Cox16p in the complex,

the linear sucrose gradient was repeated using a Cox16-V5 construct and a Cox16-TAP construct. These two constructs differ in size by ~19 kDa and thus the number of Cox16p within the complex can be determined by the difference in complex size. After two separate runs, it was determined that there were between 4-5 molecules of Cox16p within the complex, along with one or more additional unidentified proteins. The inaccuracy of the sucrose gradient technique accounted for the variability between runs and thus the number of Cox16p in the complex was to be confirmed through alternative methods, such as native PAGE. The doublet band observed in the Cox16-TAP blots is possibly due to some modification on the TAP epitope as none of the other Cox16 constructs demonstrate a visible doublet. This modification does not seem to affect any of the experiments performed with the TAP epitope.

Attempts to determine the number of Cox16p in the complex through native gels and PAGE containing a minimal amount of SDS in the running buffer were unsuccessful. Further optimization to determine the exact concentration of SDS is required. With no SDS present, the mitochondrial proteins do not properly resolve within the gel. Coomassie staining revealed that a large amount of protein remained in the stacking gel or in the region of high molecular weight proteins. At low SDS concentrations (0.01%), it is possible that a dimeric form of Cox16p was observed, although the lack of SDS reduced the definition of the band and furthermore caused improper separation of the molecular weight markers. At higher concentrations of SDS (0.1%), a strong band representing the monomeric form of Cox16p was observed with a faint band double the size, possibly representing the dimeric form. The strong signal of the monomeric form in

comparison to the faint band of the dimeric form suggests that the SDS concentration was too high, disrupting the Cox16p complex.

An alternative method to determine the number of molecules of Cox16p in the complex involves the use of sizing columns followed by immunoblot analysis. The two different epitope-tagged Cox16 constructs could be applied to separate sizing columns. The size of the complex could be determined by identifying the fraction that contains Cox16p (determined by immunoblot) and comparing the fraction to fractions containing controls of known molecular weight. This method is more accurate than linear sucrose gradients and would likely be able to determine if there are 4 or 5 molecules of Cox16p present in the complex. In addition, an immunoblot of the fractions using a Cox14-specific antibody could determine if Cox14 is located in the same fraction as Cox16. If so, it is highly suggestive that Cox14 and Cox16 are associating within the high molecular weight complex. The presence of Cox14 within this complex further implies that Mss51 is also present, as previous studies have demonstrated the association between Cox14 and Mss51 in an uncharacterized high molecular weight complex (Barrientos et al., 2004). Confirmation of this protein association between Cox16 and Cox14 (and Mss51) will have to be assessed by further experimentation, such as IP or cross-linking experiments.

The presence of 4-5 molecules of Cox16p in the complex suggested the possible formation of a pore within the IMM, perhaps transporting a particular ion or metal to the COX complex. Previous investigations suggested that Cox16p did not have a role in metal transport as the growth of the *cox16* null mutant was not rescued by supplementation of various metals to EG plates (Carlson et al., 2003). Although previous studies had shown the inability of the *cox16* null to be rescued by metal supplementation,

alterations in the Cox16p structure that reduce the protein function might be rescued by metal supplementation as the protein itself is still present. Various Cox16 mutants were tested on EG plates supplemented with a variety of metals and none demonstrated an increased growth rate in comparison to the same strains grown on an unsupplemented EG control plate. This minimizes the possibility that the Cox16p complex is involved in ion or metal transport to the COX complex through the formation of a pore. Furthermore, it suggested that none of these particular metals or ions are required as a cofactor for Cox16p function.

Further characterization of Cox16 and its associated complex was to be performed through the use of a TAP epitope tag. After the presence of Cox16 and the TAP epitope was confirmed, the construct was inserted into a single copy vector, YCplac111. Immunoblot analyses confirmed that the protein was detectable and properly localized to the mitochondria, present at a molecular weight of ~40 kDa. Initial purification experiments focused on optimizing the IgG Sepharose and calmodulin column purifications for a membrane-bound mitochondrial protein. Sample preparation, sample concentrations, wash volumes and elution conditions were all adjusted for each column to optimize the purification of Cox16-TAP. The extent of column optimization reached a point at which the Cox16-TAP protein could be eluted from the columns and detected by immunoblot with an antibody against the cleaved TAP epitope. When the elution was size fractionated and stained with either Coomassie or Silver Nitrate, the presence of a large number of high molecular weight proteins indicated that a large amount of non-specific proteins were also being eluted from the column. Additional optimization needs to be performed to reduce the amount of non-specifically binding proteins without

decreasing the concentration of Cox16-TAP in the final elution. This could be achieved by increasing the salt concentrations in the various washes in each column. A series of different concentrations and perhaps different salts would allow determination of the optimal wash for this particular protein. Once the conditions have been determined, the final elution can be resolved on an SDS-PAGE. Any additional bands other than the cleaved Cox16-TAP construct are likely involved in the high molecular weight complex. The identity of these associating proteins can be determined through mass spectrometry. Future studies of Cox16-TAP are aimed at eventually determining the crystal structure of Cox16p, as well as antibody generation for future investigations of the Cox16 mutants. A Cox16-TAP construct containing a Factor X_a protease site between the protein and the epitope tag has been generated. This construct is to be used after the column conditions have been optimized. Lysed mitochondria from a strain containing this construct will be purified by both columns and instead of reducing the calcium concentration to elute the protein from the calmodulin column, the Cox16 protein will be proteolytically cleaved and eluted by commercially purchased Factor X_a. In doing so, the remaining TAP epitope will be removed from the C-terminus of Cox16p. Instead, only two amino acids, remnants of the protease cleavage site, will remain. After running this elution on an SDS-PAGE and staining with Coomassie or Silver Nitrate, the band that associates with Cox16p (with two additional amino acids) can be isolated and used for antibody generation. In addition, elutions from the columns could also be used for crystal structure determination. Although two additional amino acids remain at the C-terminus of the protein after Factor X_a cleavage, removal of the remaining TAP epitope, specifically the calmodulin binding domain, will reduce the possibility that an antibody will be generated

against a protein other than Cox16p. Furthermore, removal of the remaining TAP epitope will enhance the accuracy of the crystal structure determination as the C-terminus of Cox16p will not contain an excessive amount of additional amino acids that could interfere with the structure. Determining the structure of Cox16p will help delineate the effects of the point mutations and deletions that were previously generated in this protein. In addition, it can provide insight into the regions of Cox16p that are necessary to associate with other proteins.

Figure 4-1 illustrates the proposed model for Cox16p and associated proteins within the high molecular weight complex.

These initial studies of Cox16 are only the beginning to determining the role of this protein in the assembly of COX. Through the generation of a Cox16-specific antibody and the optimization of Cox16 purification, the function of Cox16 can be elucidated and associating proteins can be identified. In the future, Cox16 functionality in the yeast model system can be applied to the human homolog in hopes of determining if the malfunctioning of this protein has a role in mitochondrial disease associated with COX deficiency. In the case that Cox16 malfunction is associated with human disease, understanding the important domains of Cox16 required for proper functioning can offer potential therapeutic treatments for this devastating condition.

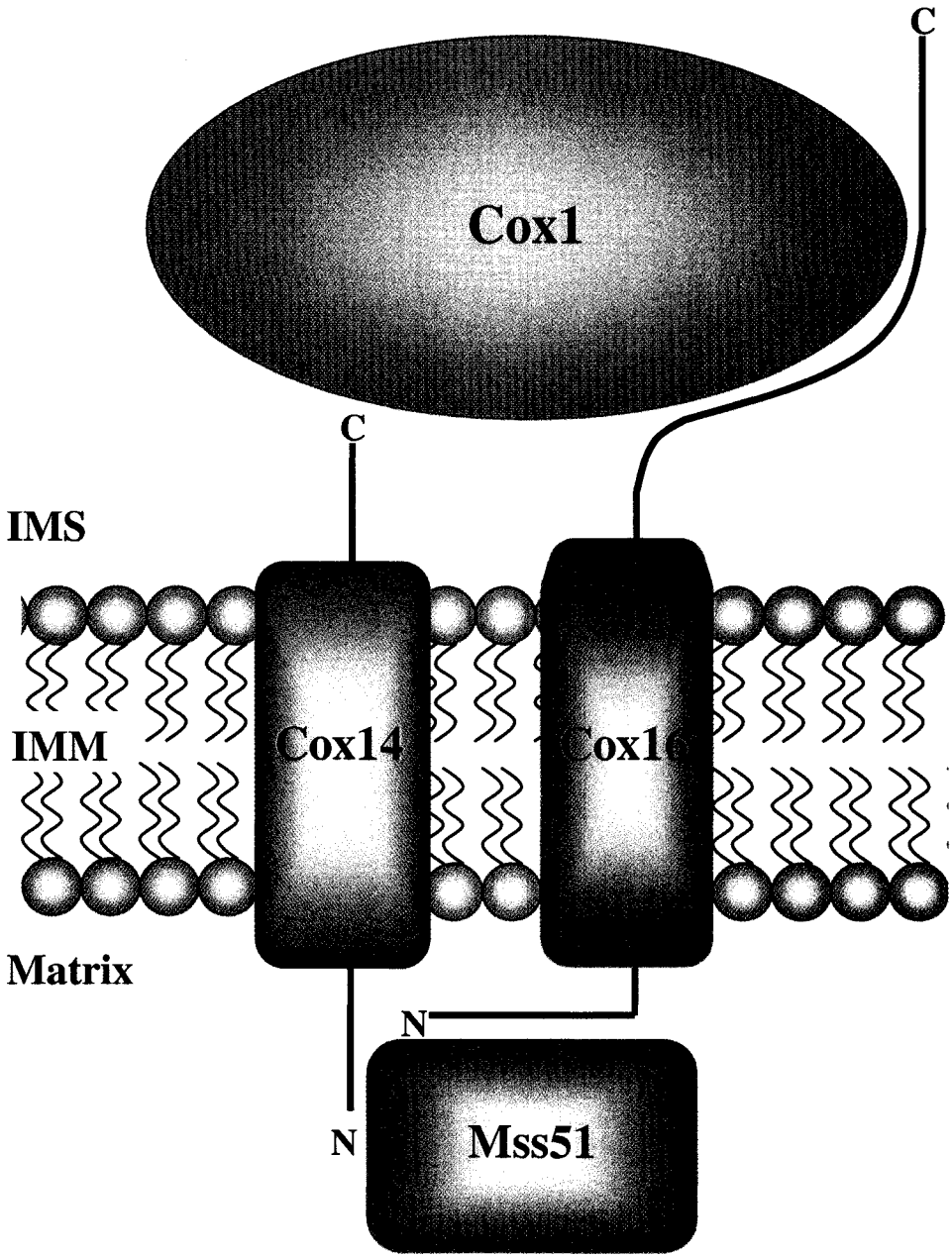

FIGURE 4-1. **Proposed model for Cox16 and associating proteins in the high molecular weight complex.** Cox16 is present in a multiple of 4 or 5 molecules. It is able to associate with Cox14 through the transmembrane region. Association of Mss51 is through the N-terminus of both Cox14 and Cox16. The C-terminus of both Cox14 and Cox16 are proposed to be involved in Cox1p stabilization prior to further COX assembly.

Bibliography

Ackrell, B.A.C. 2002. Cytopathies involving mitochondrial complex II. *Molecular Aspects of Medicine*. 23:369-84.

Antonicka, H., A. Mattman, C.G. Carlson, D.M. Glerum, K.C. Hoffbuhr, S.C. Leary, N.G. Kennaway, and E.A. Shoubridge. 2003. Mutations in *COX15* produce a defect in the mitochondrial heme biosynthetic pathway, causing early-onset fatal hypertrophic cardiomyopathy. *American Journal of Human Genetics*. 72:101-114.

Banting, G.S., and D.M. Glerum. 2006. Mutational analysis of the *Saccharomyces cerevisiae* cytochrome *c* oxidase assembly protein Cox11p. *Eukaryotic Cell*. 5:568-578.

Barrientos, A., M.H. Barros, I. Valnot, A. Rötig, P. Rustin, and A. Tzagoloff. 2002a. Cytochrome oxidase in health and disease. *Gene*. 286:53-63.

Barrientos, A., D. Korr, and A. Tzagoloff. 2002b. Shy1p is necessary for full expression of mitochondrial COX1 in the yeast model of Leigh's Syndrome. *The EMBO Journal*. 21:43-52.

Barrientos, A., A. Zambrano, and A. Tzagoloff. 2004. Mss51p and Cox14p jointly regulate mitochondrial Cox1p expression in *Saccharomyces cerevisiae*. *EMBO*. 23:3472-3482.

Barros, M.H., C.G. Carlson, D.M. Glerum, and A. Tzagoloff. 2001. Involvement of mitochondrial ferredoxin and Cox15p in hydroxylation of heme O. *FEBS Letters*. 492:133-138.

Barros, M.H., A. Johnson, and A. Tzagoloff. 2004. *COX23*, a homologue of *COX17*, is required for cytochrome oxidase assembly. *The Journal of Biological Chemistry*. 279:31943-31947.

Beers, J., D.M. Glerum, and A. Tzagoloff. 2002. Purification and characterization of yeast Sco1p, a mitochondrial copper protein. *The Journal of Biological Chemistry*. 277:22185-22190.

Borisov, V.B. 2002. Defects in mitochondrial respiratory complexes III and IV, and human pathologies. *Molecular Aspects of Medicine*. 23:385-412.

Bruno, C., A. Martinuzzi, Y. Tang, A.L. Andreu, F. Pallotti, E. Bonilla, S. Shanske, J. Fu, C.M. Sue, C. Angelini, S. DiMauro, and G. Manfredi. 1999. A stop-codon mutation in the human mtDNA cytochrome *c* oxidase I gene disrupts the functional structure of complex IV. *American Journal of Human Genetics*. 65:611-620.

Brunori, M., A. Giuffrè, and P. Sarti. 2005. Cytochrome *c* oxidase, ligands and electrons. *Journal of Inorganic Biochemistry*. 99:324-336.

Burger, G., M.W. Gray, and B.F. Lang. 2003. Mitochondrial genomes: anything goes. *TRENDS in genetics*. 19:709-716.

Capaldi, R.A. 1996. The complexity of a respiratory complex. *Nature Structural Biology*. 3:570-574.

Capaldi, R.A., and R. Aggeler. 2002. Mechanism of the F_1F_0-type ATP synthase, a biological rotary motor. *Trends in Biochemical Sciences*. 27:154-160.

Carlson, C.G., A. Barrientos, A. Tzagoloff, and D.M. Glerum. 2003. *COX16* encodes a novel protein required for the assembly of cytochrome oxidase in *Saccharomyces cerevisiae*. *The Journal of Biological Chemistry*. 278:3770-3775.

Carr, H.S., G.N. George, and D.R. Winge. 2002. Yeast Cox11, a protein essential for cytochrome *c* oxidase assembly, is a Cu(I)-binding protein. *The Journal of Biological Chemistry*. 277:31237-31242.

Carr, H.S., and D.R. Winge. 2003. Assembly of cytochrome *c* oxidase within the mitochondrion. *Accounts of Chemical Research*. 36:309-316.

Cecchini, G. 2003. Function and structure of Complex II of the respiratory chain. *Annual Reviews in Biochemistry*. 72:77-109.

Church, C., B. Goehring, D. Forsha, P. Wazny, and R.O. Poyton. 2005. A role for Pet100p in the assembly of yeast cytochrome *c* oxidase. *The Journal of Biological Chemistry*. 280:1854-1863.

Clark, K.M., R.W. Taylor, M.A. Johnson, P.F. Chinnery, Z.M.A. Chrzanowska-Lightowlers, R.M. Andrews, I.P. Nelson, N.W. Wood, P.J. Lamont, M.G. Hanna, R.N. Lightowlers, and D.M. Turnbull. 1999. An mtDNA mutation in the initiation codon of the cytochrome *c* oxidase subunit II gene results in lower levels of the protein and a mitochondrial encephalomyopathy. *American Journal of Human Genetics*. 64:1330-1339.

Cobine, P.A., F. Pierrel, and D.R. Winge. 2006. Copper trafficking to the mitochondrion and assembly of copper metalloenzymes. *Biochimica et Biophysica Acta*:Accepted 5 March 2006.

Comi, G.P., A. Brodoni, S. Salani, L. Franceschina, M. Sciacco, A. Prelle, F. Fortunato, M. Zeviani, L. Napoli, N. Bresolin, M. Moggio, C.D. Ausenda, J.-W. Taanman, and G. Scarlato. 1998. Cytochrome *c* oxidase subunit I microdeletion in a patient with motor neuron disease. *Annals of Neurology*. 43:110-116.

Crofts, A.R. 2004. The cytochrome bc_1 complex: Function in the context of structure. *Annual Reviews in Physiology*. 66:689-733.

Dickinson, E.K., D.L. Adams, E.A. Schon, and D.M. Glerum. 2000. A human *SCO2* mutation helps define the role of Sco1p in the cytochrome oxidase assembly pathway. *The Journal of Biological Chemistry*. 275:26780-26785.

Foltopoulou, P.F., G.A. Zachariadis, A.S. Politou, A.S. Tsiftsoglou, and L.C. Papadopoulou. 2004. Human recombinant mutated forms of the mitochondrial COX assembly Sco2 protein differ from wild-type in physical state and copper binding capacity. *Molecular Genetics and Metabolism*. 81:225-236.

Hanna, M.G., I.P. Nelson, S. Rahman, R.J.M. Lane, J. Land, S. Heales, M.J. Cooper, A.H.V. Schapira, J.A. Morgan-Hughes, and N.W. Wood. 1998. Cytochrome *c* oxidase deficiency associated with the first stop-codon point mutation in human mtDNA. *American Journal of Human Genetics*. 63:29-36.

Hell, K., A. Tzagoloff, W. Neupert, and R.A. Stuart. 2000. Identification of Cox20p, a novel protein involved in the maturation and assembly of cytochrome oxidase subunit 2. *The Journal of Biological Chemistry*. 275:4571-4578.

Herrmann, J.M., and S. Funes. 2005. Biogenesis of cytochrome oxidase - Sophisticated assembly lines in the mitochondrial inner membrane. *Gene*. 354:43-52.

Hirano, M. 2001. Introduction for: 'mitochondrial diseases'. *Cell & Developmental Biology*. 12:395.

Holt, I.J., A.E. Harding, and J.A. Morgan Hughes. 1988. Deletions of muschle mitochondrial DNA in patients with mitochondrial myopathies. *Nature*. 331:717-719.

Horng, Y.-C., P.A. Cobine, A.B. Maxfield, H.S. Carr, and D.R. Winge. 2004. Specific copper transfer from the Cox17 metallochaperone to both Sco1 and Cox11 in the assembly of yeast cytochrome *c* oxidase. *The Journal of Biological Chemistry*. 279:35334-35340.

Horng, Y.-C., S.C. Leary, P.A. Cobine, F.B.J. Young, G.N. George, E.A. Shoubridge, and D.R. Winge. 2005. Human Sco1 and Sco2 function as copper-binding proteins. *The Journal of Biological Chemistry*. 280:34113-34122.

Karadimas, C.L., P. Greenstein, C.M. Sue, J.T. Joseph, K. Tanji, R.G. Haller, T. Taivassalo, M.M. Davidson, S. Shanske, E. Bonilla, and S. DiMauro. 2000. Recurrent myoglobinuria due to a nonsense mutation in the *COXI* gene of mitochondrial DNA. *Neurology*. 55:644-649.

Keightley, J.A., K.C. Hoffbuhr, M.D. Burton, V.M. Salas, W.S.W. Johnston, A.M.W. Penn, N.R.M. Buist, and N.G. Kennaway. 1996. A microdeletion in cytochrome *c* oxidase (COX) subunit III associated with COX deficiency and recurrent myoglobinuria. *Nature Genetics*. 12:410-416.

Khalimonchuk, O., K. Ostermann, and G. Rödel. 2005. Evidence for the association of yeast mitochondrial ribosomes with Cox11p, a protein required for the Cu_B site formation of cytochrome *c* oxidase. *Current Genetics*. 47:223-233.

Khalimonchuk, O., and G. Rödel. 2005. Bigenesis of cytochrome *c* oxidase. *Mitochondrion*. 5:363-388.

Koerner, T.J., G. Homison, and A. Tzagoloff. 1985. Nuclear mutants of *Saccharomyces cerevisiae* with altered subunits 4, 5, and 6 of cytochrome oxidase. *The Journal of Biological Chemistry*. 260:5871-5874.

Lancaster, C.R.D. 2002. Succinate:quinone oxidoreductases: an overview. *Biochimica et Biophysica Acta*. 1553:1-6.

Lehninger, A.L., and E.P. Kennedy. 1949. Oxidation of fatty acids and tricorboxylic acid cycle intermediates by isolated rat liver mitochondria. *Journal of Biological Chemistry*. 179:957-972.

Lemire, B.D., and K.S. Oyedotun. 2002. The *Saccharomyces cerevisiae* mitochondrial succinate:ubiquinone oxidoreductase. *Biochimica et Biophysica Acta*. 1553:102-116.

Lode, A., M. Kushel, C. Paret, and G. Rödel. 2000. Mitochondrial copper metabolism in yeast: interaction between Sco1p and Cox2p. *FEBS Letters*. 485:19-24.

Lode, A., C. Paret, and G. Rödel. 2002. Molecular characterization of *Saccharomyces cerevisiae* Sco2p reveals a high degree of redundancy with Sco1p. *Yeast*. 19:909-922.

Manfredi, G., E.A. Schon, C.T. Moraes, E. Bonilla, G.T. Berry, J.T. Sladky, and S. DiMauro. 1995. A new mutation associated with MELAS is located in a mitochondrial DNA polypeptide-coding gene. *Neuromuscular Disorders*. 5:391-398.

Mashkevich, G., B. Repetto, D.M. Glerum, C. Jin, and A. Tzagoloff. 1997. *SHY1*, the yeast homolog of the mammalian *SURF-1* gene, encodes a mitochondrial protein required for respiration. *The Journal of Biological Chemistry*. 272:14356-14364.

McEwen, J.E., C. Ko, B. Kloeckner-Gruissem, and R.O. Poyton. 1986. Nuclear functions required for cytochrome *c* oxidase biogenesis in *Saccharomyces cerevisiae*. *The Journal of Biological Chemistry*. 261:11872-11879.

Mesecke, N., N. Terziyska, C. Kozany, F. Baumann, W. Neupert, K. Hell, and J.M. Herrmann. 2005. A disulfide relay system in the intermembrane space of mitochondria that mediates protein import. *Cell*. 121:1059-1069.

Michel, H., J. Behr, A. Harrenga, and A. Kannt. 1998. Cytochrome *c* oxidase: Structure and spectroscopy. *Annual Reviews in Biophysical and Biomolecular Structures*. 27:329-56.

Munnich, A., and P. Rustin. 2001. Clinical spectrum and diagnosis of mitochondrial disorders. *American Journal of Medical Genetics*. 106:4-17.

Naithani, S., S.A. Saracco, C.A. Butler, and T.D. Fox. 2003. Interactions among *COX1, COX2*, and *COX3* mRNA-specific translational activator proteins on the inner surface of the mitochondrial inner membrane of *Saccharomyces cerevisiae*. *Molecular Biology of the Cell*. 14:324-333.

Neupert, W. 1997. Protein import into mitochondria. *Annual Reviews in Biochemistry*. 66:863-917.

Nijtmans, L.G.J., M. Artal Sanz, M. Bucko, M.H. Farhoud, M. Feenstra, G.A.J. Hakkaart, M. Zeviani, and L.A. Grivell. 2001. Shy1p occurs in a high molecular weight complex and is required for efficient assembly of cytochrome *c* oxidase in yeast. *FEBS Letters*. 498:46-51.

Nijtmans, L.G.J., J.-W. Taanman, A.O. Muijsers, D. Speijer, and C. van den Bogert. 1998. Assembly of cytochrome-*c* oxidase in cultured human cells. *European Journal of Biochemistry*. 254:389-394.

Nittis, T., G.N. George, and D.R. Winge. 2001. Yeast Sco1, a protein essential for cytochrome *c* oxidase function is a Cu(I)-binding protein. *The Journal of Biological Chemistry*. 276:42520-42526.

Papadopoulou, L.C., C.M. Sue, M.M. Davidson, K. Tanji, I. Nishino, J.E. Sadlock, S. Krishna, W. Walker, J. Selby, D.M. Glerum, R.V. Coster, G. Lyon, E. Scalais, R. Lebel, P. Kaplan, S. Shanske, D.C. DeVivo, E. Bonilla, M. Hirano, S. DiMauro, and E.A. Schon. 1999. Fatal infantile cardioencephalomyopathy with cytochrome *c* oxidase (COX) deficiency and mutations in *SCO2*, a human COX assembly gene. *Nature Genetics*. 23:333-337.

Pedersen, P.L. 1999. Mitochondrial events in the life and death of animal cells: A brief overview. *Journal of Bioenergetics and Biomembranes*. 31:291-304.

Péquignot, M.O., R. Dey, M. Zeviani, V. Tiranti, C. Godinot, A. Poyau, C. Sue, S. DiMauro, M. Abitbol, and C. Marsac. 2001. Mutations in the *SURF1* gene assocaited with leigh syndrome and cytochrome *c* oxidase deficiency. *Human Mutation*. 17:374-381.

Punter, F.A., and D.M. Glerum. 2003. Mutagenesis reveals a specific role for Cox17p in copper transport to cytochrome oxidase. *The Journal of Biological Chemistry*. 278:30875-30880.

Rahman, S., J.-W. Taanman, J.M. Cooper, I. Nelson, I. Hargreaves, B. Meunier, M.G. Hanna, J.J. García, R.A. Capaldi, B.D. Lake, J.V. Leonard, and A.H.V. Schapira. 1999. A missense mutation of cytochrome oxidase subunit II causes defective assembly and myopathy. *American Journal of Human Genetics*. 65:1030-1039.

Rentzsch, A., G. Krummeck-Weib, A. Hofer, A. Bartuschka, K. Ostermann, and G. Rödel. 1999. Mitochondrial copper metabolism in yeast: mutational analysis of

Sco1p involved in the biogenesis of cytochrome *c* oxidase. *Current Genetics*. 35:103-108.

Rigaut, G., A. Shevchenko, B. Rutz, M. Wilm, M. Mann, and B. Séraphin. 1999. A generic protein purification method for protein complex characterization and proteome exploration. *Nature Biotechnology*. 17:1030-1032.

Saracco, S.A., and T.D. Fox. 2002. Cox18p is required for the export of the mitochondrially encoded *Saccharomyces cerevisiae* Cox2p C-tail and interacts with Pnt1p and Mss2p in the inner membrane. *Molecular Biology of the Cell*. 13:1122-1131.

Shoubridge, E.A. 2001. Cytochrome *c* oxidase deficiency. *American Journal of Medical Genetics*. 106:46-52.

Souza, R.L., N.S. Green-Willms, T.D. Fox, A. Tzagoloff, and F.G. Nobrega. 2000. Cloning and characterization of *COX18*, a *Saccharomyces cerevisiae PET* gene required for the assembly of cytochrome oxidase. *The Journal of Biological Chemistry*. 275:14898-14902.

Taanman, J.-W. 1997. Human cytochrome *c* oxidase: Structure, function and deficiency. *Journal of Bioenergetics and Biomembranes*. 29:151-163.

Taanman, J.-W., and S.L. Williams. 2001. Assembly of cytochrome *c* oxidase: what can we learn from patients with cytochrome *c* oxidase deficiency? *Biochemical Society Transactions*. 29:446-451.

Tay, S.K.H., S. Shanske, P. Kaplan, and S. DiMauro. 2004. Association of mutations in *SCO2*, a cytochrome *c* oxidase assembly gene, with early fetal lethality. *Arch Neurology*. 61:950-952.

Tiranti, V., P. Corona, M. Greco, J.-W. Taanman, F. Carrara, E. Lamantea, L. Nijtmans, G. Uziel, and M. Zeviani. 2000. A novel frameshift mutation of the mtDNA *COIII* gene leads to impaired assembly of cytochrome *c* oxidase in a patient affected by Leigh-like syndrome. *Human Molecular Genetics*. 9:2733-2742.

Tiranti, V., K. Hoertnagel, R. Carrozzo, C. Galimberti, M. Munaro, M. Granatiero, L. Zelante, P. Gasparini, R. Marzella, M. Rocchi, M.P. Bayona-Bafaluy, J.-A. Enriquez, G. Uziel, E. Bertini, C. Dionisi-Vici, F. Franco, T. Meitinger, and M. Zeviani. 1998. Mutations of SURF-1 in leigh disease associated with cytochrome *c* oxidase deficiency. *American Journal of Human Genetics*. 63:1609-1621.

Tokatlidis, K., and G. Schatz. 1999. Biogenesis of mitochondrial inner membrane proteins. *The Journal of Biological Chemistry*. 274:35285-35288.

Triepels, R.H., B.J. Hanson, L.P. van den Heuvel, L. Sundell, M.F. Marusich, J.A. Smeitink, and R.A. Capaldi. 2001. Human Complex I defects can be resolved by monoclonal antibody analysis into distinct subunit assembly patterns. *The Journal of Biological Chemistry*. 276:8892-8897.

Trounce, I. 2000. Genetic control of oxidative phosphorylation and experimental models of defects. *Human Reproduction*. 15:18-27.

Tsukihara, T., H. Aoyama, E. Yamashita, T. Tomizaki, H. Yamaguchi, K. Shinzawa-Itoh, R. Nakashima, R. Yaono, and S. Yoshikawa. 1995. Structures of metal sites of oxidized bovine heart cytochrome *c* oxidase at 2.8 A. *Science*. 269:1069-1074.

Tzagoloff, A., and C.L. Dieckmann. 1990. *PET* genes of *Saccharomyces cerevisiae*. *Microbiological Reviews*. 54:211-225.

Valnot, I., S. Osmond, N. Gigarel, B. Mehaye, J. Amiel, V. Cormier-Daire, A. Munnich, J.-P. Bonnefont, P. Rustin, and A. Rötig. 2000a. Mutations of the *SCO1* gene in mitochondrial cytochrome *c* oxidase deficiency with neonatal-onset hepatic failure and encephalopathy. *American Journal of Human Genetics*. 67:1104-1109.

Valnot, I., J.-C. von Kleist-Retzow, A. Barrientos, M. Gorbatyuk, J.-W. Taanman, B. Mehaye, P. Rustin, A. Tzagoloff, A. Munnich, and A. Rötig. 2000b. A mutation in the human heme A:farnesyltransferase gene (*COX10*) causes cytochrome *c* oxidase deficiency. *Human Molecular Genetics*. 9:1245-1249.

Winge, D.R. 2003. Let's Sco1, oxidase! Let's Sco! *Structure*. 11:1313-1314.

Xu, F., C. Morin, G. Mitchell, C. Ackerley, and B.H. Robinson. 2004. The role of the *LRPPRC* (leucine-rich pentatricopeptide repeat cassette) gene in cytochrome oxidase assembly: mutation causes lowered levels of COX (cytochrome *c* oxidase) I and COX III mRNA. *Biochemical Journal*. 382:331-336.

Yano, T. 2002. The energy-transducing NADH: quinone oxidoreductase, complex I. *Molecular Aspects of Medicine*. 23:345-368.

Yao, J., and E.A. Shoubridge. 1999. Expression and functional analysis of *SURF1* in Leigh sundrome patients with cytochrome *c* oxidase deficiency. *Human Molecular Genetics*. 8:2541-2549.

Yoshikawa, S. 1999. X-ray structure and reaction mechanism of bovine heart cytochrome *c* oxidase. *Biochemical Society Transactions*. 27:351-362.

Yu, C.-A., H. Tian, L. Zhang, K.-P. Deng, S.K. Shenoy, L. Yu, D. Xia, H. Kim, and J. Deisenhofer. 1999. Structural basis of multifunctional bovine mitochondrial cytochrome bc_1 complex. *Journal of Bioenergetics and Biomembranes*. 31:191-199.

Zhu, Z., J. Yao, T. Johns, K. Fu, I. De Bie, C. Macmillan, A.P. Cuthbert, R.F. Newbold, J.-c. Wang, M. Chevrette, G.K. Brown, R.M. Brown, and E.A. Shoubridge. 1998. *SURF1*, encoding a factor involved in the biogenesis of cytochrome *c* oxidase, is mutated in Leigh syndrome. *Nature Genetics*. 20:337-343.